8-2018

THE COMPARISON OF EFFECTS OF SYNTHETIC AND NATURAL ARACHIDIN-3 ON ROTAVIRUS INFECTED CELLS

Rebekah Napier-Jameson
Stephen F Austin State University, napierjar@jacks.sfasu.edu

THE COMPARISON OF EFFECTS OF SYNTHETIC AND NATURAL ARACHIDIN-3 ON ROTAVIRUS INFECTED CELLS

Creative Commons License

THE COMPARISON OF EFFECTS OF SYNTHETIC AND NATURAL ARACHIDIN-3 ON ROTAVIRUS INFECTED CELLS

By

REBEKAH NAPIER-JAMESON, B.S BIOLOGY, B.S ENVIRONMENTAL SCIENCE

Presented to the Faculty of Graduate School of

Stephen F. Austin State University

In Partial Fulfillment

Of the Requirements

For the Degree of

Master of Science in Biotechnology

STEPHEN F. AUSTIN STATE UNIVERSITY

August 2018

THE COMPARISON OF EFFECTS OF SYNTHETIC AND NATURAL ARACHIDIN-3 ON ROTAVIRUS INFECTED CELLS

By

REBEKAH NAPIER-JAMESON, B.S BIOLOGY, B.S ENVIRONMENTAL SCIENCE

APPROVED:

_____
Rebecca D. Parr, Ph.D., Thesis Director

_____
Judith Ball, Ph.D., Committee Member

_____
Josephine Taylor, Ph.D., Committee Member

_____
Donald Pratt, Ph.D., Committee Member

_____
Pauline M. Sampson, Ph.D.
Dean of Research and Graduate Studies

ABSTRACT

Rotavirus (RV) causes severe, life-threatening diarrhea, in infants, young children and immunocompromised adults. There are several effective vaccines for young children, however they are strain specific and are not protective against many RV strains in developing countries. Therefore, it is important to investigate anti-RV therapeutic agents. Our laboratory has shown arachidin-1 (A1) and arachadin-3 (A3) significantly inhibit RV replication in two cell lines, however the molecular mechanism(s) of action are not known. A synthetic molecule of A3 (sA3) has been produced, but its' antiviral effects have not been examined. Our hypothesis is that sA3 produces the same effects on RV-infected cells as natural A3. This study used plaque forming unit (PFU) assays to show a significant decrease in the amount of infectious RV particles released from arachidin treated cells, and tunable resistive pulse sensing technology (TRPS) revealed changes in the size distribution of released nanoparticles. Transmission electron microscopy (TEM) was utilized to observe alterations of nucleus to cytoplasm ratios which were confirmed with whole cell fluorescent staining techniques. This suggested that the arachidins modified the apoptosis and autophagy pathways. To support these observations, transcripts of initiator genes in both pathways were investigated using qRT-PCR, and the expression of two effector proteins in

the apoptosis pathway were measured. Only small changes in the transcripts and proteins were detected which implied the regulation of other genes in the cell death signaling pathways that requires further examination. Both A3 and sA3 have similar antiviral activity that results in significant decreases in the production of infectious RV particles, thus revealing therapeutic potential for rotavirus infections.

ACKNOWLEDGEMENTS

TABLE OF CONTENTS

LIST OF FIGURES

LIST OF TABLES

LIST OF ABBREVIATIONS

Symbol	Description
A1	Arachidin 1
A3	Arachidin 3
AGE	Acute gastroenteritis
ANOVA	Analysis of variance
BSA	Bovine serum albumin
cDNA	Complementary DNA
Ct	Threshold cycle
DLP	Double Layer Particles
DMEM	Dulbecco's Modified Eagle's Medium
DNA	Deoxyribose Nucleic Acid
dNTP	Deoxy ribonucleotide triphosphate
dsRNA	double stranded Ribonucleic Acid
ER stress	Endoplasmic reticulum stress
$_{e}$RV	Enveloped Rotavirus particle
FBS	Fetal bovine serum
GI	Gastrointestinal

HPCCC	High Performance Countercurrent Chromatography
HPI	Hours post infection
HT29	Human colon adenocarcinoma cell line
HT29.f8	Spontaneously polarizing human colon adenocarcinoma cell line
MA104	African green monkey kidney cell line
MEM	Minimum essential media
MOI	multiplicity of infection
mRNA	Messenger Ribonucleic Acid
$_{ne}$RV	Non-enveloped Rotavirus particle
NV	No Virus
PCR	Polymerase chain reaction
PFU	Plaque Forming Unit assay
qRT-PCR	Quantitative real time polymerase chain reaction
RFU	Relative Fluorescence Units
RNA	Ribonucleic acid
RV	Rotavirus
RV+A3	Rotavirus with 20μM A3
RV+sA3	Rotavirus with 20μM sA3

SA11.4f	Simian rotavirus strain
sA3	Synthetic Arachidin 3
SD	Standard Deviation
SDS	Sodium dodecyl sulfate
TEM	Transmission Electron Microscopy
TLP	triple layered particles
TRPS	Tunable Resistive Pulse Sensing Technology
VP	Viral protein
Wa	Human rotavirus strain

INTRODUCTION

Rotavirus (RV) is a member of the Reoviridae family and is a major source of viral gastroenteritis affecting infants and young children (Bernstein, 2009; Ward, 1996) as well as in immunocompromised adults such as those with SCIDs, HIV, chemotherapy patients, or transplant patients (Bakare *et al.*, 2010; Stelzmuller *et al.*, 2007, Cui *et al.*, 2015; Lee and Ison, 2014; Sugata, *et al.*, 2012; Yin *et al.*, 2015; Liakopoulou *et al.,* 2005; Anderson and Weber, 2004; Patel *et al.*, 2010). RV infections are characterized by vomiting, fever, and watery diarrhea with symptoms usually lasting for 4-6 days (Heymann, 2015). The prevalent nature of RV and the serious health risks it poses have made it a major studied pathogen over the past 70+ years (Bernstein, 2009). Globally, by the age of five almost all children have been infected by RV (Ward, 1996). It is estimated that approximately 215,000 rotavirus deaths in children under the age of five occur globally each year (Tate, *et al.*, 2016). RV is transmitted via the fecal-oral route and is extremely contagious (Cook, 1990). Infected persons may remain asymptomatic or have an acute gastroenteritis (AGE) with mild to severe Diarrhea and vomiting (Desselberger, 2014). AGE can lead to a massive electrolyte imbalance; leading to severe dehydration (Desselberger, 2014).

Dehydration and cardiac failure are the leading causes of deaths associated with RV infections (Desselberger, 2011; Tate *et al.*, 2012). The WHO recommends oral rehydration therapy and zinc supplementation for rotavirus-induced diarrhea management (Gandhi *et al.*, 2016).

In 1973, stool samples from several severe gastroenteritis cases in young children at the Royal Children's Hospital in London, England, were obtained for transmission electron microscopy (TEM) and spherical particles were observed (Bishop *et al.*, 1973). These 1973 TEM images were the first authentication of RV infection in humans using TEM and led to the use of EM in the diagnosis of RV infections (Bishop *et al.*, 1973). Polyacrylamide gel electrophoresis (PAGE), enzyme linked immunosorbent assays (ELISA), and latex agglutination tests are used to test for RV infections (Esona and Gautam, 2015; Heymann, 2015). After the visualization of RV using EM in 1973 one of Ruth Bishop's collaborators, Thomas Flewett, and his team put forward the Latin name "rota", meaning wheel, due to RV's unique wheel-like microscopic appearance (Flewett and Woode, 1978). Four years later, in 1977, the International Committee on Taxonomy of Viruses agreed to officially name the pathogen "rotavirus" (Mathews, 1979).

The Centers for Disease Control (CDC) and the World Health Organization (WHO) report that fatality rates associated with RV have fallen steadily since 1980 (Bishop, 2009; Gandhi *et al.*, 2016). This decline is attributed mainly to the use of RV vaccines and the improvement of treatment protocols

(Bishop, 2009; Jiang *et al*., 2010). There are two licensed attenuated RV vaccines: RotaTeq® (Merck) and RotaRix® (GlaxoSmithKline). Rotarix® is an attenuated human RV vaccine made with a tissue-culture-adapted human strain, and RotaTeq® is a bovine (WC3)-human reassortment vaccine composed of 5 strains, each containing a human rotavirus gene (Angel *et al.,* 2007). These vaccines only protect against specific RV strains (Leshem *et al*., 2014). Recently a new attenuated RV vaccine, Rotavac®, was recently released in India by Hyderabad-based Bharat Biotech International (Bhandari *et al*., 2014; John, 2014). Rotavac® only protects against an RV strain that is a common cause of severe diarrhea in children in India (Bhandari *et al*., 2014).

Vaccines represent a major means in which to prevent the severe negative outcomes of rotavirus infection, especially in impoverished regions where resources and access to care may be limited (Madhi *et al*., 2016). However, the vaccines efficacies are dependent on the timing of vaccination, and are designed to protect against common RV strains in specific areas of the world and therefore do not provide universal protection (Glass, 2006; John, 2014). Neither natural RV infections nor RV vaccines provide full protection from future infections (Centers for Disease Control and Prevention, 2017). Vaccinated children are much less likely to get sick from rotavirus, and if they do, their symptoms are usually much less severe than unvaccinated children (Centers for Disease Control and Prevention, 2017).

Mature RVs are segmented double-stranded RNA viruses (Patton, 2012). RV particles (virions) are approximately 75 nanometers (nm) in diameter, non-enveloped, and have three concentric icosahedral protein layers that encapsulate 11 double stranded RNA segments (Estes, 2001; Heymann, 2015). Each RNA segment codes for one viral protein (VP) except for gene segment 11 which codes for two proteins (Estes, 2001). There are six viral structural proteins (VP1-VP4, VP6 and VP7) and six nonstructural proteins (NSP1-NSP6) (Matthijnssens, *et al.,* 2008). VP4 is then cleaved into two polypeptides, VP5 and VP8 (Jayaram *et al.*, 2004).

These proteins function either as a structural component of the virus particle (VP) or as a nonstructural protein (NSP) which is involved in various aspects of the viral replication cycle (Jayaram *et al*, 2004). The inner core of the RV particle is made up of 60 dimers of VP2 and encloses the complete viral genome as well as viral RNA dependent RNA polymerase, VP1 and the capping enzyme VP3 (Desselberger, 2014; Jayaram *et al.*, 2004; Patton, 1995). The intermediate capsid layer is composed of VP6 and is arranged in a lattice form with 260 trimers forming the icosahedral layer (Desselberger, 2014; Payne *et al.*, 2006).

In immature virus particles, the outside protein coats are made from only VP6 (Payne *et al.*, 2006). These immature particles are known as noninfectious double layered particles (DLPs) (Payne *et al.*, 2006). VP6 is large in size and

participates in communication with the inner VP2 layer in addition to the outer proteins, VP4, and VP7 (Payne *et al.*, 2006). Rotavirus particles contain large channels that breach through the VP7 and VP6 layers (Payne *et al.*, 2006). These channels facilitate the passage of aqueous materials through the capsid (Payne *et al.*, 2006). When an RV particle contains both VP4 and VP7 it is considered a triple layered particle (TLP) and is considered infectious (Payne *et al.* 2006). The outermost layer consists of an icosahedral capsid made of VP7, a glycoprotein, with 60 projecting spikes that are made up of VP4 dimers (Payne *et al.*, 2006). These spikes are required by the virions for efficient cell entry (Payne *et al.*, 2006). When RV attaches to the host's cell surface VP4 is cleaved by the small intestine enzyme trypsin (Estes *et al.*, 1981). This produces a conformational change and the production of VP5 and VP8 which are necessary for viral entry into the host cell (Estes *et al.*, 1981).

The process of viral entry is still not wholly understood. The process of receptor mediated endocytosis was the first accepted method of RV entry (Bernstein, 2009). It has also been found that low calcium levels in endosomes make it possible for direct membrane penetration via the solubilization of the outer capsid protein VP7 (Desselberger, 2014).

The newly formed transcriptionally active DLPs are released into the cytoplasm (Gardet *et al.*, 2006). The DLPs make their way into specialized

structures called viroplasms where viral replication begins to take place (Patton, 1995).

Viroplasms vary in size and shape depending on the replication cycle but are usually located adjacent to the nucleus (Desselberger, 2014). Viroplasms produce new DLPs which then bud into the endoplasmic reticulum (ER) by the attachment to a nonstructural protein (NSP4) (Desselberger, 2014; Greenberg and Estes, 2009). As VP4 and VP7 assemble, the ER membranes are removed, resulting in a mature TLP (Greenberg and Estes, 2009). TLPs are released in epithelial cells via budding (Gardet *et al*., 2006).

There are many challenges in the attempt to combat RV. One major challenge is posed by reassortment, which leads to new RV strains (Patton, 2012). All of the 11 rotavirus gene segments are responsible in creating rotavirus diversity in nature (Matthijnssens, *et al.,* 2008). Reassortment can take place during co-infections producing novel RV strains (Ball, *et. al*., 2005; Patton, 2012; Yakshe *et al*., 2015). The differences in the efficacies of vaccines in developed and developing countries are also a major challenge (Lopman *et al*, 2012).

Recent studies in the Parr laboratory have shown that two stilbenoids Arachidin-1 and -3 (A1 and A3) (natural products from peanut hairy root cultures) significantly reduce the production of infectious RV particles and decrease viral replication (Ball *et al*., 2015). These findings demonstrate the potential for the development of these stilbenoids as antiviral therapeutics.

Stilbenoids are secondary metabolites which act as phytoalexins (a substance that is produced by plant tissues in response to contact with a parasite and that specifically inhibit the growth of that parasite) which are produced by plants including grape, berry, and peanut plants in response to pathogens and are derived from the phenylpropanoid/ acetate pathway (Huang *et al.*, 2010; Moss *et al.*, 2013). Phytoalexins tend to accumulate rapidly in areas of pathogenic infection and demonstrate anti-oxidative/anti-pathogenic properties (Chong *et al.*, 2009; Jeandet *et al.*, 2010).

Resveratrol is a stilbenoid commonly found in grapes used for making red wine, has received much attention due to its wide range of biological activities and potential health benefits (Berardi *et al.*, 2009; Moss *et al.*, 2013). These benefits may include: anti-oxidative-, anti-inflammatory-, cardioprotective-, antiviral-, anticancer-, and anti-aging-properties (Huang *et al.*, 2010, Sobolev *et al.*, 2006, Velayudhan *et al.*, 2014).

Many *in vitro* and *in vivo* studies have demonstrated significant biological effects of resveratrol (Berardi *et al.*, 2009; Nakamura *et al.*, 2010; Palamara *et al.*, 2005). However, at times it lacks biological activity due to its limited oral bioavaibility (Gambini *et al.*, 2015; Vitaglione *et al.*, 2005). Rapid absorption and metabolism leading to the formation of various metabolites such as resveratrol glucoronides and sulfates which are quickly released from the body may be

responsible for resveratrols curbed oral bioavailability (Gambini *et al.*, 2015; Vitaglione *et al.*, 2005).

Resveratrol strongly inhibits the replication of influenza virus, improves survival, and decreases pulmonary viral infectivity titers in influenza virus-infected mice (Palamara *et al.*, 2005). Furthermore, resveratrol exhibits no toxic effects *in vitro* or *in vivo* (Palamara *et al.*, 2005). However, another study testing the effects of different concentrations of resveratrol on polyomavirus showed cytotoxicity in a time- and dose-dependent manner and inhibition of polyomavirus DNA synthesis (Berardi *et al.*, 2009). Another study identified resveratrol derivatives with potent anti-HSV-1 and HSV-2 activity showing antiherpetic activity at single-digit micromolar concentrations (Chen *et al.*, 2012).

In peanuts, the some of the known stilbenoids are prenylated, having an isopentenyl moiety as in A1 and A3 (Sobolev *et al.*, 2006). Studies have shown that A1 has a higher efficacy in inducing programmed cell death in leukemia HL-60 cells (Huang *et al.*, 2010). These results show the potential use of A1 as an anti-cancer drug.

Once peanut (*Arachis hypohaea*) hairy root cultures are exposed to abiotic (environmental) and biotic (caused by living organisms) stresses they produce stilbenoids including: resveratrol, piceatannol, A3 and A1 (Chong *et al.*, 2009). These stilbenoids have been shown to possess anti-inflammatory, anti-cancer and anti-proliferative properties (Chang *et al.,* 2006; Djoko *et al.,* 2007).

8

A synthetic version of A3 (sA3) has been produced by the laboratory of Dr. Medina-Bolivar (personal communications). A U.S. utility patent 9,981,895 was awarded on May 29, 2018 titled "Compositions and Methods of Synthesizing Arachidin-3 from Resveratrol". Briefly, organic synthesis using primary alkylamines or primary hydroxyalkyl amines, or carboxy amines with natural carboxylic acids as catalysts to react isovaleraldehyde with trans-resveratrol is utilized in the production of sA3 (Clayton and Bandy, 2018). An azeotropic mixture comprising toluene with pyridine, n-butanol, n-propanol, 2-propanol, 2-methyl-1-propanol, or other alcohols that form an azeotrope with toluene used as the organic solvent in which the synthesis is carried out (Clayton and Bandy, 2018). Column chromatography (neutral), high performance liquid chromatography (HPLC), high performance counter-current chromatography, thin layer chromatography (TLC), nuclear magnetic resonance spectroscopy (NMR), and infrared spectroscopy (IR) are all utilized as purification and qualification analysis techniques in sA3 production (Clayton and Bandy, 2018).

One study suggests that the enhanced therapeutic activity of stilbenoids is likely the result from the increased ability to dissolve fats, oils, and non-polar solvents which is imparted by single or multiple groups present within their structure (Huang *et al.*, 2010). It has been proposed that the greater lipophilicity of prenylated trans-Resveratrol (t-Res) analogues may allow for easier interactions between substances and cell membranes (Huang *et al.*, 2010). This

may increase access and association with potential membrane-bound molecular targets responsible for the beneficial activities of these compounds (Huang *et al.*, 2010). Another study suggests that the lipophilic side chain (3-methyl-1-butenyl group) might hinder the addition of glucuronic acid to a substrate and thereby enhance the bioavailability of the analogues (Brents *et al.*, 2012). Additionally, A3 exhibits higher biological activities both *in vitro* and *in vivo* when compared to resveratrol, also demonstrating antiviral activity (Ball *et al.*, 2015; Yang *et al.*, 2015).

Our hypothesis is that the addition of the sA3 to RV-infected HT29.f8 cells decreases the amount of infectious viral particles in an infection and produces the same effects on the host cell as the natural A3. My hypothesis is that the addition of either the natural A3 or sA3 to a human RV-infected HT29.f8 cell line effects the infected host and effects the maturation of infectious RV particles. This results in the decrease of infectious viral particles produced, changes in the host cell ultrastructure, and regulation of the host gene transcripts. This hypothesis will be tested using four objectives:

(1) Establish that the viability of the cells are not affected with the addition of 20 µM final concentration sA3 by performing cell viability assays;

(2) Measure the progeny infectious RV particles using plaque forming unit (PFU) assays and total RV particles using tunable pulse sensing technology (TRPS);

(3) Visualize the effects of treatments on the cells using TEM, whole cell fluorescent staining, and morphometric analysis;

(4) Determine the effects of treatments on gene expression and regulation of cell death pathways in treated host cells using qRT-PCR.

Materials and Methods

Cells, MycoFind™ Mycoplasma PCR detection kit, and virus

MA104 cells were obtained from ATCC (Rockville, MD) and HT29.F8 cells, a spontaneously polarizing cell line, were derived from the parent human adenocarcinoma (HT29) intestinal line (Mitchell & Ball, 2004). RV Wa (G[1] P[8] genotype) (Matthijnssens *et al.*, 2008) was amplified, viral titers determined to be 3.66E+11 PFU/mL by plaque forming unit (PFU) assays using MA104 cells, and stored at -80°C. Stilbenoid efficacy against RV was tested using HT29.f8 cells obtained from Dr. Judith Ball (Texas A&M University, College Station, TX). The cell line was maintained in Dulbecco's Modified Eagle Medium (DMEM; Genesee Scientific, San Diego, CA) supplemented with 7.5% fetal bovine serum (FBS; Caisson, Smithfield, UT), L-glutamine (2 mM) (Caisson, Smithfield, UT), penicillin-streptomycin (100 µg/mL) (Caisson, Smithfield, UT) and non-essential amino acids (Caisson, Smithfield, UT) as a 100X solution. The amino acids were used at a 1X concentration of 100 µM each.) (Mitchell & Ball, 2004). The cell lines were confirmed to be free of mycoplasma contamination using the PCR Mycoplasma Test Kit I/C (PromoKline, PromoCell GmbH, Heidelberg, Germany).

Briefly, the cell lines were cultured for 2 weeks in media lacking Pen/Strep. 1 mL of supernatants from each cell line was transferred into sterile labelled 1.5 mL microfuge tubes and centrifuged at 500 x *g* for 5 minutes in order to pellet cellular debris. The supernatants were then transferred into fresh sterile 1.5mL microfuge tubes and centrifuged at 14,000 x *g* for 15 minutes. The cell pellets were re-suspended with 100 µL of DNA free water. The test samples, positive control, and negative control were prepared as per Table 1.

Table 1. PCR Mycoplasma Test Kit I/C sample preparation

	Test sample	Positive Control	Negative Control
Rehydration Buffer	23 µL	23 µL	23 µL
Sample	2 µL		
DNA-free water		2 µL	
Fresh Cell Culture Medium			2 µL

The contents of the test sample tubes, positive control tube, and negative control tube were mixed thoroughly via flicking the tubes. The lyophilized

components were allowed to dissolve by incubating the tubes for 5 minutes at 25°C. The thermal cycling parameters laid out in Table 2 were used.

Table 2. Thermal Cycling parameters used for PCR Mycoplasma Test Kit I/C

1 cycle	95° for 2 minutes
40 cycles	94°C for 30 seconds
	55°C for 30 seconds
	72°C for 40 seconds
Hold	4°C

The tubes were quickly tap-spun and 8 µL of the resulting products were run on a 1.5% agarose gel (0.75g Molecular Biology Certified agarose (IBI Scientific, Peosta, CA), 50 mL 1X TAE (Apex BioResearch Products, Genesee Scientific, San Diego, CA), 5 µL GelRed dye (Biotium Inc., Fremont, CA)) alongside the Apex 100 bp-Mid DNA marker (Genesee Scientific, San Diego, CA) for 1 hour at 100 volts using the BioRad PowerPac and Mini-Sub Cell GT (BioRad Laboratories, Hercules, CA). The gel was visualized on the Typhoon FLA 9000 (GE Healthcare Life Sciences, Uppsala, Sweden) using the following settings: Fluorescence, EtBr, 100 µM.

Bio-production of stilbenoids in peanut hairy root cultures

Natural A3 were purified from methyl-β-cyclodextrin (CD)-elicited peanut (*A. hypogea*) hairy root cultures as recently described (Abbott *et al.*, 2010; Condori *et al.*, 2010; Yang *et al.*, 2015). Briefly, 9-day peanut hairy root cultures, line 3 (Condori *et al.* 2010), were elicited with methyl-β-cyclodextrin (fresh MSV medium with 9 g/L methyl-β-cyclodextrin (Cavasol$^{®}$ W7 M)) (Medina-Bolivar *et al.* 2007; Medina-Bolivar *et al.* 2010). Cultures were incubated in the dark at 28$^{°}$C for an additional 72 hours to induce synthesis and secretion of stilbenoids into the culture medium (Abbott *et al.*, 2010; Yang *et al.*, 2015). After the elicitation period, the culture medium was removed from each flask and combined. This pooled medium was mixed with an equal volume of ethyl acetate in a separator funnel to extract the stilbenoids as described previously (Jose Condori *et al.*, 2010). The ethyl acetate phase was recovered and dried in a rotavapor (Buchi Corp., New Castle, DE), and A3 was purified from the extract with HPCCC. Fractions were collected every 30 seconds, dried in a speed-vac and selected fractions were checked for purity by mass spectrometry using an UltiMate 3000 ultrahigh performance liquid chromatography (UHPLC) system (Dionex, Thermo Scientific, Waltham, WA) coupled with a LTQ XL linear ion trap mass spectrometer (Thermo Scientific, Waltham, MA) as previously described (Marsh *et al.*, 2014). HPCCC fractions containing A3 with over 95% purity based on HPLC analysis (UV 340 nm) were combined, dried under a nitrogen stream and

used for viral assays. The dry mass of the purified stilbenoids were reconstituted in 0.02% DMSO with 1 µg/mL Worthington trypsin (WT) (Worthington Biochemical, Lakewood, NJ) in MEM medium.

A synthetic version of A3 (sA3) has been produced by the laboratory of Dr. Medina-Bolivar (personal communications). A U.S. utility patent application was filed on March 29, 2016 titled "Compositions and Methods of Synthesizing Arachidin-3 from Resveratrol". Briefly, organic synthesis using primary alkylamines or primary hydroxyalkyl amines, or carboxy amines with natural carboxylic acids as catalysts to react isovaleraldehyde with trans-resveratrol is utilized in the production of sA3 (Clayton and Bandy, 2018). An azeotropic mixture comprising toluene with pyridine, n-butanol, n-propanol, 2-propanol, 2-methyl-1-propanol, or other alcohols that form an azeotrope with toluene used as the organic solvent in which the synthesis is carried out (Clayton and Bandy, 2018). Column chromatography (neutral), high performance liquid chromatography (HPLC), high performance counter-current chromatography, thin layer chromatography (TLC), nuclear magnetic resonance spectroscopy (NMR), and infrared spectroscopy (IR) are all utilized as purification and qualification analysis techniques in sA3 production (Clayton and Bandy, 2018).

RV Infections in HT29.f8 Cells

To test the biological activity of A3 and sA3 on RV infections in HT29.f8 cells, the cells were grown to 80% confluence in T25 tissue culture flasks (Corning Life Sciences); starved for fetal bovine sera 8 hours prior to infection, and then infected with RV Wa as previously described *(*Arnold *et al.,* 2009*;* Ball *et al.*, 2015; Yakshe *et al.*, 2015). Briefly, Wa RV stock was sonicated 10 min using a cup horn attachment and ice bath in a Misonix Sonicator 3000 (Misonix, Inc., Farmingdale, NY) and incubated in serum-free DMEM with 10 μg/mL trypsin (WT) for 45 min at 37°C. The activated viral inoculum was incubated with the cells for 1 hour at 37°C in 5% CO_2 at an MOI of 2. At the scheduled collection times, cells were washed with Dulbecco's PBS (Caisson Laboratories, Smithfield, UT) and released from the flasks using a 0.25% trypsin (0.25% trypsin in HBSS, Caisson Labs (North Logan, UT)). The supernatants were collected, clarified at 10 000 *x g* for 5 min, and stored at -80°C for plaque assays and TRPS analysis (see below). The cells were washed in 1X cold Dulbecco's PBS   (Caisson Laboratories, Smithfield, UT), fixed with 5% glutaraldehyde and used for TEM analysis as described below.

Toxicity of A3 and sA3 to HT29.f8 cells: Trypan Blue cell exclusion viability assay

Viability assays were performed with RV alone, RV + 0.02% DMSO (bioWORLD, Dublin, OH), RV with 20 µM A3 or sA3, 20 µM A3 alone, 20 µM sA3 alone, cells without treatments (NV, no virus), and cell with 0.02% DMSO using the trypan blue cell exclusion assay (Ball *et al.*, 2015; Freshney, 1994). Briefly, HT29.f8 cells were grown to 80% confluence in 6-well tissue culture plates (Corning Life Sciences, Corning, NY); starved from fetal bovine sera 8 hours prior to the addition of 0.02% DMSO, 0.02% DMSO with 20 µM concentrations of the arachidins, RV (MOI 2), and RV (MOI 2) with 20 µM concentrations of the arachidins. At 18 hours after the treatments, a suspension of ~10^6 cells/mL was diluted 1:1 with a 0.4% trypan blue solution (Sigma-Aldrich, St. Lois, MO. T8154, Lot RNBC8659), and loaded onto a Neubauer-improved hemocytometer (Paul Marienfeld Gmbh & Co. Kg., Lauda-Königshofen, Germany). Each of the four corner squares was used for counts. Any cell sitting on or outside a division line was not counted. The number of stained dead cells and total number of cells were counted, and the calculated percentage of live cells was reported. Each treatment was performed in triplicate, Data were statistically analyzed in Microsoft Office Excel 2016 software using one-way analysis of variance (ANOVA) and two-tailed Student's t tests (significance level,

P <0.05) with Bonferroni's *post hoc* test to correct for multiple comparisons ($P < 0.004545$).

Production of infectious virus particles with the addition of A3 or sA3

6-well, flat bottom tissue culture plates (Olympus plastics, tissue culture plate, 6-well, flat bottom, cat. #25-105, Genesee Scientific) in were seeded with approximately $0.5X10^6$ MA104 cells/well with 3mL complete MEM. Cells were grown to confluency (approximately 2 days). Plaque forming unit (PFU) assays were performed in triplicate as previously described *(Arnold et al., 2009; Ball et al.*, 2015; Yakshe *et al.*, 2015). Briefly, 0.5 mL of 10-fold dilutions of RV alone and RV with 20 µM of A3 or sA3 supernatants collected at 18hpi from previous infections were added to serum starved MA104 cells for 1 hour at 37°C, 5% CO_2. The virus inoculum was removed and the wells were washed gently with pre-warmed Dulbecco's PBS (GE Healthcare Life Sciences, HyClone Laboratories, Logan, Utah) after which 3 mL of a medium overlay consisting of a 1:3 mixture of 5% agarose (Apex Low Melting Point Agarose, Genesee Scientific Inc., San Diego, CA) and complete serum-free MEM with a 1:100 dilution of 100X Pen/Strep was overlaid and allowed to set and incubated at 37°C in 5% CO_2 for approximately 1-2 days or until plaques became visible. A neutral red overlay consisting of a 1:3 mixture of 5% agarose with serum-free MEM containing 50

µg/mL neutral red was prepared and 1 mL per well of stain overlay was added on top of the first agarose/medium overlay and allowed to set. The six-well plates were incubated at 37°C until plaques were clearly visible (approximately 12 to 36 hours). The individual plaques were counted, and the titers were calculated as follows:

Number of plaques x 1/dilution factor x 1/ (mL of inoculum) = PFU/mL

Plaque forming assays were performed four times in triplicate as outlined above. Data were expressed as mean ± SD, and comparisons were statistically evaluated by analysis of variance (ANOVA) and two-tailed Student's t tests using Microsoft Excel 2016 software (significance level, $P < 0.05$).

Quantification of nanoparticles and size distribution by TRPS analysis

TRPS analysis using the qNano system (Izon Science, Cambridge, MA) was performed on the RV-infected cell supernatants to display the concentration of virus particles/mL, diameter of RV particles and size distribution of particles. TRPS is based on a coulter counter that is composed of two fluid reservoirs filled with an electrolyte or other conductive medium and separated by a membrane

containing a nanopore (Kozak *et al.*, 2011; Weatherall *et al.*, 2016). When an electrical field is applied across the pore, the resistance to the resulting ionic current is indirectly proportional to the cross-sectional area of the pore. When a non-conducting particle passes through the pore, the increase in resistance is proportional to the particle volume relative to pore size. This change in resistance is detected as a pulse in an ionic current. The pulse frequency is proportional to particle flow rate and particle concentration (DeBlois, 1970). This system provides a quick and accurate method with which to measure sizes of individual nanoparticles and their volume in a solution. All qNano experiments were performed using the manufacturer's established protocols (Bo *et al.*, 2014; Jones, 2015; Vogel *et al.*, 2011). Briefly, samples were purified using a qEV 10 size exclusion column from Izon (Izon Scientific, Cambridge, MA) (containing resin with approximately 75nm pore size). The samples were suspended in Dulbecco's PBS with 0.025% Tween 20 to reduce particle aggregation and facilitate the wetting of the nanopore. A 1:1000 dilution of the sample was placed on the qNano size-tunable nanopore (NP100, Izon), and each sample was measured as a transient change in the ionic current flow using the custom assistant application in IZON proprietary software v3.2.2.268 (Izon). Samples are driven through the nanopore by applying a combination of pressure and voltage, and each particle causes a blockade signal which is detected and measured by the application software. Blockade magnitude is proportional to the volume of each particle

(Vogel *et al.*, 2012), and the blockade frequency is used to determine particle concentration (Roberts *et al.*, 2012). These values are converted into particle properties (size and concentration, respectively) by calibration with particles of known size and concentration (CPX100B, Izon). The size distribution and concentration analysis was performed using IZON proprietary software v3.2.2.268 (Izon).

TEM morphometric analysis of arachidin treated RV-infected HT29.f8 cells

TEM analysis was performed on RV-infected HT29.f8 cells to visualize the effects of A3 and sA3 on progeny virus and cellular morphology as described by Wright (2000). Briefly, RV-infected HT29.f8 cells with and without 20 µM A3 or sA3 were incubated for 16 and 18 hpi, washed with Dulbecco's PBS and then trypsinized. Cells were pelleted and fixed with 5% glutaraldehyde (Electron Microscopy Sciences, Hatfield, PA) and refrigerated overnight at 4°C. The cells were post-fixed with 2% osmium tetroxide (Electron Microscopy Sciences, Hatfield, PA) followed by an overnight incubation in a uranyl acetate solution (Electron Microscopy Sciences, Hatfield, PA). Cells were dehydrated with a graded ethanol series (2x wash with deionized water at 10-15 minute intervals, followed by ethanol series at 10-15 minute intervals: 20% EtOH, 40% EtOH, 60% EtOH, 80% EtOH, 95% EtOH, 2x 100% EtOH, 2x 100% Acetone) (Electron

Microscopy Sciences, Hatfield, PA). Acetone was used for the transitional solvent, after which the samples were infiltrated and embedded in Spurr's resin (Electron Microscopy Sciences, Hatfield, PA) (70% Spurr's resin, 30% Acetone, replaced with 100% Spurr's resin after 8 hours and polymerized at 70°C overnight in a Robbins Scientific Model 400 Hybridization Incubator (Robbins Scientific Corporation, Sunnyvale, CA)). Ultra-thin sections (~50-80 nm) were obtained with an RMC MT-X ultra-microtome (Boeckeler instruments, Tucson, AZ) and stained with uranyl acetate and lead citrate (Electron Microscopy Sciences, Hatfield, PA). Samples were examined and photographed with a Hitachi H-7000 transmission electron microscope operating at 75 KeV (Wright, 2000), negatives were digitized at 600 dpi using the HP Scanjet G4050 (HP Inc., Palo Alto, CA), and image analysis was performed using Macnification Version 2 (Orbicule, Inc., www.orbicule.com). The mean ratio of the cell nucleus to cytoplasm was determined using 10 micrographs of cells from each treatment to compare between test and control groups. Data were statistically analyzed in Microsoft Office Excel 2016 software using one-way analysis of variance (ANOVA) and two-tailed Student's t tests (significance level, $P < 0.05$) with Bonferroni's *post hoc* test to correct for multiple comparisons ($P < 0.0033$).

Whole cell fluorescent staining for morphometric analysis

The nucleus and plasma membranes of HT29.f8 cells were fluorescently labelled to determine the ratios of the nucleus to cytoplasm of whole cells to compare to the nucleus to cytoplasm ratios obtained with TEM. Briefly, cells were grown to 80% confluence in 8-well slides (Lab-Tek Chamber Slide System, Nunc, Inc. Naperville, IL) and RV-infected and treated with the arachidins as described above (RV alone, RV with 20 µM A3 or A3, 20 µM sA3 alone, or 20 µM sA3 alone, and cells without treatments (NV-no virus). At 18 hpi, the cells were washed with PBS 1x one time at 25°C, and then fixed with 1% Glutaraldehyde (Electron Microscopy Science, Hatfield, PA) for one hour at 25°C in a fume hood (Harlow and Lane, 1988). Following fixation, the cells were washed twice with PBS 1x at 25°C. The Image-IT™ LIVE Plasma Membrane and Nuclear Labeling Kit (I34406) (Molecular Probes, Invitrogen detection Technologies, Eugene, OR) was used to label the cells. Briefly, one solution for the single step staining for both stains was prepared by adding 5.0 µg/mL Alexa Flour 594-labeled wheat germ agglutinin and 1 µM Hoechst 33342 stain into 1x PBS. Two hundred µLs of the labelling solution was added to each well in 8-well chambered slides, and incubated for ten minutes at 25ºC, removed and the cells were washed twice with PBS 1x, and mounted in PBS 1x. The microscopic analysis was carried out using the Olympus BX50 with DP Manager System compound light microscope with epifluorescense illumination for Alexa Flour 594 labeled wheat germ (Excitation

480-550nm, dichroic mirror DM 570nm, barrier filter 590nm) and Hoechst 33342 (Excitation 330-385nm, dichroic mirror DM 400nm, barrier filter BA420nm) with the DP71 camera (Olympus Corporation, Shinjuku, Tokyo, Japan) equipped with x 40 and X100 objectives. The images were digitized using the DP Controller software (Olympus Corporation), and the pixels of the nucleus and whole cell were measured using Macnification Version 2 (Orbicule, Inc., www.orbicule.com). Excel was used to determine the mean nucleus to cytoplasm ratio of the cells (N = 50 cells of each treatment). Data were statistically analyzed in Microsoft Office Excel 2016 software using one-way analysis of variance (ANOVA) and two-tailed Student's t tests (significance level, P <0.05) with Bonferroni's *post hoc* test to correct for multiple comparisons (P <0.0033).

Quantification of Transcripts for Cell Death Pathway Genes in HT29.f8 Cells

QuantiFluor dsDNA System

The QuantiFluor dsDNA System contains a fluorescent DNA-binding dye ($504nm_{EX}/531nm_{EM}$) that enables sensitive quantitation of small amounts of double-stranded DNA (dsDNA) in a purified sample. Before conducting the qRT-PCR studies a QuantiFluor assay standard curve was conducted to determine accuracy of pipettes and handling. Briefly, a working solution was prepared by diluting the QuantiFluor dsDNA dye 1:400 in 1X TE buffer to make the

Quantifluor dsDNA de working solution. A standard curve was prepared resulting

in 0.05-200ng/well as shown in table 3.

Table 3. Preparing Recommended dsDNA standard Curve Samples.

Standard	Volume of dsDNA Standard (µl)	Volume of 1X TE Buffer (µl)	Final dsDNA Concentration (ng/µl)
A	20	80	20
B	25 of standard A	75	5
C	25 of standard B	75	1.25
D	25 of standard C	75	0.31
E	25 of standard D	75	0.078
F	25 of standard E	75	0.02
G	25 of standard F	75	0.005

200µl of QuantiFluor dsDNA Dye working solution was pipetted into each

well intended for an unknown, blank or standard. Each standard and unknown

was performed in triplicate. 10 µl of the dsDNA standards prepared as in table 3

was dispensed into the plate using a multichannel pipet. For the blanks, 10 µl of

1X TE buffer was loaded into the blank wells. 10-fold dilutions of the unknown

were made and plated in triplicate. The plate was loaded into the VERSA$_{max}$

tunable microplate reader (Molecular Devices, Sunnyvale, CA) and the plate was

shaken for 10 seconds to facilitate thorough mixing. The plate was incubated at

room temperature for 5 minutes protected from light. The fluorescence

($504nm_{EX}/531nm_{EM}$) was measured using VERSA$_{max}$ tunable microplate reader

(Molecular Devices, Sunnyvale, CA) and the SoftMax Pro v5 software (Molecular

Devices Corp., Sunnyvale, CA). The dsDNA was calculated as follows: the

florescence of the blank sample (1X TE Buffer) was subtracted from all of the

standard and unknown samples. The corrected data from the DNA standards

was then used to generate a standard curve of fluorescence versus DNA

concentration. The unknown samples DNA concentration was then determined

from the standard curve and multiplying the resulting number by the dilution

factor if applicable.

Efficiency Assay

Robust and accurate qPCR assays are typically associated with high PCR

efficiencies (Bustin *et al.*, 2009). The ΔΔCt method was utilized to determine

differences in concentrations between samples and is based on normalization

with a reference gene(s) (Bustin *et al.*, 2009). The ΔΔCt method assumes a

uniform PCR amplification of 100% across all samples (Rao *et al.*, 2014).

Therefore, genes must be amplified with comparable efficiencies for this

comparison to be accurate (Bustin *et al.*, 2009). Efficiencies usually are not exactly 100% due to factors such as the presence of PCR inhibitors or enhances, RNA extraction, and different uses of probes, primers, and enzymes (Rao *et al.,* 2014). Efficiencies of 90-100% are considered usable for publication (Rao *et al.*, 2014). Amplification efficiency should be determined from the slope of the log-linear portion of the calibration curve (Bustin *et al.*, 2009).The equation:

$$\text{PCR efficiency} = 10^{-1/slope} - 1$$

In which the logarithm of the initial template concentration is plotted on the x axis and the Ct is plotted on the y axis was used to determine efficiencies. The theoretical maximum of 1.00 (100%) indicates that the amount of product doubles with each cycle (Bustin *et al.*, 2009).

RNA was extracted from each experimental set described above. The ZYMO Research Quick-RNA Miniprep (Catalog number R1054) (Zymo research corp., Irvine, CA) was used to extract and purify total RNA according to the manual protocol. cDNA was synthesized using the ThermoFisher cDNA synthesis kit (Thermo Fisher Scientific, Inc., Waltham, MA). Efficiency assays were run using the suggested Luna Universal Probe and qPCR Master Mix (New England Biolabs, Ipswich, MA) thermal cycling protocol described below.

Briefly, the samples were lysed and homogenized by adding 600 μL of lysis buffer directly to each T75 flask, rocking gently, transferring cells to 1.5 mL microfuge tubes, and passing each sample through a clean 26G$^{3/8}$ syringe 5-10 times. Sample cleaning and gDNA removal was performed by centrifuging the samples at 12 000 x g for 1 minute, transferring the samples to spin-away filters (yellow) in a collection tube and centrifuging at 12 000 x g for 1 minute. The flow-through was used for RNA purification. RNA purification was performed by adding 1 volume of 200-proof ethanol to each RNA sample and mixing well. The samples were then transferred to Zymo-spin III CG columns (green) in collection tubes and centrifuged at 12 000 x g for 30 seconds. In-column DNase I treatment was then performed: The samples were washed with 400 μL RNA wash buffer, centrifuged at 12 000 x g for 30 seconds, the flow-through discarded, and then 80 μL of DNase I treatment mix (5 μL DNase I, 75 μL DNA digestion buffer) was added to each column matrix and incubated at room temperature for 15 minutes followed by a 12 000 x g centrifugation for 30 seconds. The samples were washed with 400 μL RNA prep buffer and centrifuged at 12 000 x g for 30 seconds. 700 μL of RNA wash buffer was added to each sample and they were centrifuged at 12 000 x g for 30 seconds. A further wash was performed using 400 μL RNA wash buffer and a centrifugation at 12 000 x g for 2 minutes. The columns were places in RNase-free tubes and 50 μL of DNase/RNase free deionized water was used to elute the samples; after placing the 50 μL of water

on each sample they were spun at top speed for 30 seconds, the flow through was recovered and re-applied to the columns for a further spin at top speed for 30 seconds. Total RNA was analyzed using a full spectrum analysis at 240 nm-300 nm in the Cary 50 spectrophotometer (Agilent, Corp., Santa Clara, CA). The total RNA was stored at -80°C for future studies. A conversion factor of 40 µg/mL was used to convert the A_{260} to concentration and the value of 10 corrected for path length of 0.1 mm (Sean and Wiley, 2008). The concentration of RNA was calculated using the formula as follows:

Concentration of RNA= A_{260} x 40 µg/mL x 10 x Dilution factor

cDNA was then synthesized using the Thermo Scientific Verso cDNA Synthesis Kit from each experimental set using 500 ng of purified total RNA. A Master Mix was prepared as described in the manufacturer's protocol as shown in Table 4 (Thermo Fisher Scientific, Inc., Waltham, MA).

Table 4. cDNA Master Mix

	Volume (µL)	Final Concentration
5x cDNA synthesis buffer	4	1x
dNTP Mix	2	500µM each
Anchored oligo dT and random hexamer mix [a]	1	
Verso Enzyme Mix	1	
RT enhancer	1	
Template RNA	5	500ng/5µL
Nuclease-free water	6	
Total volume	20	

[a] 3:1 mix of random hexamer and anchored oligo dT

The samples were then placed into the BioRad Real-Time System C1000 Thermal Cycler Instrument (BioRad, Hercules, CA) for the following cycle (Table 5).

Table 5. cDNA synthesis thermal cycling parameters.

	Temperature	Time	Number of cycles
cDNA synthesis	42°C	30 min	1 cycle
Inactivation	95°C	2 min	1 cycle

cDNA samples were purified using the Monarch PRC & DNA Cleanup Kit (New England Biolabs, Ipswich, MA) as per the quick protocol for oligonucleotide cleanup and then quantified using the Cary 50 spectrophotometer (Agilent, Corp., Santa Clara, CA). Briefly, samples were brought up to 50 µl with nuclease-free

water. 100 µl of DNA Cleanup Binding Buffer was added to each 50 µl sample after which 300 µl of 200-proof ethanol (Decon Laboratories Inc., King of Prussia, PA) was added to each sample. The samples were mixed well by gentle pipetting. Samples were loaded onto columns in collection tubes and centrifuged at 16 000 x g for 1 minute, the flow-through discarded, and the columns re-inserted into the collection tubes. Two washed with 500 µL of DNA Wash Buffer were performed at 16 000 x g for 1 minute with the flow-through discarded. The columns were transferred into clean 1.5 mL microfuge tubes and 10 µl of elution buffer placed in the center of the matrix and incubated for 1-2 minute before centrifuging at 16 000 x g for 1 minute. An additional 5 µl of elution buffer was added to the matrix and incubated for 1-2 minutes before spinning at 16 000 x g for 1 minute. The cDNA of the same samples was pooled.

Total cDNA was analyzed using a full spectrum analysis at 230 nm- 300 nm in the Cary 50 spectrophotometer (Agilent, Corp., Santa Clara, CA). Total cDNA concentrations were calculated using the formula as follows:

$$\text{Concentration of cDNA} = A_{260} \times 33\ \mu g/mL \times 10 \times \text{dilution factor}$$

Samples of cDNA were stored at $-20^{\circ C}$ and were diluted to a 50 ng/ 5 µl concentration as needed for qRT-PCR experiments.

The qRT-PCR experiment was performed using a CFX96 Touch Real-Time PCR Detection System (BioRad, Des Plaines, IL). For all experiments, reactions were performed in triplicate with Luna Universal qPCR Master Mix 2X concentration (New England Biolabs, Ipswich, MA) that contained all necessary components to perform a DNA-binding dye base real-time DNA amplification experiment. Primers were purchased from Integrated DNA Technologies (Coralville, IA) with the sequences, Tm, and base pairs sizes of the products shown in Table 6.

Table 6. Primers for qRT-PCR studies

Genes	Primer name	Primer sequence (5′-3′)	Size (bp)	Ref Number
GAPDH	GAPDH For	GAGTCCACTGGCGTCTTCA	190	NM_001289746.1
	GAPDH Rev	GGGGTGCTAAGCAGTTGGT		
β-Actin	β-Actin For	ATCCTCACCCTGAAGTACCC	183	NM_001101.3
	β-Actin Rev	TAGAAGGTGTGGTGCCAGAT		
Caspase 3	Casp3 For	AGAACTGGACTGTGGCATTGAG	191	NM_004346.3
	Casp3 Rev	GCTTGTCGGCATACTGTTTCAG		
Caspase 6	Casp6 For	ACAGGAGGAGAGGAATTGCT	201	NM_001226.3
	Casp 6 Rev	GGCTAACAGTTGACACCTCATG		
Caspase 7	Casp 7 for2	TCAGTGGATGCTAAGCCAGA	199	NM_001267056.1
	Casp 7rev2	GAACGCCCATACCTGTCACT		
Caspase 8	Casp8 For	GGTCACTTGAACCTTGGGAA	146	NM_001080124.1
	Casp8 Rev	CGGAATGTAGTCCAGGCTCA		
Caspase 9	Casp9 For	ACACCCAGACCAGTGGACAT	148	NM_001229.4
	Casp9 Rev	CACGGCAGAAGTTCACATTG		
BCL2	BCL2 For	CAGTTGGGCAACAGAGAACCAT	171	NM_000633.2
	BCL2 Rev	AGCCCTTGTCCCCAATTTGGAA		

Each reaction mixture contained 10 μl of 2X Luna Universal qPCR Master Mix, 0.5 μl of 10 μM forward/reverse primers, 5 μl template cDNA (200ng, 100ng, 50ng, 25ng, 12.5ng, and 6.25ng) and nuclease-free water to a final volume of 20 μl. The 96-well plates were centrifuged at 2500 x g for 4 minutes using the Beckman induction drive centrifuge J-6M (Beckman Coulter, Brea, CA). The suggested Luna thermal cycling protocol (Table 7) was used for the initial time course study.

Table 7. LUNA PCR thermal cycling conditions used for qRT-PCR.

Initial denaturation	95°C	1 minutes
PCR (45 cycles)	95°C	15 seconds
	60°C	30 seconds
Melt curve	60-95°C	Increments of 0.5°C 5 seconds

In order to conduct the efficiency assays duplicated of cDNA dilutions were plated in concentrations of 200 ng, 100 ng, 50 ng, 25 ng, 12.5 ng, and 6.25 ng/well. With the appropriate 0.5 µl forward and reverse primers, 10 µl Luna Universal qPCR Master Mix (NEB BioLabs, Ipswich, MA) and 4 µl RNase and DNase free water.

The following thermal cycling conditions were used:

Table 8. qRT-PCR thermal cycling parameters

Initial denaturation	95°C	1 minutes
PCR (45 cycles)	95°C	15 seconds
	60°C	30 seconds
Melt curve	60-95°C	Increments of 0.5°C 5 seconds

The Ct values obtained were exported into Microsoft Excel and the logarithm of the initial cDNA template concentration is plotted on the x axis and the Ct is plotted on the y axis per primer set (GOI). A standard curve was created and the equation and R^2 inserted. The slope from the generated equation was inserted into the following equation in order to determine the efficiencies.

$$E=10^{(-1/slope)}-1 \times 100 \text{ to determine \% efficiency}$$

Experiments were performed twice in duplicate. Due to the fact that the efficiency for BCL2 could not be determined it was dropped from further studies and I concentrated on the caspase GOI.

Quantitative real time polymerase chain reaction assays (qRT-PCR)

The structural changes observed by TEM and whole cell staining were validated by quantitative real-time polymerase chain reaction (qRT-PCR) assays.

Infections, RNA extraction at 6-, 7-, 8-, and 9-hpi, and cDNA synthesis were performed as previously described. 50ng of cDNA was used per reaction. Plates were run in triplicate as previously described.

GAPDH and β-actin were used as housekeeping genes to normalize for relative expression analyses. The cycle threshold (Ct) value or cycle number obtained from a single reaction for each standard reaction were all values that fell within a linear portion of the standard curve. The obtained Ct values from the qRT-PCR experiment were exported to Microsoft Excel 2016 for data analyses. Fold change in signals of expression of the genes of interest relative to GAPDH and β-Actin were determined by using the $\Delta\Delta$Ct method. The results were expressed as mean $\pm$ SD.

CellTiter 96 AQ$_{ueous}$ One Solution Cell Proliferation Cell Viability Assay

 Determining seeding density

In order to get accurate readings for the CellTiter 96 AQ$_{ueous}$ One Solution Cell Proliferation Cell Viability Assay (Promega, Madison, WI) readings at 490nm need to be less than 1 abs on the VERSA$_{max}$ tunable microplate reader and

SoftMax Pro software (Molecular Devices, Sunnyvale, CA). In order to determine what seeding density of cells would give accurate measurements and what incubation period to use cells were seeded at 10^5, 10^4, 10^3, 10^2, and media only in triplicate and incubated at 37°C, 5% CO_2 for approximately 24 hours. Cells were serum starved for 8 hours by replacing the media with DMEM +all without FBS media and incubated at 37°C, 5% CO_2. Treatments were prepared as previously described. Briefly, 25 μL/well of DMEM +all without FBS + 1:1000 WT was used for the NV treatments. 25 μL/well of RV treatment made up in DMEM + all without FBS + 1:1000 WT having an MOI of 2 was used for the RV treatment. DMEM + all without FBS + 1:1000 WT was placed in the blank wells. Treatments were left on for an hour as previously described. After an hour the treatment were removed and replaced with DMEM + all without FBS + 1:10 000 WT and incubated at 37°C, 5% CO_2 for 18 hours. At 18 hpi 20 μL of AQ_{ueous} One Solution Reagent was added to each well. The plate was incubated at 37°C, 5% CO_2 for 1 hour protected from light. At the one hour incubation period the plate was transferred to the $VERSA_{max}$ tunable microplate reader (Molecular Devices, Sunnyvale, CA) where it was mechanically shaken for 10 seconds before the 490 nm absorbance was recorded. The data was then blanked using the blank row. The cell viability was calculated as follows:

$$\text{Cell viability (\%)} = \text{Treatment}_{abs}/\text{NV}_{abs} \times 100$$

The results from the initial cell seeding experiment were used when designing the protocol for the full CellTiter 96 AQ_{ueous} One Solution Cell Proliferation Cell Viability Assay and APO 3/7 assay.

CellTiter 96 AQ_{ueous} One Solution Cell Proliferation Cell Viability Assay

Viability assays were performed with RV alone, RV with 20 µM A3 or sA3, 20 µM A3 or sA3 alone, and cells without treatment (NV) using the CellTiter 96 AQ_{ueous} One Solution Cell Proliferation Assay (Promega, Madison, WI). Briefly, cells were seeded at a density of 10^4 in 96 well plates (Evergreen Scientific, Los Angeles, CA). Approximately 24-hours after plating the cells were serum starved for 8 hours by replacing the media with DMEM + all without FBS media and incubated at 37°C, 5% CO_2. Treatments prepared as described in the RV Infection section were performed. Briefly, Wa RV stock was sonicated 10 min using a cup horn attachment and ice bath in a Misonix Sonicator 3000 (Misonix, Inc., Farmingdale, NY) and incubated in serum-free DMEM with 10 µg/mL trypsin (WT) for 45 min at 37°C. The activated viral inoculum was incubated with the cells for 1 hour at 37°C in 5% CO_2 at an MOI of 2. After which the treatments were removed and DMEM + all without FBS + 1:10 000 WT was placed on the cells (100 µl/well) and incubated for 12-18 hours at 37°C, 5% CO_2. At 12-, 14-, 16-, and 18hpi 20 µl of the CellTiter 96 AQ_{ueous} One Solution Reagent was added to each well containing 100 µl of culture medium using a multi-channel pipet. The

plates were incubated at 37°C, 5% CO_2 for 1 hour protected from light. After the incubation time the plates were read on the VERSA$_{max}$ tunable microplate reader and SoftMax Pro software (Molecular Devices, Sunnyvale, CA). The plates were shaken for 10 seconds and then the absorbance at 490 nm was recorded. Cell viability was calculated by blanking data against the blank well (media + AQ$_{ueous}$ One Solution Reagent). The blanked data was then used to calculate the cell viability using the following formula:

Treatment 490nm absorbance/NV 490nm absorbance x 100 = % cell viability

Each treatment was performed in triplicate and experiments were repeated three times. Data were statistically analyzed in Microsoft Office Excel 2016 software using one-way analysis of variance (ANOVA) and two-tailed Student's t tests (significance level, $P < 0.05$) with Bonferroni's *post hoc* test to correct for multiple comparisons ($P < 0.005$).

Apo-ONE Homogeneous Caspase-3/7 Assay

Apo-ONE Homogeneous Caspase-3/7 assays were carried out at 12-, 14-, 16-, and 18-hpi using the Apo-ONE Homogeneous Caspase-3/7 Assay (Promega, Madison, WI). Briefly, HT29.f8 cells were plated in 96-well tissue culture microplates (#333-8000-01F) (Evergreen Scientific, Los Angeles, CA) per

time point at 10^4 cells/well and incubated at 37°C, 5% CO_2 for 24 hours. The cells were then serum starved overnight by replacing media with DMEM + all without FBS. The cells were infected as previously described and accounting for blanks and negative controls. After treatment 100 μl of DMEM + all without FBS + 1:10 000 WT was placed in each well. At the 12-, 14-, 16-, and 18-hpi time points the media was removed and replaced with 25 μl/well of fresh DMEM + all without FBS media. 25 μl of Apo-ONE Caspase-3/7 Reagent was added to each well and the plates shaken for 15 minutes using the Bio-Rad iMark Microplate Reader (Bio-Rad, Hercules, CA) and then kept in the dark at room temperature for a further 45 minutes. The contents of the wells were then transferred to a microplate 96 well black plate (Greiner bio-one, 655096) (Greiner bio-one Inc., Denver, CO). The contents of the wells were gently spun down at 2500 rpm using the Beckman Coulter Avanti J-15R centrifuge (Beckman Coulter, Brea, CA).

Fluorescence was measured at 499nm using the Typhoon FLA 9000 (GE Healthcare Bio-Sciences AB, Uppsala, Sweden) and determined empirically.

Caspase-3/7 activity was calculated as follows:

Assay RFU-Blank RFU

Blanked Assay RFU- Blanked Negative Control RFU/Negative control

The percent cell viability for each treatment obtained from the AQ_{eous} One assay was used to further correct the data.

Data were statistically analyzed in Microsoft Office Excel 2016 software using one-way analysis of variance (ANOVA) and two-tailed Student's t tests (significance level, $P < 0.05$) with Bonferroni's *post hoc* test to correct for multiple comparisons ($P < 0.005$).

RESULTS

Mycoplasma Detection

The PCR Mycoplasma Test Kit I/C from PromoKine was used to detect over seven species of Mycoplasma. The positive control shows a distinct band at 265-278bp which represents a highly conserved 16S rRNA operon region in the Mycoplasma genome. The negative internal control and both samples only showed a band at 479bp indicating that the amplification process was successful and that both cell lines are mycoplasma free (Fig. 1).
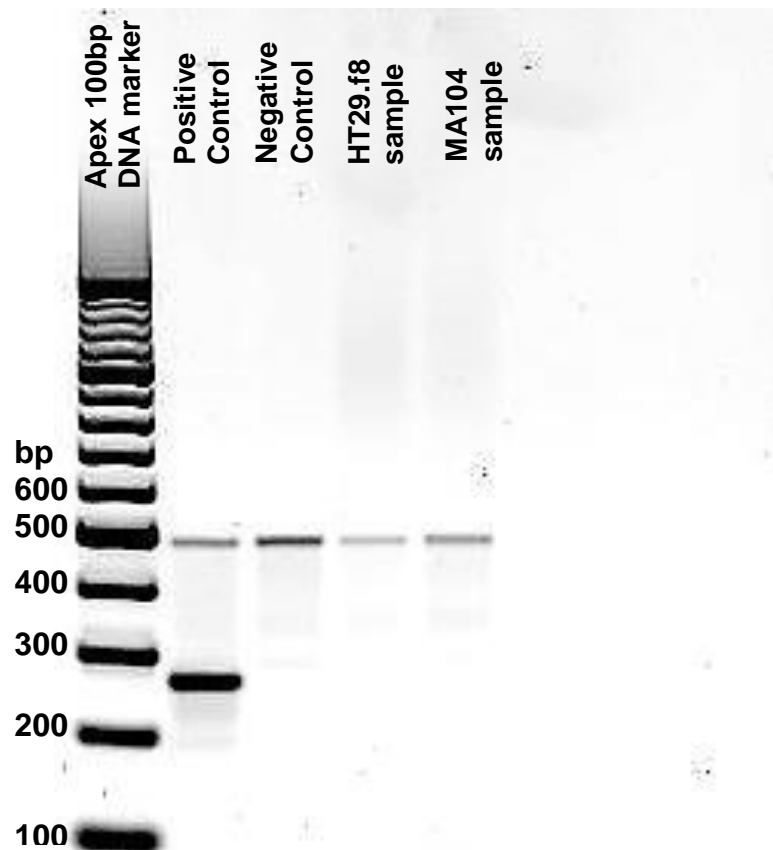
Figure 1. PCR Mycoplasma testing in HT29.f8 and MA104 cell lines. PCR products from the PCR Mycoplasma Test Kit I/C and the Apex 100 bp-Mid DNA marker (Genesee Scientific, San Diego, CA) were run on a 1.5% agarose gel, and visualized on the Typhoon FLA 9000 (GE Healthcare Life Sciences, Pittsburgh, PA). The positive control shows a distinct band at 265-278 bp. The internal control band was present in all samples at 479bp indicating that the PCR reaction was successful in all samples and that both cell lines are mycoplasma free.

Toxicity of A3 and sA3 on HT29.f8 cells

Percent live/dead cells were calculated using the trypan blue exclusion dye assay as previously described (Ball *et al.*, 2015). At 18hpi, the cells treated with NV, A3, and sA3 had cell viabilities of 93.5% ±1.73, 95.25% ±2.50, and 93.75% ±2.06, respectively. Cells infected with RV alone had a viability of 90.75% ±2.06 and cells with RV and 0.02% DMSO had a viability of 91.25% ±1.89. RV-infected cells treated with the A3 and sA3 showed an increased viability of 94.75% ±2.22 and 92.50% ±1.25, respectively (Fig. 2). Therefore, the arachidins had no cytotoxic effect on the cells when applied at 20 μM concentrations.

HT29.f8 18hpi Trypan Blue Cell Viabilitie Assay Results

	RV	RV+DMSO	RV+3	RV+sA3	A3	sA3	NV	NV+DMSO
▪ Cell Viability (%)	90.75	91.25	94.75	92.50	95.25	93.75	93.50	94.00
Standard Deviations	2.06	1.89	2.22	1.29	2.50	2.06	1.73	1.41

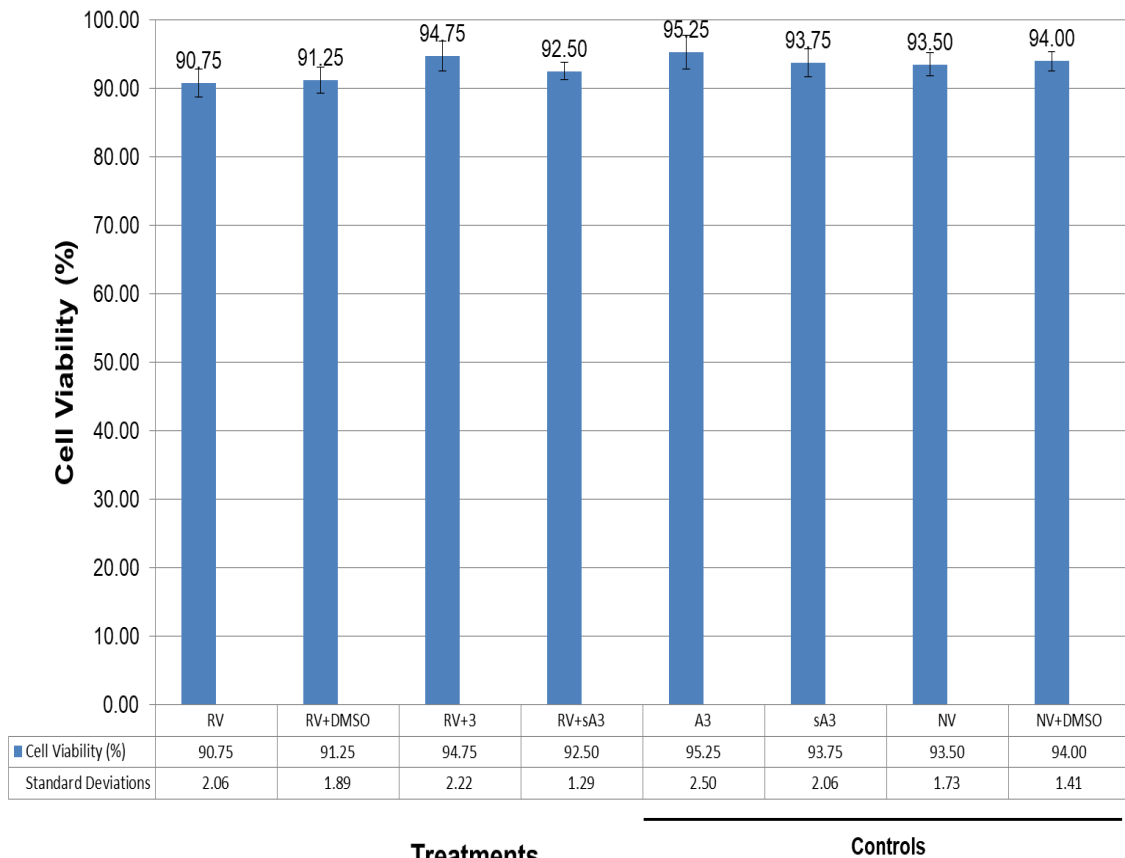Treatments   Controls

Figure 2. HT29.f8 cell viability assay at 18hpi using a trypan blue exclusion dye assay. Cells were counted in quadruplicate for each treatment at 18hpi and percent live/dead cells were calculated. Data were statistically analyzed in Microsoft Office Excel 2016 software using a one-way analysis of variance (ANOVA) and a two-tailed Student's t tests (significance level, P <0.05) with Bonferroni's *post hoc* test to correct for multiple comparisons (P < 0.004545).

Production of infectious RV with the addition of A3 and sA3

Supernatants collected at 18hpi from the RV-infected and RV-infected with 20 μM concentrations of A3 or sA3 were used for plaque forming assays to quantify the amount of infectious viral progeny produced (Arnold *et al.*, 2009). The PFU assays demonstrated statistically significant differences between RV and RV+A3 ($P = 0.0075$) and RV and RV+sA3 ($P = 0.0075$); representing 48-fold change decrease in PFU with A3 treatment and a 51-fold change decrease in PFU with sA3 treatment (Fig.3).

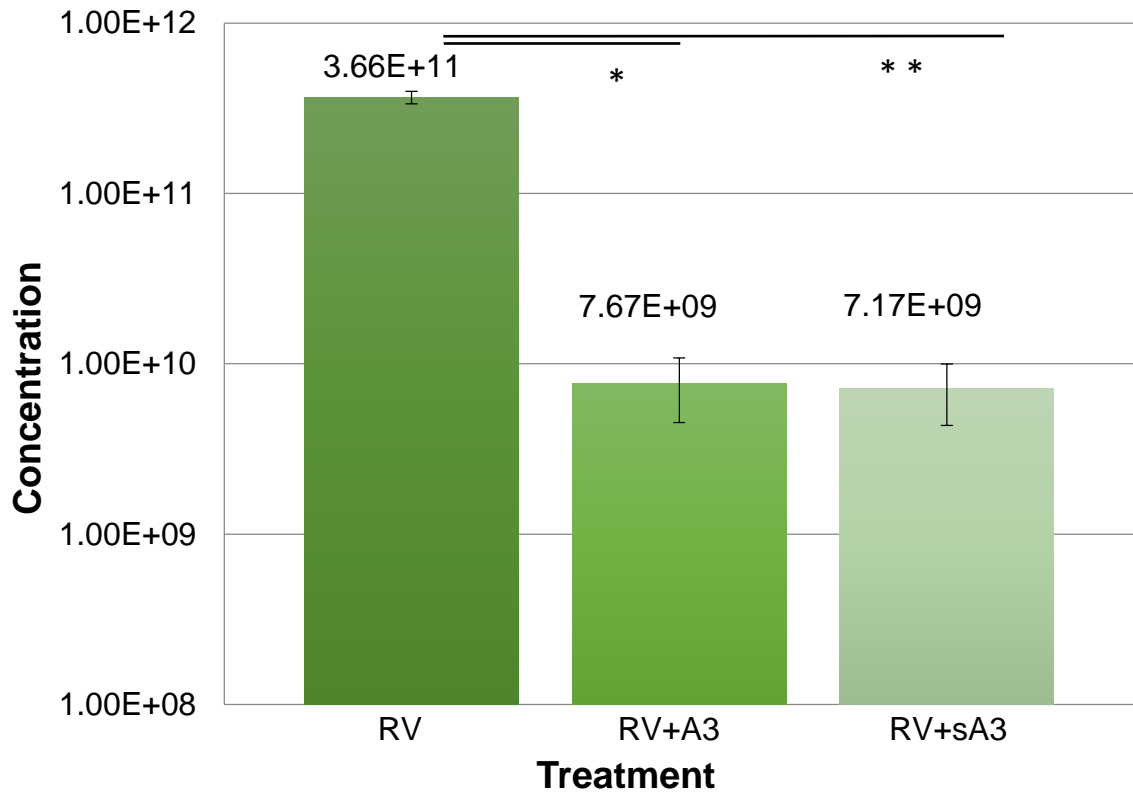**PFU/mL for HT29.f8 cells with/without arachidin treatments**

Figure 3. Quantification of infectious Wa RV particles using plaque forming assays (PFU/mL) at 18 hpi. HT29.f8 cells were infected with RV, RV+20 µM A3, or RV +20 µM sA3. At 18 hpi, the supernatants were collected, clarified by centrifugation, and used in plaque forming assays. The RV titer was 3.66E11, RV with A3 titer was 7.67E09, and RV with A3 titer was 7.17E09. Experiments were conducted in triplicate during four different experiments. *Comparison of RV only and RV+A3, *P*= 0.0075 **Comparison of RV only and RV+sA3, *P*= 0.0075.

Quantification of nanoparticles and size distribution by TRPS analysis

The concentrations and diameters of nanoparticles (~50-150 nm) were measured using the Izon qNano system at 16 and 18hpi. Figure 4 are the resultant images created from one representative run in the IZON proprietary software v3.2.2.268 (Izon). RV-only samples showed the concentration of 1.71E13 and 2.13E13 particles/mL at 16 and 18hpi, respectively (Fig. 4A), and the average particle populations' diameter was 79 nm and 74 nm at 16 and 18hpi (Fig. 4A). RV-infected cells treated with A3 demonstrated a nanoparticle concentration of 1.71E13 and 2.01E13 particles/mL at 16 and 18hpi, respectively (Fig. 4B). However, the RV-infected cell treated with A3 demonstrated nanoparticle diameter averaged 97 nm at 16 hpi that shifted to a population of larger particles (116 nm) particles at 18hpi (Fig. 4B). Likewise, RV-infected cells treated with sA3 demonstrated a nanoparticle concentration of 2.01E13 and 2.10E13 particles/mL at 16 and 18hpi, respectively (Fig. 4C). With sA3 treatment 16hpi nanoparticle sizes were averaging 95 nm; however, at 18hpi a shift to a population of larger particles (117 nm) was revealed (Fig. 4C).

Data from triplicate runs at 16 and 18hpi were statistically analyzed in Microsoft Office Excel 2016 software using a one-way analysis of variance (ANOVA) and a two-tailed Student's t tests (significance level, $P < 0.05$) with

Bonferroni's *post hoc* test to correct for multiple comparisons ($P < 0.017$) is shown in table 9. At both the 16 and 18hpi time points there was a statistical difference in the mean nanoparticle diameter of the RV and RV with the addition of either of the arachadins (A3 or sA3). (16hpi: RV/RV+A3 ($P= 0.000133986$), RV/RV+sA3 ($P= 0.000218321$), 18hpi: RV/RV+A3 ($P= 0.000242047$), RV/RV+sA3 ($P= 0.000181715$).
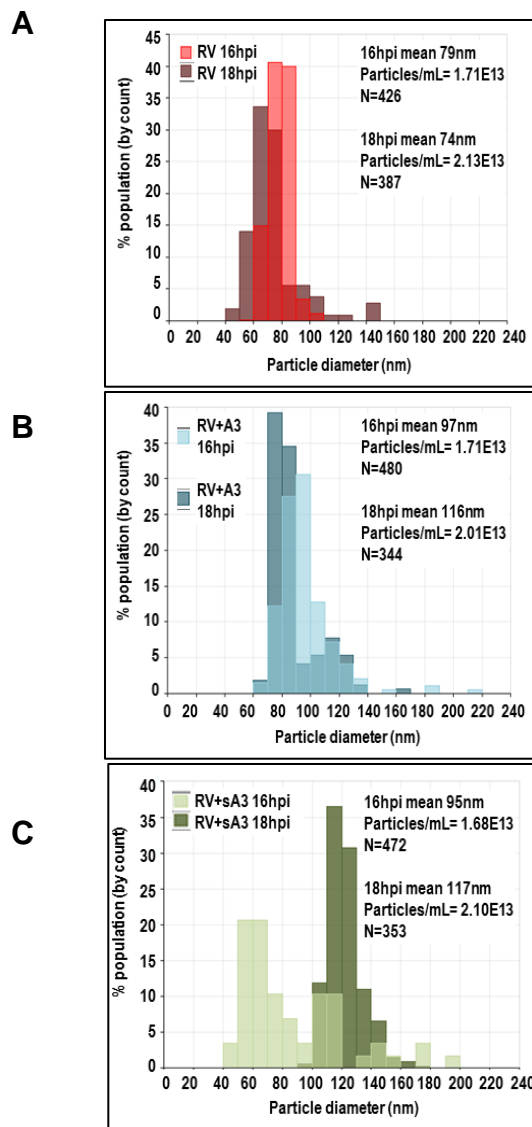
Figure 4. Overlaid tunable resistant pulse sensing technology (TRPS) analyses of nanoparticles/mL released from RV-infected and RV-infected-arachidin treated HT29.f8 cells at 16 and 18hpi. 4A (RED **RV 16hpi** **RV 18hpi**) RV only 16 and 18hpi particles/mL= 1.71E13 and 2.13E13 respectively, mean diameter (nm)= 79 and 74 respectively, and N= 426 and 387 respectively. 4B (BLUE **RV+A3 16hpi** **RV+A3 18hpi**) RV+A3 16 and 18hpi particles/mL= 1.71E13 and 2.01E13 respectively, mean diameter (nm)= 97 and 116 respectively, and N= 480 and 344 respectively. 4C (GREEN **RV+sA3 16hpi** **RV+sA3 18hpi**) RV+sA3 16 and 18hpi particles/mL= 1.68E13 and 2.10E13 respectively, mean diameter (nm)= 95 and 117 respectively, and N= 472 and 353 respectively.

Table 9. Statistical analysis of triplicate TRPS runs

		16hpi	18hpi
Particle concentration (particles/mL)	RV	2.07E+13 ±3.93E+12	2.56E+13 ± 5.56E+12
	RV+A3	1.49E+13 ±3.81E+12	1.91E+13 ± 1.79E+12
	RV+sA3	1.58E+13 ±1.79E+12	2.07E+13 ±5.20E+11
Mean diameter (nm)	RV	77.67 ±1.53[a,b]	73.33 ±5.03 [c, d]
	RV+A3	95.67 ±1.53[a]	113.67 ±2.52[c]
	RV+sA3	96.67 ±2.08[b]	115.33 ±2.08[d]
N (Average number of particles counted in triplicate runs per sample)	RV	296.67 ±112.12	293.00 ±91.60
	RV+A3	346.33 ±116.07	324.00 ±23.58
	RV+sA3	405.67 ±91.72	331.33 ±33.29

[a-d] Data from triplicate runs at 16 and 18hpi were statistically analyzed in Microsoft Office Excel 2016 software using a one-way analysis of variance (ANOVA) and a two-tailed Student's t tests (significance level, P <0.05) with Bonferroni's *post hoc* test to correct for multiple comparisons (P <0.017) is shown in table 9. At both the 16 and 18hpi time points there was a statistical difference in the mean nanoparticle diameter of the RV and RV with the addition of either of the arachadins. (16hpi: [a]RV/RV+A3 (P= 0.000133986), [b]RV/RV+sA3 (P= 0.000218321), 18hpi: [c]RV/RV+A3 (P= 0.000242047), [d]RV/RV+sA3 (P= 0.000181715).

TEM and whole cell fluorescent analyses of nucleus to cytoplasm ratios of HT29.f8 cells

TEM and fluorescent analysis was performed on HT29.f8 cells infected with RV, RV with A3, and RV with sA3. These were compared to the three controls, NV, A3, and sA3. TEM analysis was performed at 16 and 18hpi and fluorescent analysis was performed at 18hpi (Fig 5, 6, and 7).

TEM analysis revealed that at 16 hpi, the mean ratio of RV-infected cells was 0.87 ±0.51, showing an increase in comparison to the control cells (NV, A1and A3 alone) as shown in figure 5. At the same time point, RV-infected cells treated with A3 had a smaller average nucleus/cytoplasm ratio of 0.41 ±0.19 at 16hpi (Fig. 5). RV+sA3 cells had an average nucleus/cytoplasm ratio of 0.51 ±0.22 at 16hpi (Fig.5).
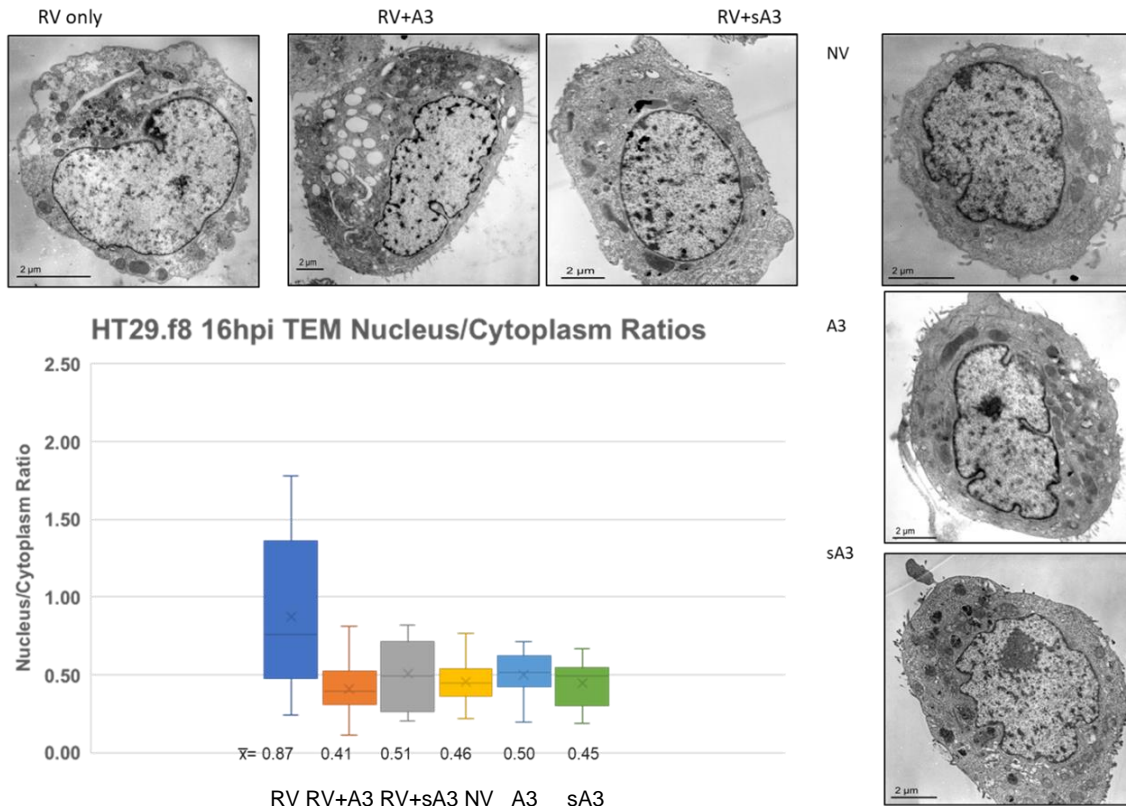
Figure 5. 16hpi HT29.f8 TEM nucleus/cytoplasm ratios. Data expressed at mean ±SD, N= 10. RV only, RV+A3, and RV+sA3 representative cells along top. Representative cells of the controls NV, A3, and sA3 to the side. Scale bars = 2μm. Data were statistically analyzed in Microsoft Office Excel 2016 software using a one-way analysis of variance (ANOVA) (significance level, P <0.05). No statistical difference between groups was detected. The data was graphed using a whisker and box plots. The box represents all the data points within the lower (Q1) and upper (Q3) quartiles with vertical lines with an x that represents the median. The whiskers go from each quartile to the minimum and maximum data points. Data points falling outside the overall pattern of distribution were plotted as dots that represent outliers.

At 18 hpi, the ultrastructural appearance and mean nuclear to cytoplasm ratios of the control cells with A3 (0.50 ±0.15) and sA3 (0.47 ±0.09) were similar to the cells with no treatment (0.46 ±0.15) (Fig. 6). An increase in the number of mitochondria, autophagosomes, RV particles and viroplasms was demonstrated in RV-infected cells, and RV-infected cells. At 18 hpi, the RV-infected cells demonstrated an increased nucleus to cytoplasm ratio of 1.18 ±0.34 while RV-infected cells treated with either arachidin had similar mean ratios, 0.42 ±0.17 and 0.65 ±0.25, respectively, and both A3 or sA3 treatments showed relatively normal ultrastructure (Fig. 6). RV was statistically different from NV ($P=$ 9.23E-06); RV+A3 ($P=$ 6.56E-06); RV+sA3 ($P=$ 0.00098); A3 ($P=$ 1.94E-05); and sA3 ($P=$ 6.01E-06).
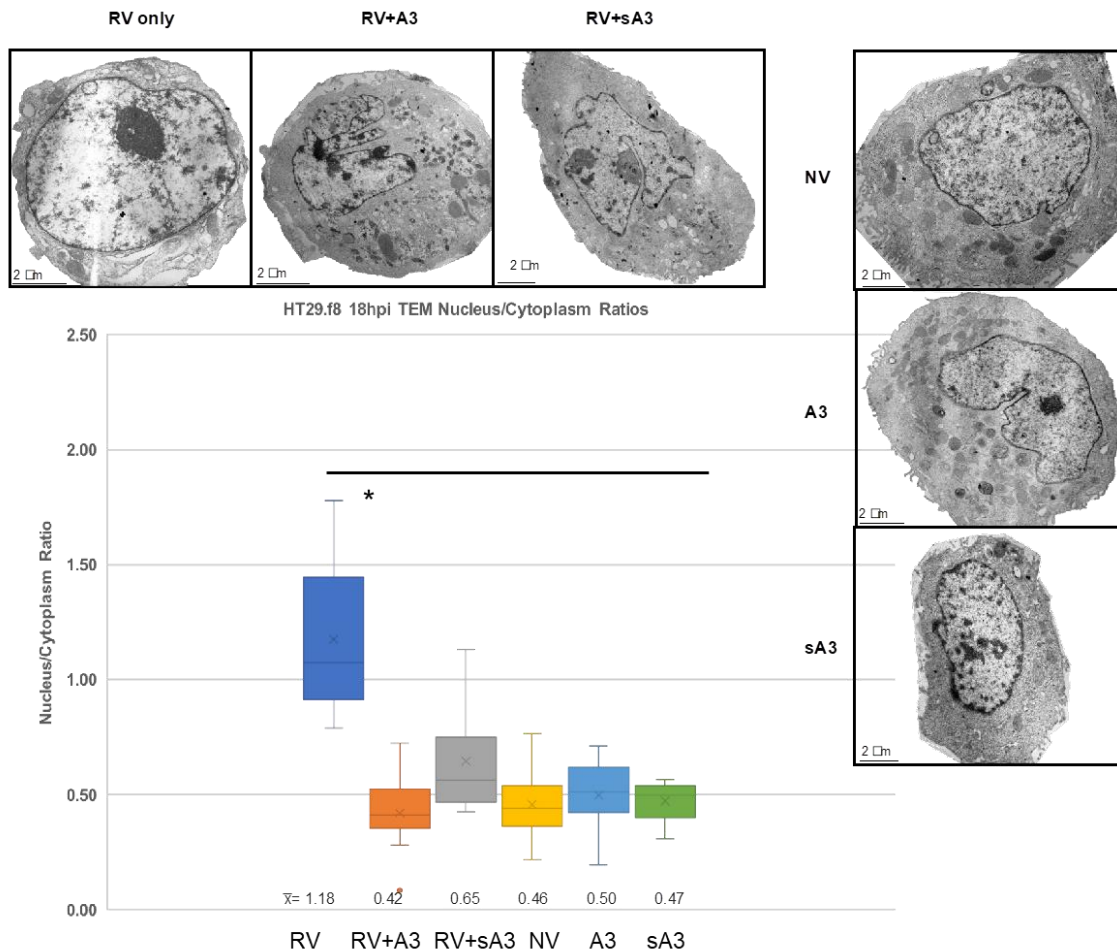
Figure 6. 18hpi HT29.f8 TEM nucleus/cytoplasm ratios. Data expressed as mean ±SD, N= 10. RV only, RV+A3, and RV+sA3 representative cells along top. Representative cells of the controls NV, A3, and sA3 to the side. Scale bars = 2µm. Data were statistically analyzed in Microsoft Office Excel 2016 software using a one-way analysis of variance (ANOVA) and a two-tailed Student's t tests (significance level, P <0.05) with Bonferroni's *post hoc* test to correct for multiple comparisons (P <0.0033). The data was graphed using whisker and box plots. The box represents all the data points within the lower (Q1) and upper (Q3) quartiles with vertical lines with an x that represents the median. The whiskers go from each quartile to the minimum and maximum data points. Data points falling outside the overall pattern of distribution were plotted as dots that represent outliers. RV was statistically different from NV (P= 9.23E-06); RV+A3 (P= 6.56E-06); RV+sA3 (P= 0.00098); A3 (P= 1.94E-05); and sA3 (P= 6.01E-06).

At 18 hpi whole cell staining was used to verify the TEM results (Fig. 7). The nucleus/cytoplasm ratios obtained from the live staining supports the TEM data. Although exact ratios where slightly different the general trends remained the same. Nucleus/cytoplasm ratios at 18hpi were as follows: RV= 1.04 ±0.63, RV+A3= 0.61 ±0.24, RV+sA3= 0.53 ±0.2, NV= 0.67 ±0.26, A3 only= 0.58 ±0.19, and sA3 only= 0.51 ±0.13. RV was statistically different from NV (P= 0.00041); RV+A3 (P=2.1E-05); RV+sA3 (P= 3.6E-07); A3 only (P= 2.7E-06); and sA3 (P= 1.3E-07). NV was statistically different from sA3 (P= 0.00028).
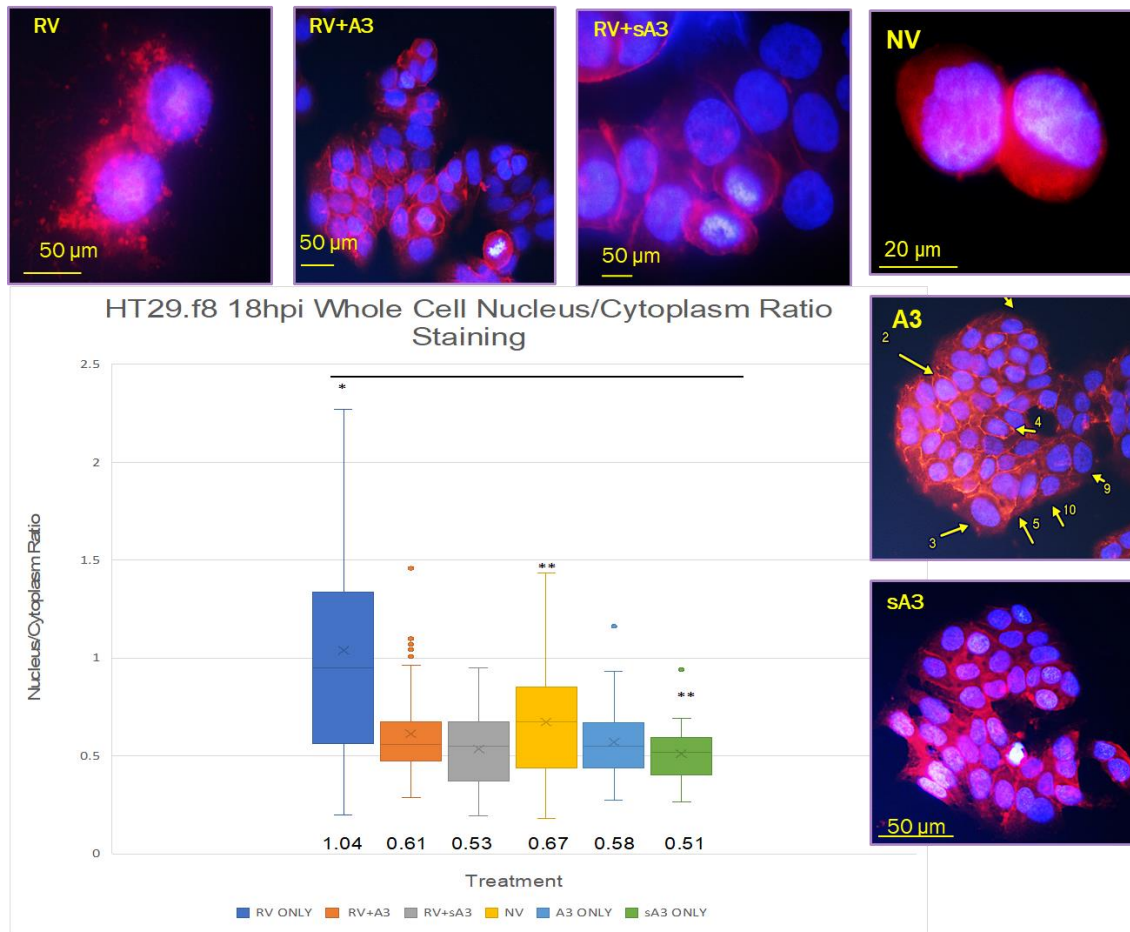
Figure 7. 18hpi whole cell staining nucleus/cytoplasm (N/C) ratios. Data expressed as mean ±SD.N/C ratios of 50 cells per treatment were averaged and statistically analyzed using Microsoft Office Excel 2016 software using a one-way analysis of variance (ANOVA) and a two-tailed Student's t tests (significance level, P <0.05) with Bonferroni's *post hoc* test to correct for multiple comparisons (P <0.0033). The data was graphed using whisker and box plots. The box represents all the data points within the lower (Q1) and upper (Q3) quartiles with vertical lines with an x that represents the median. The whiskers go from each quartile to the minimum and maximum data points. Data points falling outside the overall pattern of distribution were plotted as dots that represent outliers. Averages were as follows: RV= 1.04 ±0.63 RV+A3= 0.61 ±0.24, RV+sA3= 0.53 ±0.2, NV= 0.67 ±0.26, A3 only= 0.58 ±0.19, and sA3 only= 0.51 ±0.13. RV was statistically different from NV (P= 0.00041); RV+A3 (P=2.1E-05); RV+sA3 (P= 3.6E-07); A3 only (P= 2.7E-06); and sA3 (P= 1.3E-07). NV was statistically different from sA3 (P= 0.00028).

Quantification of transcripts for cell death pathway genes in HT29.f8

cells

QuantiFluor dsDNA assay

The QuantiFluor dsDNA assay was conducted to assure pipetting and plating accuracy. Table 10 and figure 8 show the representative data for the dsDNA Standard Curve and QuantiFluor dsDNA Dye while Table 11 shows the unknown dilutions and average fluorescence.

Table 10. Representative Data for the dsDNA Standard Curve and QuantiFluor dsDNA dye

Standard (ng/well)	Average Fluorescence (RFU)
20	12207257.44
5	3364591.47
1.25	813147.44
0.31	252417.07
0.078	120794.85
0.02	79405.14
0.005	33035.88

The data from the QuantiFluor was graphed and the standard curve was created using Microsoft Office Excel 2016 software (Figure 8). The generated equation of y= 608459x+92471 (x=(y-92471)/608459) was used to determine the original concentrations of the diluted unknown sample that were performed in triplicate.

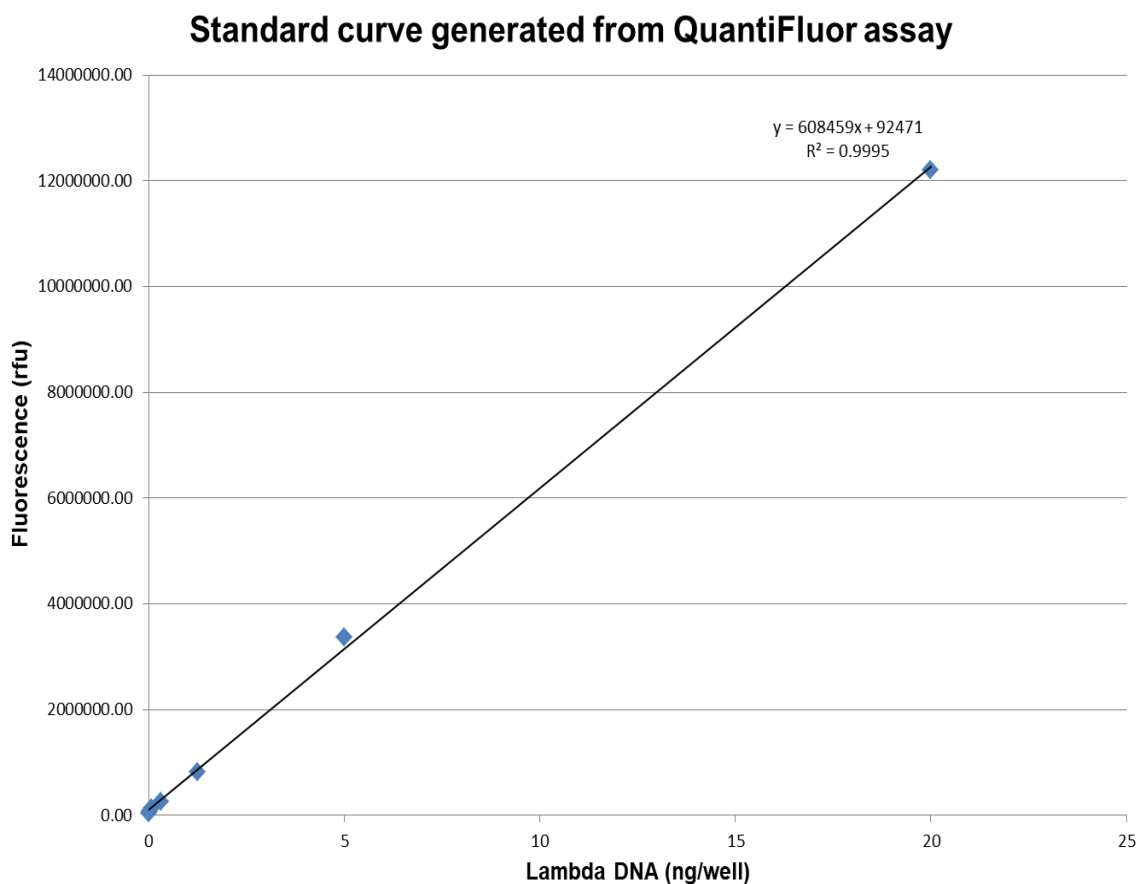**Standard curve generated from QuantiFluor assay**

Figure 8. Standard curve plotted using the fluorescence (rfu) and lambda DNA (ng/well) values. The equation generated was used to calculate the unknown DNA concentrations in triplicate.

The R^2 value was 0.9995. Table 11 shows the calculated concentrations.

The unknown concentration was determined to be between 7.14 ng/µl-8.3ng/µl.

Table 11. Sample Dilution Series and QuantiFluor dsDNA dye of lambda DNA

lambda DNA dilution	Average Fluorescence (RFU)	Calculated DNA concentration (ng/µl)
1/10	4434040	7.14
1/100	548533.2	7.5
1/1000	143109.2	8.3
Average calculated DNA concentration (ng/µl)		**7.6**

Efficiency Assays

Efficiency assays were performed twice in duplicate on the GOI primers. The housekeeping and caspase primers showed efficiencies ranging from 92.55-110.52%. BCL2 efficiency could not be calculated and therefore it was decided to drop BCL2 and the other Autophagy GOI from this study and concentrate on the caspase GOI.

Primer	Calculated % efficiency
GAPDH	92.55
β-actin	110.52
CASP 3	105.44
CASP 6	105.31
CASP 7.2	103.0
CASP 8	103.75
CASP 9	105.65
BCL 2	

Table 12. PCR efficiencies calculated from two duplicate run efficiency assays. Efficiencies were calculated from two experiments conducted in duplicate.
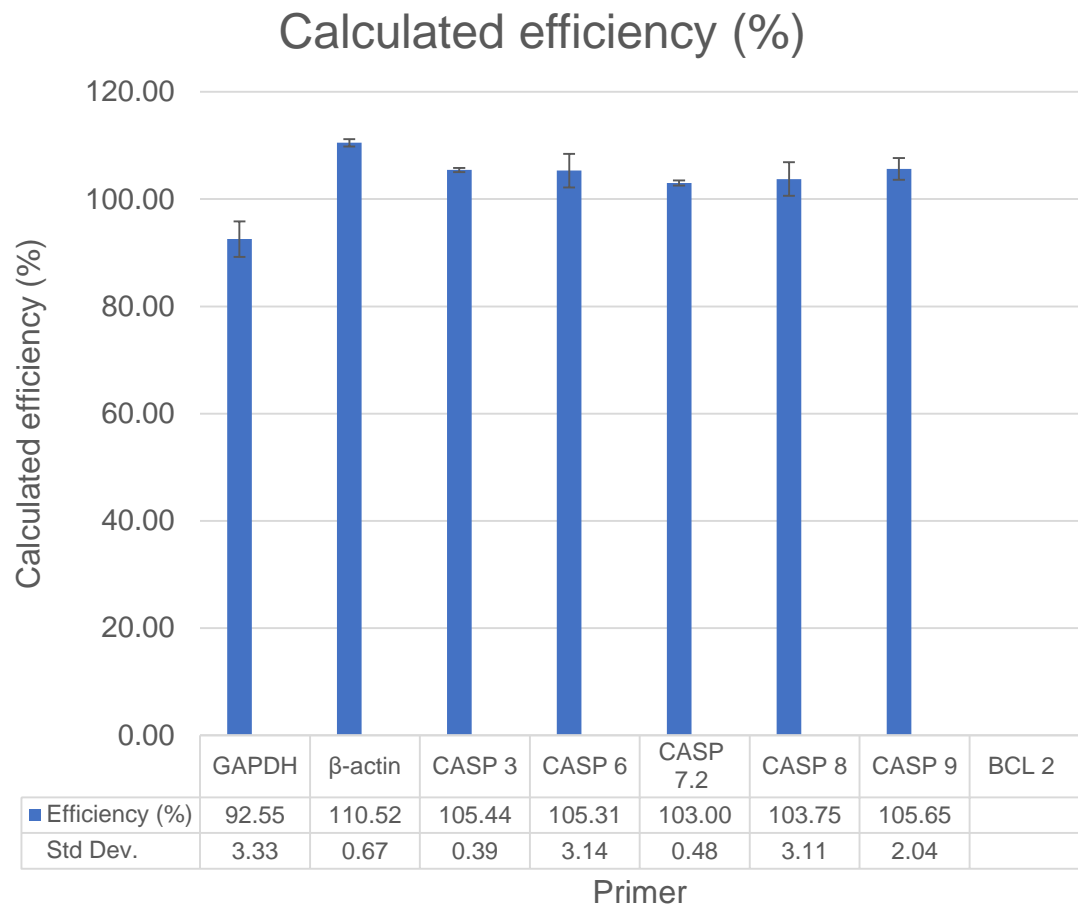
Calculated efficiency (%)

	GAPDH	β-actin	CASP 3	CASP 6	CASP 7.2	CASP 8	CASP 9	BCL 2
■ Efficiency (%)	92.55	110.52	105.44	105.31	103.00	103.75	105.65	
Std Dev.	3.33	0.67	0.39	3.14	0.48	3.11	2.04	

Figure 9. Calculated efficiencies for GOI primers from two efficiency assays run in duplicate. Data expressed at mean ± SD.

qRT-PCR

To determine if the arachidins regulated the transcripts of genes that encoded for proteins that initiated either the apoptosis or autophagy pathways, qRT-PCR experiments were performed on arachidin treated RV-infected HT29.f8 cells at 6, 7, 8, and 9hpi (Figure 10-18).

At 6hpi (figure 10) there appears to be a slight upregulation of caspase 3, 6, 7, and 8 with sA3 alone (1.19 ±0.11, 1.33 ±0.09, 1.28 ±0.07, and 1.37 ±0.05 respectively). The other treatments appear to cause slight down or no regulation of caspase 3, 6, 7, and 8. All the treatments had little or no effect on the regulation of caspase 9.

At 7hpi (figure 11) caspase 3 is not regulated by RV, RV+A3, or RV+sA3 while it is slightly upregulated by A3 and sA3 (1.55 ±0.11, and 1.20 ±0.06 respectively). Caspase 6 is slightly upregulated by all the treatments (RV 1.15 ±0.03, RV+A3 1.29 ±0.05, RV+sA3 1.02 ±0.11, 1.31 ±0.06, and 1.32 ±0.07). Caspase 7 is slightly upregulated by all the treatments (RV 1.18 ±0.09, RV+A3 1.33 ±0.08, RV+sA3 1.07 ±0.08, A3 1.20 ±0.06, and sA3 1.21 ±0.07). RV, RV+A3, and RV+sA3 cause slight down regulation of caspase 8 (0.85 ±0.05, 0.79 ±0.03, and 0.9 ±0.07 respectively) while A3 and sA3 alone cause slight upregulation of caspase 8 (1.17 ±0.1, and 1.21 ±0.05). RV, RV+A3, and RV+sA3 cause the slight downregulation of caspase 9 (0.76 ±0.02, 0.71 ±0.07, and 0.83

±0.1) while A3and sA3 cause the slight to no regulation of caspase 9 (1.15 ±0.1, and 0.99 ±0.07).

At 8hpi (figure 12) caspase 3 is down regulated by all the treatments (RV 0.63 ±0.04, RV+A3 0.69 ±0.05, RV+sA3 0.52 ±0.03, A3 0.9 ±0.08, and sA3 0.39 ±0.03). RV, RV+sA3, and sA3 downregulate caspase 6 (0.79 ±0.03, 0.82 ±0.13, and 0.84 ±0.08 respectively) while RV+A3 and A3 upregulate caspase 6 (1.28 ±0.05 and 1.44 ±0.08 respectively). Caspase 7 is downregulated by both RV and sA3 (0.88 ±0.04, and 0.86 ±0.08 respectively) while RV+A3, RV+sA3, and A3 all slightly upregulate caspase 7 (1.27 ±0.09, 1.13 ±0.06, and 1.17 ±0.12 respectively). Caspase 8 is slightly downregulated by RV, RV+sA3, and sA3 (0.92 ±0.08, 0.85 ±0.09, and 0.98 ±0.1) and slightly upregulated by RV+A3 and A3 (1.14 ±0.05 and 1.05 ±0.09). RV, RV+A3, RV+sA3 and A3 slightly downregulate caspase 9 (0.8 ±0.04, 0.93 ±0.04, 0.8 ±0.06 and 0.97 ±0.06) while sA3 slightly upregulates caspase 9 (1.01 ±0.09).

At 9 hpi (figure 13) all treatments downregulated caspase 3 (RV 0.67 ±0.06, RV+A3 0.72 ±0.05, RV+sA3 0.54 ±0.03, A3 0.94 ±0.08, and sA3 0.4 ±0.03). RV, RV+sA3, and sA3 downregulated caspase 6 (0.8 ±0.03, 0.84 ±0.13, and 0.85 ±0.09 respectively) while RV+A3 and A3 slightly upregulated caspase 6 (1.32 ±0.04 and 1.16 ±0.09 respectively). RV and sA3 downregulated caspase 7 (0.9 ±0.04 and 0.89 ±0.09 respectively) while RV+A3, RV+sA3, and A3 slightly

upregulated caspase 7 (1.29 ±0.1, 1.17 ±0.06, and 1.21 ±0.12 respectively). RV, A3, and sA3 slightly downregulated caspase 8 (0.89 ±0.12, 0.83 ±0.09, and 0.96 ±0.1 respectively) while RV+A3 and RV+sA3 slightly upregulated caspase 8 (1.13 ±0.04 and 1.03 ±0.08). All treatments slightly downregulated or did not regulate caspase 9 (RV 0.77 ±0.04, RV+A3 0.9 ±0.03, RV+sA3 0.8 ±0.06, A3 0.97 ±0.06, and sA3 1.01 ±0.09).

Figure 14 shows a time course of caspase 3 regulation with the various treatments. At appears that RV, RV+A3, and RV+sA3 have a similar time course pattern (slight down regulation at 6hpi, less downregulated at 7hpi, down regulated at 8 and 9hpi. A3 and sA3 show a similar time course pattern; both being upregulated at 6 and 7hpi and downregulated at 8 and 9 hpi. This time course study suggests that 7-8hpi is of particular importance in terms of changes in this system.

Figure 15 shows a time course of caspase 6 regulation with the various treatments. RV switches from upregulating caspase 6 at 6 and 7hpi to downregulating caspase 6 during 7 and 8hpi. Again showing 7-8hpi being an important time point in terms of changes. RV+A3 initially downregulates caspase 6 and 6hpi but then upregulates it during 7, 8, and 9hpi. RV+sA3 showed a different pattern; downregulating caspase 6 at 6hpi, showing very little regulation at 7hpi, and then downregulating caspase 6 at 7 and 8hpi. A3 and sA3 also

showed different time course patterns. At 6hpi A3 downregulated caspase 6 but at 7, 8, and 9hpi A3 upregulates caspase 6. sA3 upregulated caspase 6 at 6 and 7hpi but then downregulated caspase 6 at 7 and 8hpi.

Figure 16 shows a time course of caspase 7 regulation with the various treatments. RV slightly upregulated caspase 7 at 6 and 7hpi and then downregulated caspase 7 at 8 and 9hpi; again showing 7-8hpi being an important time point in terms of changes. Both RV+A3 and RV+sA3 slightly down regulated caspase 7 and 6 hpi but then slightly upregulated caspase 7 at 7, 8, and 9hpi. A3 and sA3 showed different time course patterns. A3 down regulated caspase 7 at 6 hpi but then upregulated caspase 7 at 7, 8, and 9hpi while sA3 slightly upregulated caspase 7 at 6 and 7hpi and then down regulated caspase 7 at 8 and 9hpi.

Figure 17 shows a time course of caspase 8 regulation with the various treatments. The time course patterns for the various treatments showed variable time course patterns for caspase 8. RV initially slightly upregulated caspase 8 at 6hpi and then slightly down regulated caspase 8 at 7, 8, and 9hpi. RV+A3 slightly upregulated caspase 8 at 6hpi, then down regulated caspase 8 at 7hpi, and then slightly upregulated caspase 8 at both 8 and 9hpi. RV+sA3 slightly downregulated caspase 8 at 6, 7, and 8hpi and then ever so slightly upregulated caspase 8 at 9hpi. A3 slightly upregulated caspase 8 at 6, 7, and 8hpi and then

slightly downregulated caspase 8 at 9hpi. sA3 slightly upregulated caspase 8 at 6 and 7hpi and then slightly down regulated caspase 8 at 8 and 9hpi.

Figure 18 shows a time course of caspase 9 regulation with the various treatments. RV, RV+A3, and RV+sA3 all slightly downregulated caspase 9 over all the time points investigated (6, 7, 8, and 9hpi). A3 initially slightly upregulated caspase 9 at 6 and 7hpi ad then slightly downregulated/ did not regulate caspase 9 at 8 and 9hpi. sA3 initially slightly upregulated caspase 9 at 6hpi and then did not regulate/ ever so slightly down regulated caspase 9 at 7, 8, and 9hpi.

Many of the up and down regulations noted where very slight. However, very small changes in the transcript expression may lead to large changes in the system.
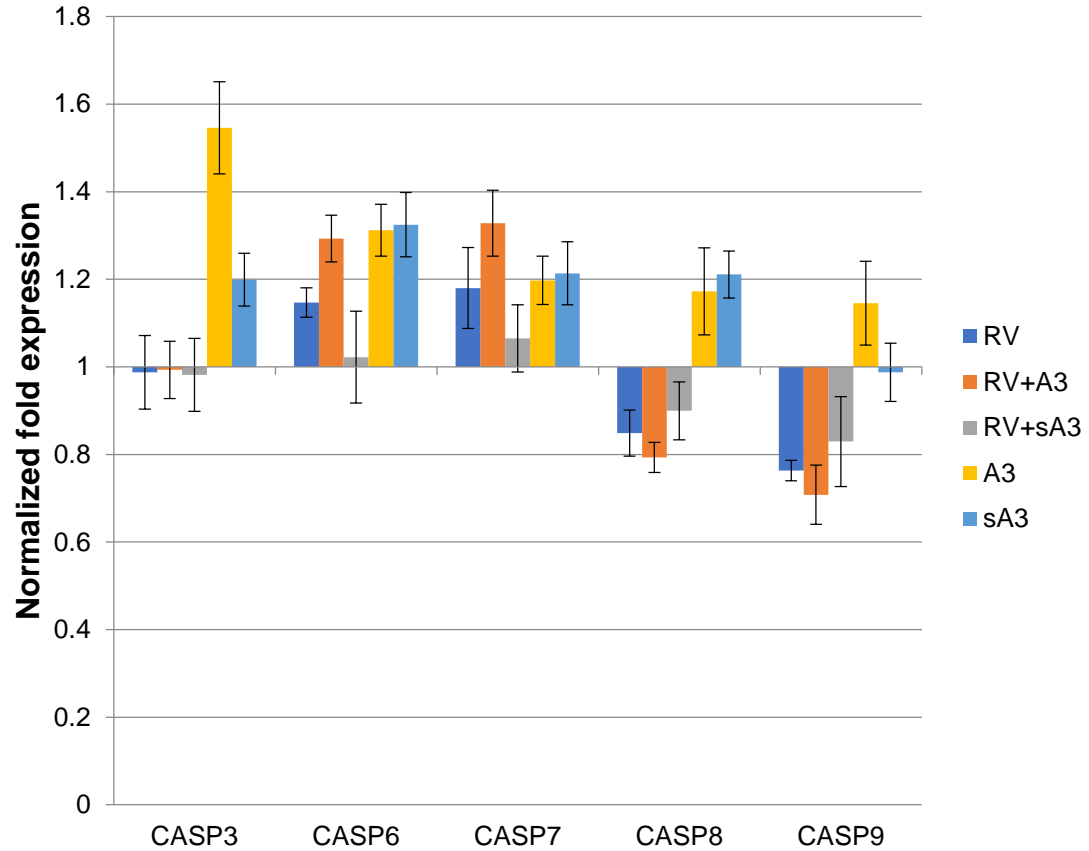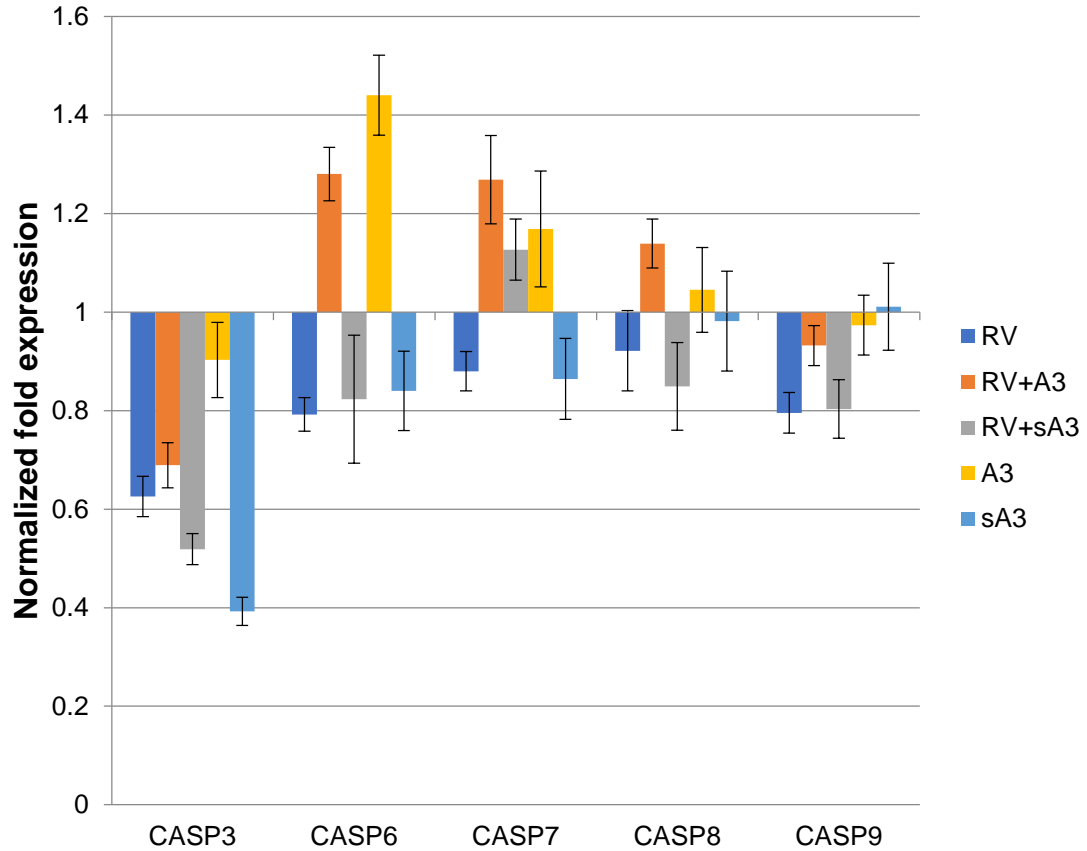
6hpi Caspase expression
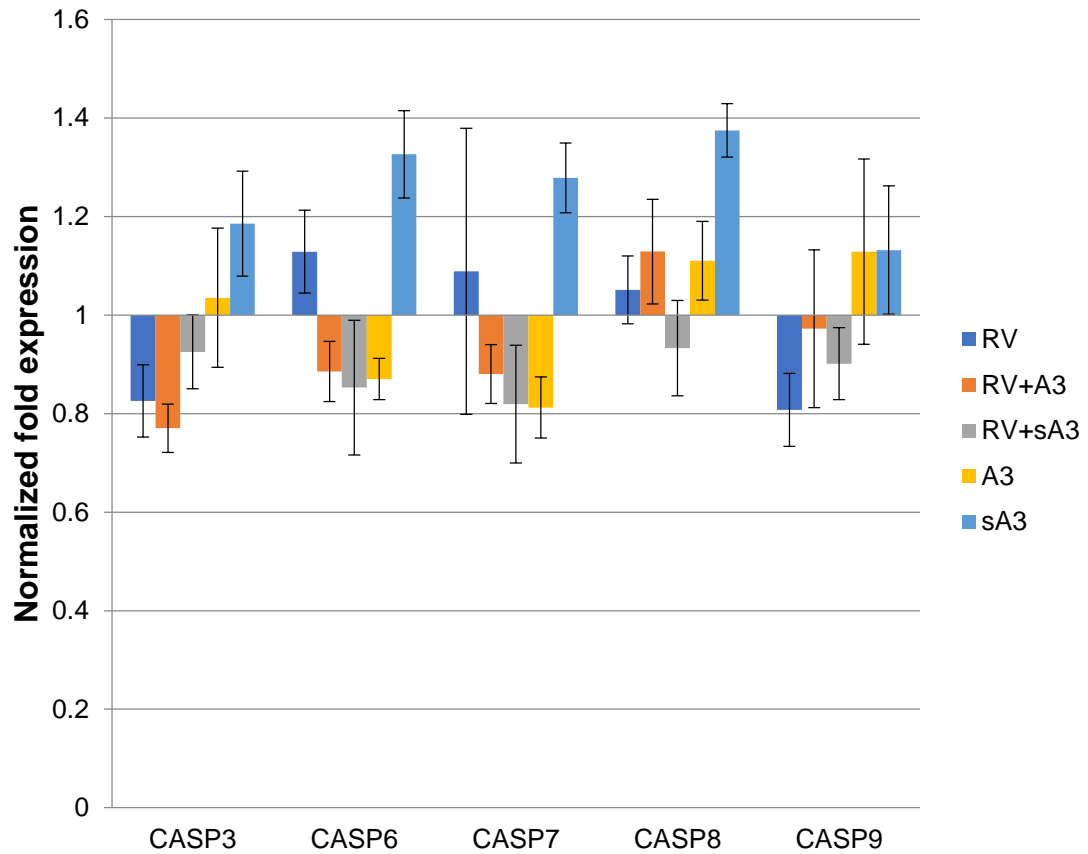
Figure 10. Changes in gene transcription in HT29.f8 cells 6hpi. Fold change in signals of expression of GOI relative to GAPDH and β-actin were determined using the ΔΔCT method. The results are expressed as mean ±SD. Experiments were performed in triplicate.
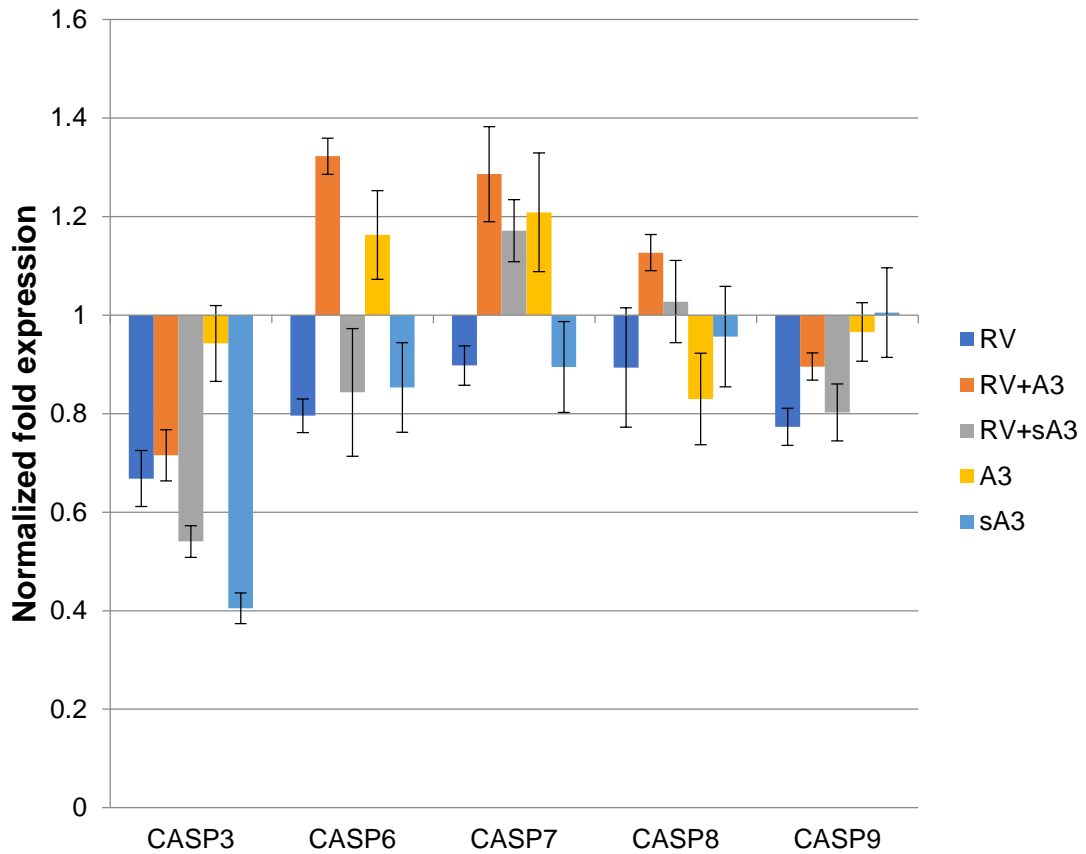
7hpi Caspase expression

Figure 11. Changes in gene transcription in HT29.f8 cells 7hpi. Fold change in signals of expression of GOI relative to GAPDH and β-actin were determined using the ΔΔCT method. The results are expressed as mean ±SD. Experiments were performed in triplicate.

8hpi Caspases

Figure 12. Changes in gene transcription in HT29.f8 cells 8hpi. Fold change in signals of expression of GOI relative to GAPDH and β-actin were determined using the ΔΔCT method. The results are expressed as mean ±SD. Experiments were performed in triplicate.

9hpi Caspases

Figure 13. Changes in gene transcription in HT29.f8 cells 9hpi. Fold change in signals of expression of GOI relative to GAPDH and β-actin were determined using the ΔΔCT method. The results are expressed as mean ±SD. Experiments were performed in triplicate.

Caspase 3 time course

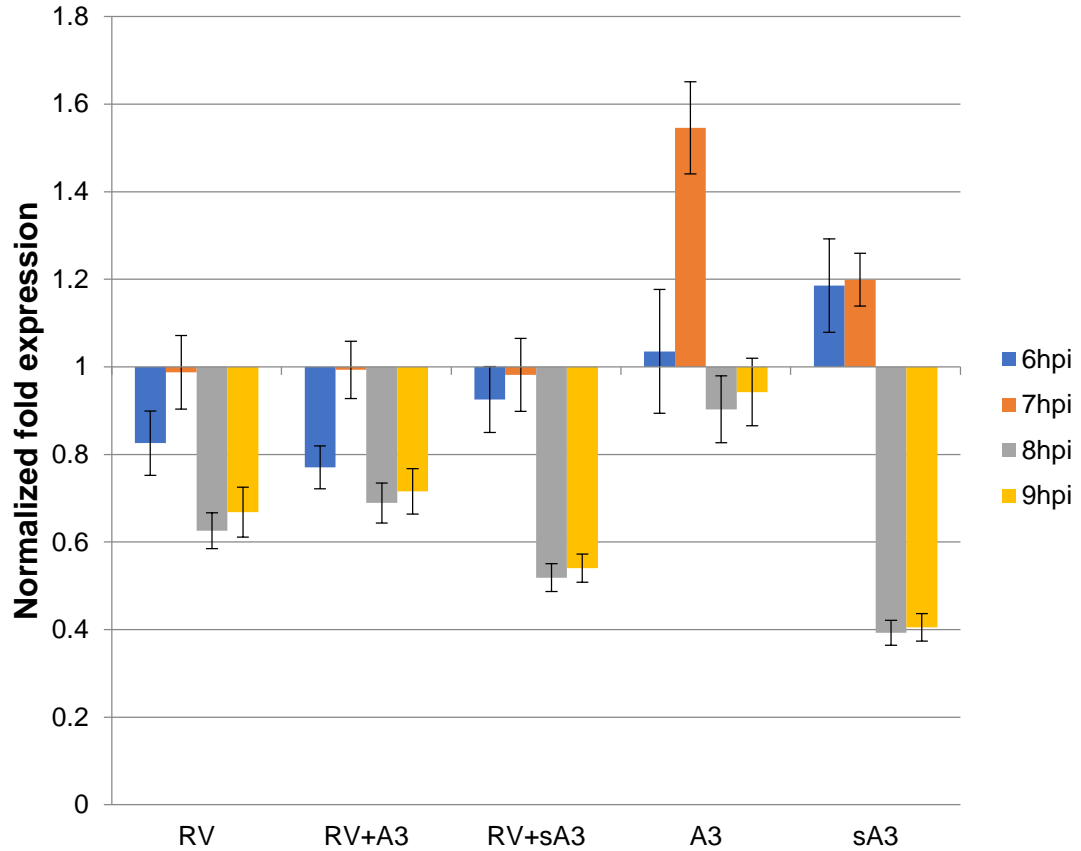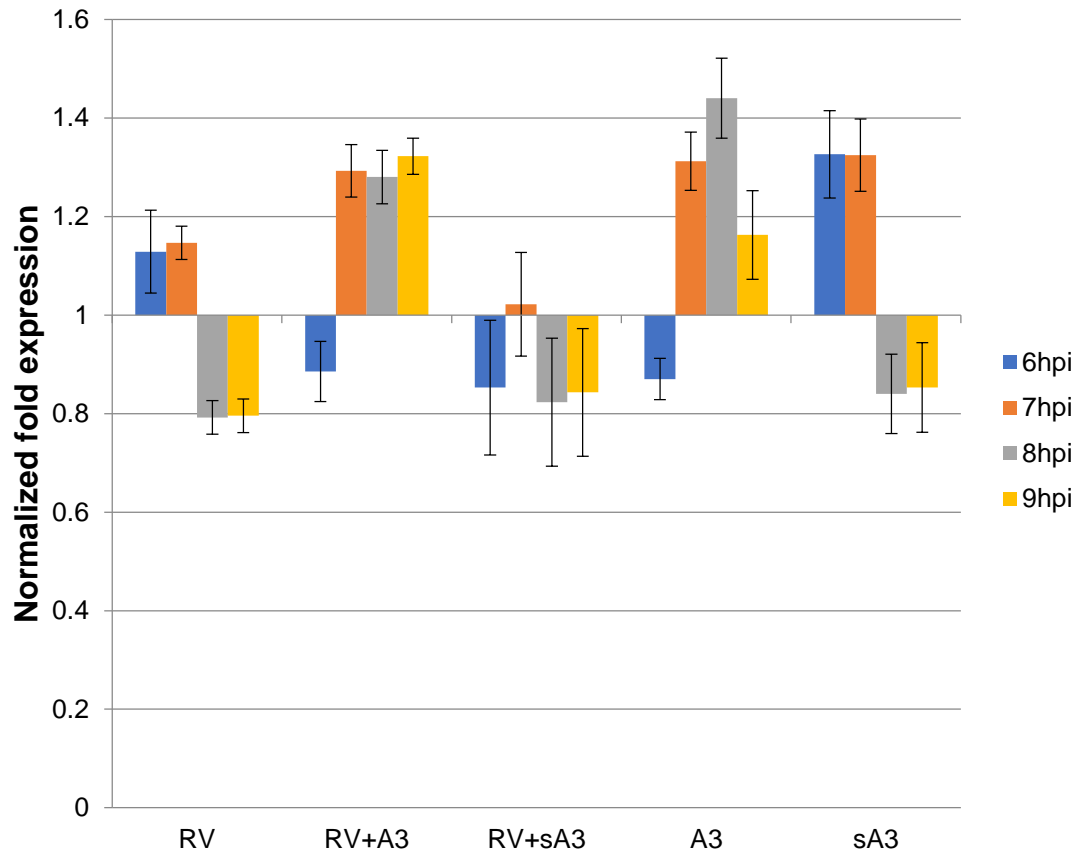Figure 14. Changes in caspase 3 gene expression in HT29.f8 cells 6-9hpi. Fold change in signals of expression of GOI relative to GAPDH and β-actin were determined using the ΔΔCT method. The results are expressed as mean ±SD. Experiments were performed in triplicate.

Caspase 6 time course

Figure 15. Changes in caspase 6 gene expression in HT29.f8 cells 6-9hpi. Fold change in signals of expression of GOI relative to GAPDH and β-actin were determined using the ΔΔCT method. The results are expressed as mean ±SD. Experiments were performed in triplicate
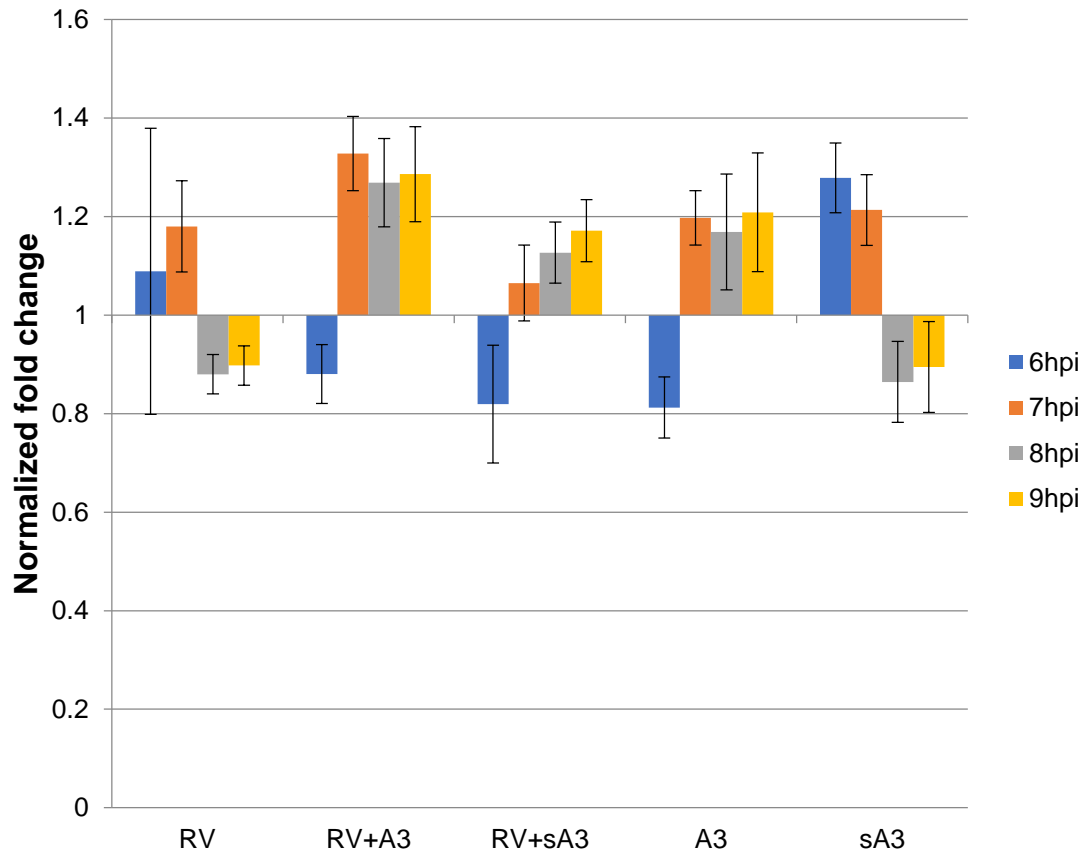
Caspase 7 time course

Figure 16. Changes in caspase 7 gene expression in HT29.f8 cells 6-9hpi. Fold change in signals of expression of GOI relative to GAPDH and β-actin were determined using the ΔΔCT method. The results are expressed as mean ±SD. Experiments were performed in triplicate
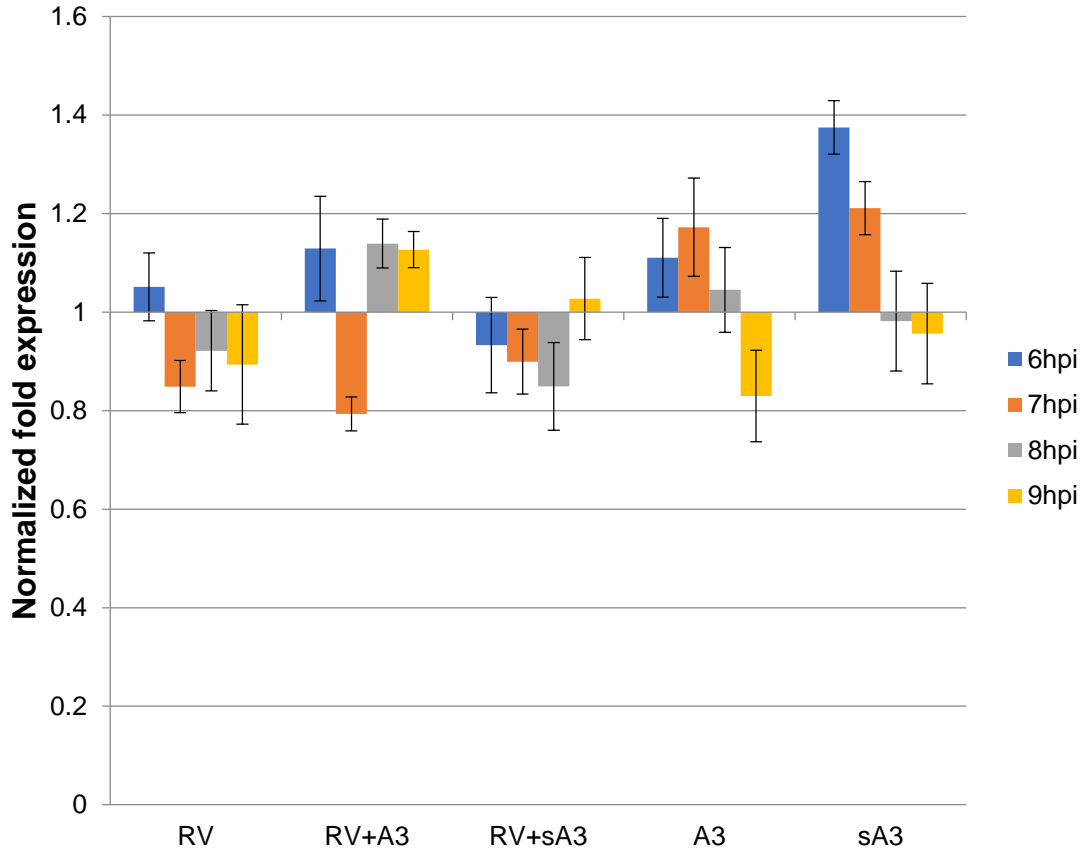
Caspase 8 time course

Figure 17. Changes in caspase 8 gene expression in HT29.f8 cells 6-9hpi. Fold change in signals of expression of GOI relative to GAPDH and β-actin were determined using the ΔΔCT method. The results are expressed as mean ±SD. Experiments were performed in triplicate
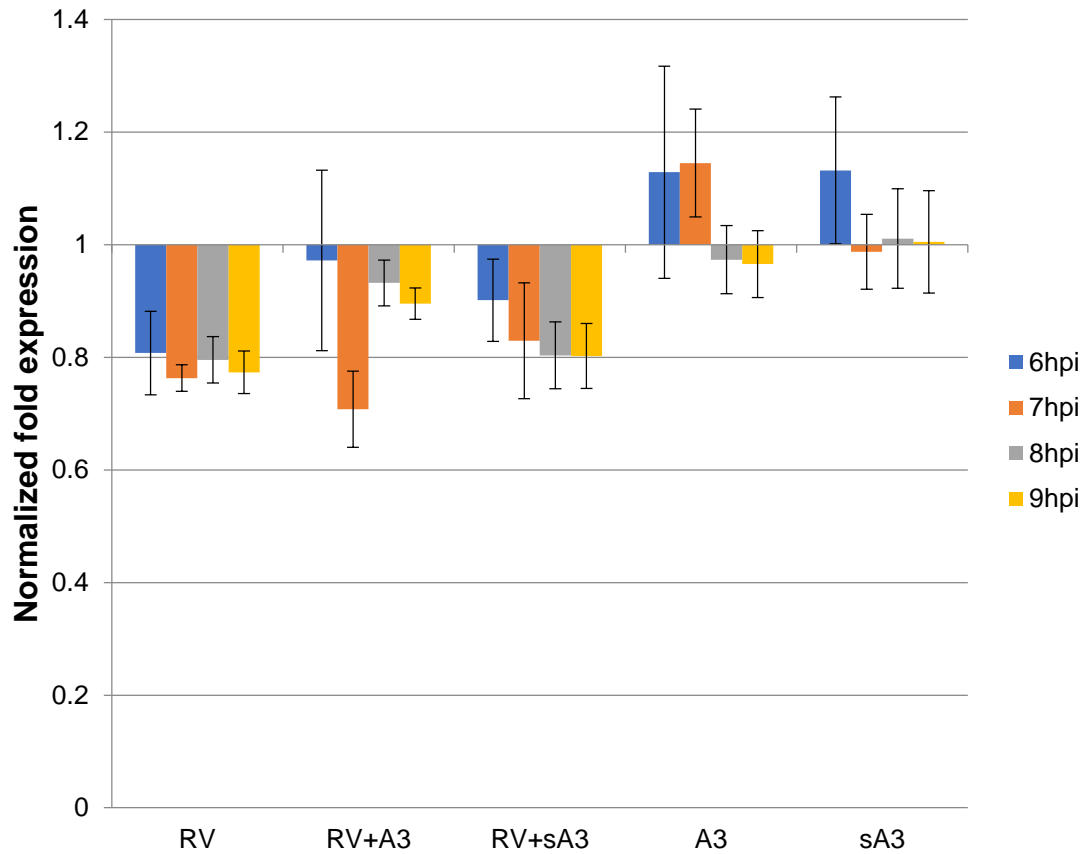
Caspase 9 time course

Figure 18. Changes in caspase 9 gene expression in HT29.f8 cells 6-9hpi. Fold change in signals of expression of GOI relative to GAPDH and β-actin were determined using the ΔΔCT method. The results are expressed as mean ±SD. Experiments were performed in triplicate

AQ$_{ueous}$ One Solution Cell Proliferation Assay

In order to get accurate readings in the CellTiter 96 AQ$_{ueous}$ One Solution Cell Proliferation Assay cell seeding density had to be determined in order to obtain 490nm absorbance values below one. During the cell seeding experiments (Fig. 19) 10^4 cells/well was determined to be the ideal seeding density for future experiments as 10^5 cells/well gave readings above 1abs at 490nm wavelength whilst seeding densities below 10^4 did not give consistent readings.
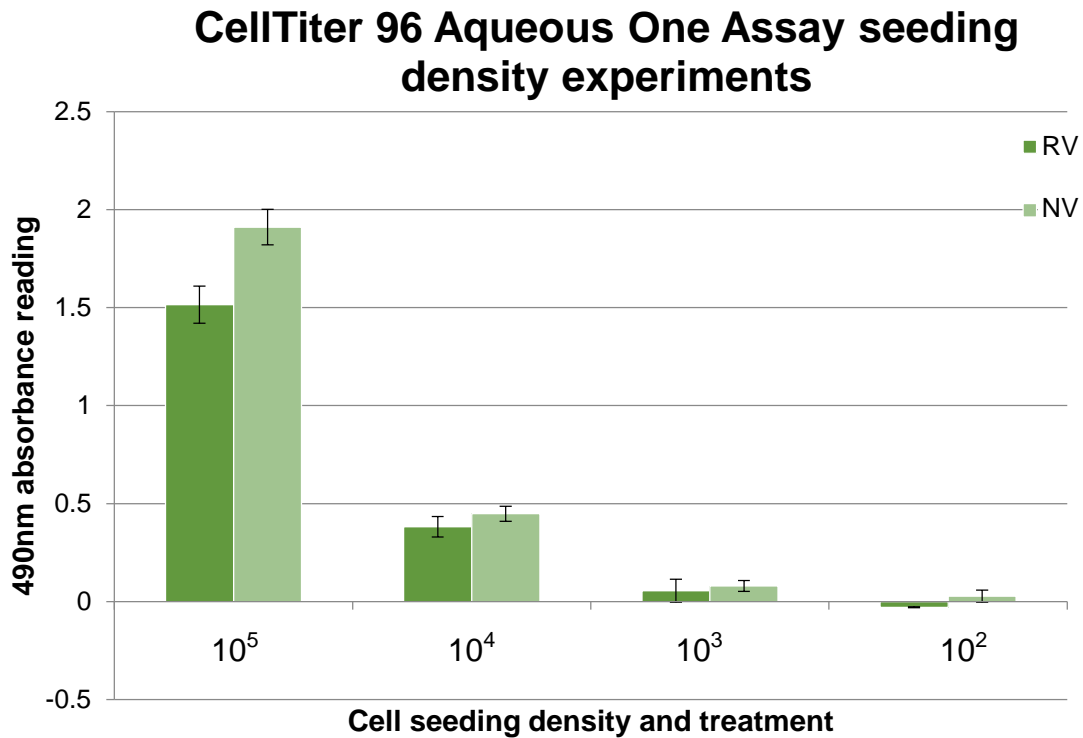

Figure 19. Absorbance at 490nm was noted for cells seeded in triplicate at 10^5, 10^4, 10^3, and 10^2 cells/well at 18hpi with NV and RV treatments. 10^4 cells/well was determined to be the ideal seeding density for future CellTiter 96 AQ$_{ueous}$ One Solution Cell Proliferation Assay experiments.

The CellTiter 96 AQ$_{ueous}$ One Solution Cell Proliferation Assay was performed in triplicate three times for 12-18hpi and resulted in cell viabilities ranging from 65.37-80.69% at 18hpi (Fig. 24). At 12hpi (Fig. 20) RV cell viability was 88.46 ±1.90%, RV+A3 was 90.14 ±3.54%, RV+sA3 was 91.37 ±5.48%, A3 was 93.98 ±3.04%, and sA3 was 89.79 ±4.47%. At 12hpi RV treatment cell viability is only slightly lower than the other treatments with no statistically significant differences being noted.
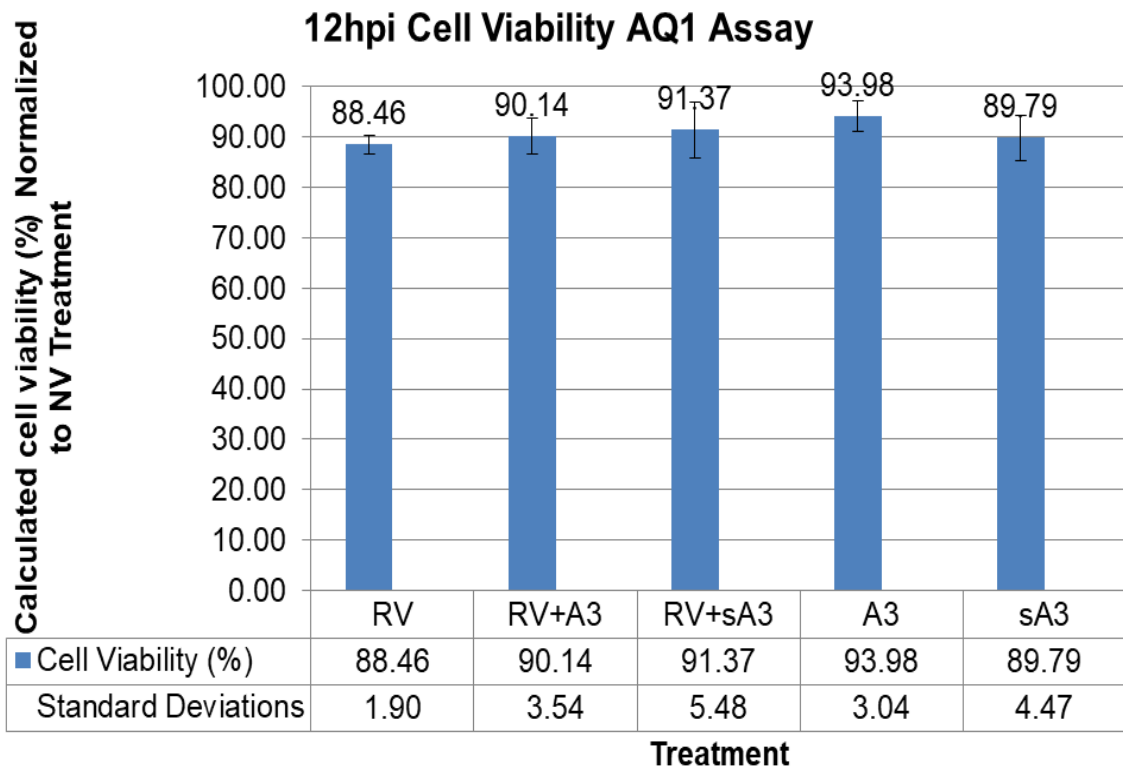
12hpi Cell Viability AQ1 Assay

	RV	RV+A3	RV+sA3	A3	sA3
Cell Viability (%)	88.46	90.14	91.37	93.98	89.79
Standard Deviations	1.90	3.54	5.48	3.04	4.47

Calculated cell viability (%) Normalized to NV Treatment / *Treatment*

Figure 20. CellTiter 96 AQ$_{ueous}$ One Solution Cell Proliferation Assay results at 12hpi for each treatment. Experiments were conducted three times in triplicate. Data were statistically analyzed in Microsoft Office Excel 2016 software using a one-way analysis of variance (ANOVA) and a two-tailed Student's t tests (significance level, $P <0.05$) with Bonferroni's *post hoc* test to correct for multiple comparisons ($P <0.005$).

At 14hpi cell viability (Fig. 21) for each treatment decreased from the 12hpi viabilities. RV treatment cell viability was 75.89 ±3.75%, RV+A3 was 83.93 ±5.52%, RV+sA3 was 85.08 ±0.62%, A3 was 87.85 ±3.49%, and sA3 was 87.99 ±4.56%. The RV treatment cell viability was statistically different from each treatment with P values of 0.002, 1.79E-06, 2.8E-06, and 1.3E-05 respectively.

14hpi Cell Viability AQ1 Assay

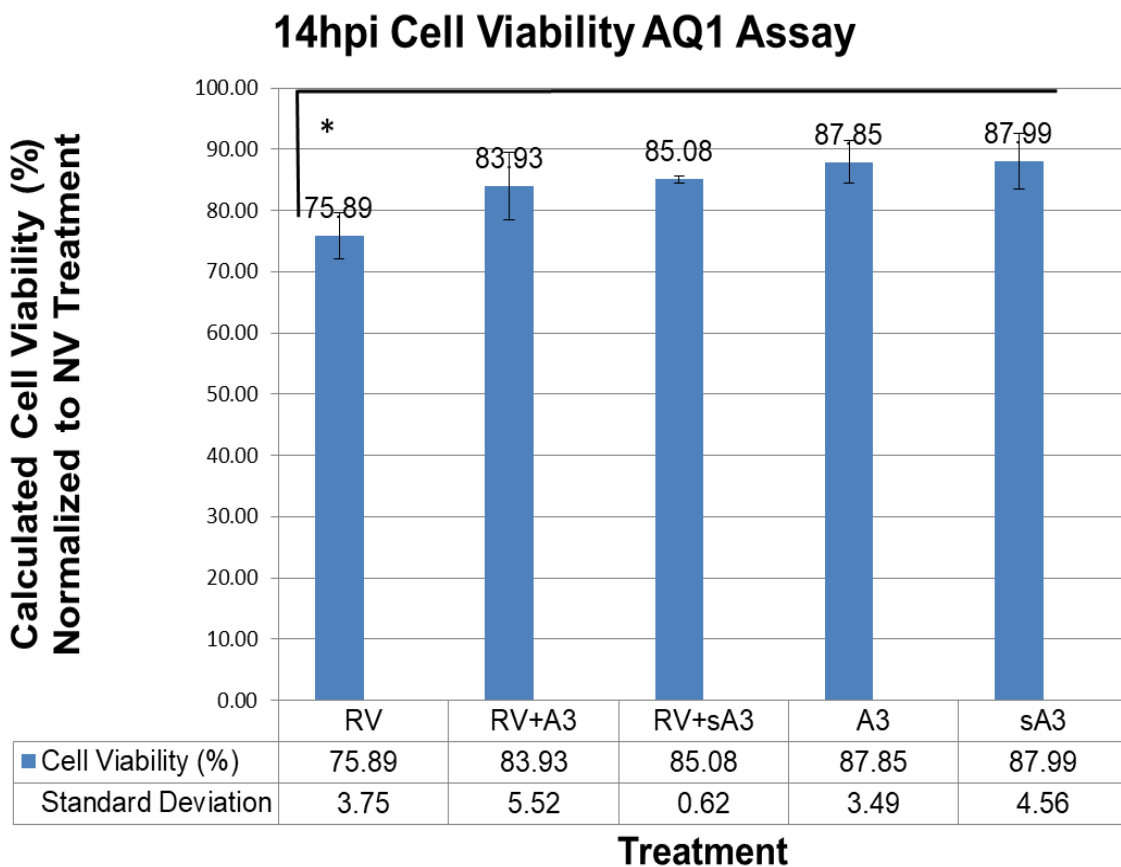|	RV	RV+A3	RV+sA3	A3	sA3
Cell Viability (%)	75.89	83.93	85.08	87.85	87.99
Standard Deviation	3.75	5.52	0.62	3.49	4.56

Figure 21. CellTiter 96 AQ$_{ueous}$ One Solution Cell Proliferation Assay results at 14hpi for each treatment. Experiments were conducted three times in triplicate. Data were statistically analyzed in Microsoft Office Excel 2016 software using a one-way analysis of variance (ANOVA) and a two-tailed Student's t tests (significance level, P <0.05) with Bonferroni's *post hoc* test to correct for multiple comparisons (P <0.005). RV was statistically different from RV+A3 (P= 0.002); RV+sA3 (P= 1.79E-06), A3 (P= 2.8E-06); and sA3 (P= 1.3E-05).

At 16hpi the cell viabilities were further decreased (Fig. 22). RV treatment cell viability was 69.96 ±0.39%, RV+A3 was 77.55 ±6.79%, RV+sA3 was 78.20 ±4.34%, A3 was 86.02 ±6.30%, and sA3 was 86.61 ±6.93%. RV treatment cell viability was statistically different from each of the other treatments with P values of 0.004, 3.24E-05, 9.77E-07, and 2.07E-06 respectively.

16hpi Cell Viability AQ1 assay

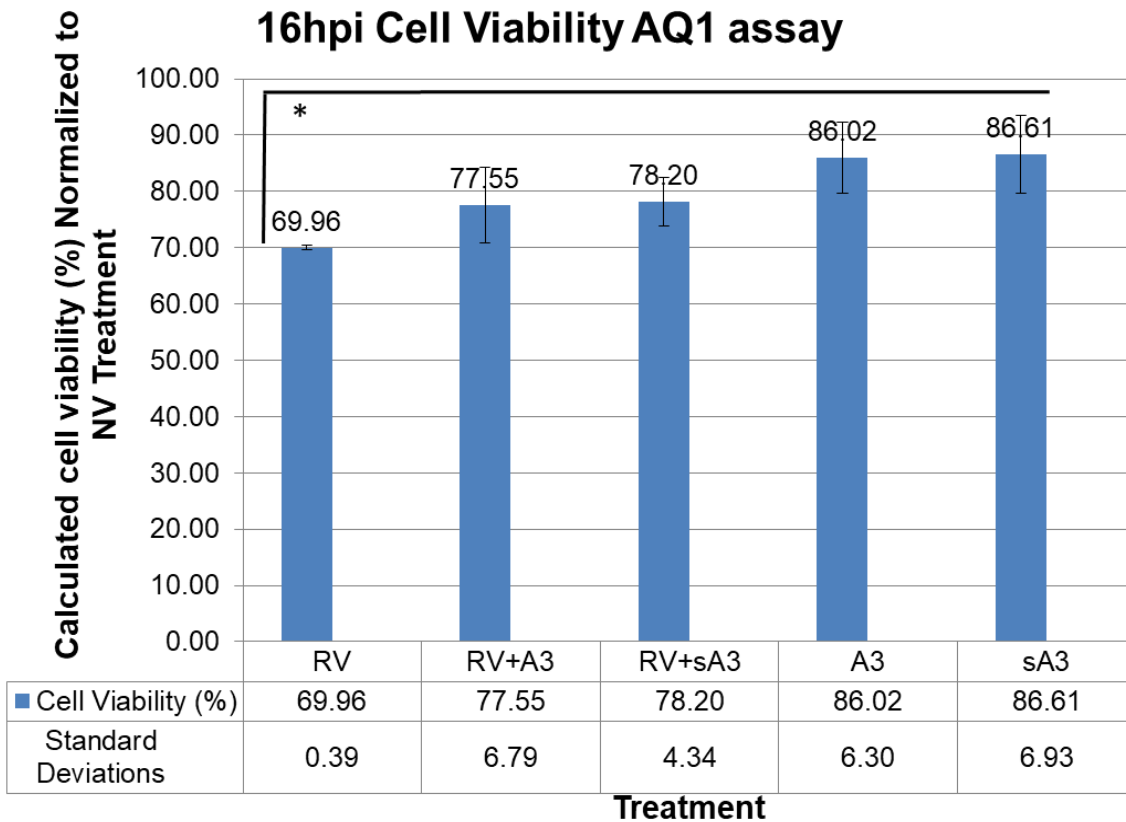|	RV	RV+A3	RV+sA3	A3	sA3
Cell Viability (%)	69.96	77.55	78.20	86.02	86.61
Standard Deviations	0.39	6.79	4.34	6.30	6.93

Treatment

Figure 22. CellTiter 96 AQ$_{ueous}$ One Solution Cell Proliferation Assay results at 16hpi for each treatment. Experiments were conducted three times in triplicate. Data were statistically analyzed in Microsoft Office Excel 2016 software using a one-way analysis of variance (ANOVA) and a two-tailed Student's t tests (significance level, P <0.05) with Bonferroni's *post hoc* test to correct for multiple comparisons (P <0.005). RV was statistically different from RV+ A3 (P= 0.0038); RV+sA3 (P= 3.24E-05); A3 (P= 9.77E-07); and sA3 (P= 2.07E-06).

At 18hpi the cell viabilities were further decreased (Fig. 23). RV treatment cell viability was 64.64 ±3.56%, RV+A3 was 76.18 ±4.53%, RV+sA3 was 76.20 ±2.21%, A3 was 83.60 ±6.50%, and sA3 was 81.99 ±2.93%. RV treatment cell viability was statistically different from each of the other treatments with P values of 1.75E-05, 3.3E-07, 9.2E-07, and 4.8E-09 respectively. RV+A3 was just statistically different from A3 with a P value of 0.00494. RV+sA3 was just statistically different from A3 with a P value of 0.00497.

18hpi Cell Viability AQ1 assay

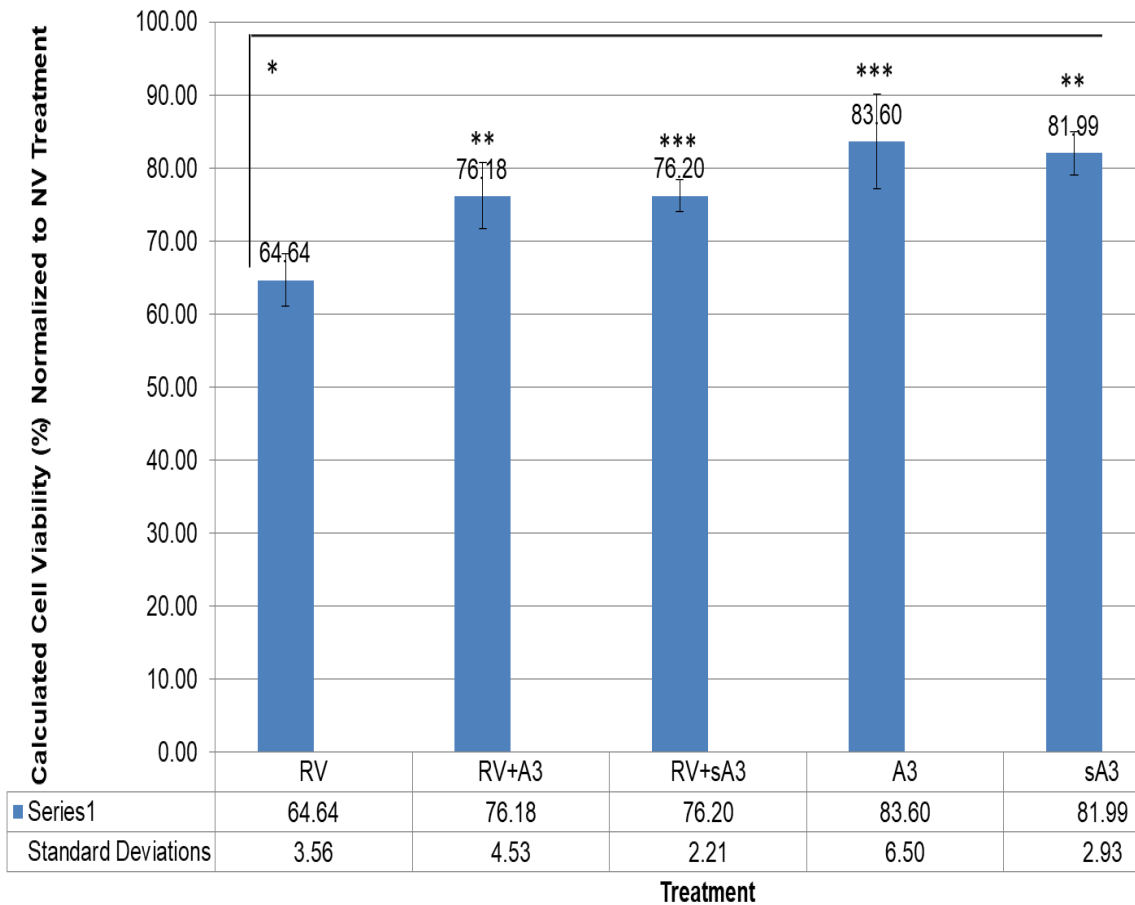|	RV	RV+A3	RV+sA3	A3	sA3
■ Series1	64.64	76.18	76.20	83.60	81.99
Standard Deviations	3.56	4.53	2.21	6.50	2.93

Figure 23. CellTiter 96 AQ$_{ueous}$ One Solution Cell Proliferation Assay results at 18hpi for each treatment. Experiments were conducted three times in triplicate. Data were statistically analyzed in Microsoft Office Excel 2016 software using a one-way analysis of variance (ANOVA) and a two-tailed Student's t tests (significance level, P <0.05) with Bonferroni's *post hoc* test to correct for multiple comparisons (P <0.005). RV was statistically RV+A3 (P= 1.75E-05); RV+sA3 (P= 3.3E-07); A3 (P= 9.2E-07); and sA3 (P= 4.8E-09). RV+A3 was statistically different from A3 (P= 0.00494). RV+sA3 was statistically different from A3 (P = 0.00497).

Data showing cell viability for each treatment over the 12-18hpi time points (Fig. 24) demonstrates the increased rate of decreased cell viability in the RV treated cells compared to RV+A3/sA3 or A3/sA3 alone. This suggests that A3 and sA3 may be conveying a protective effect to the cells both when introduced to RV infections as well as by themselves.

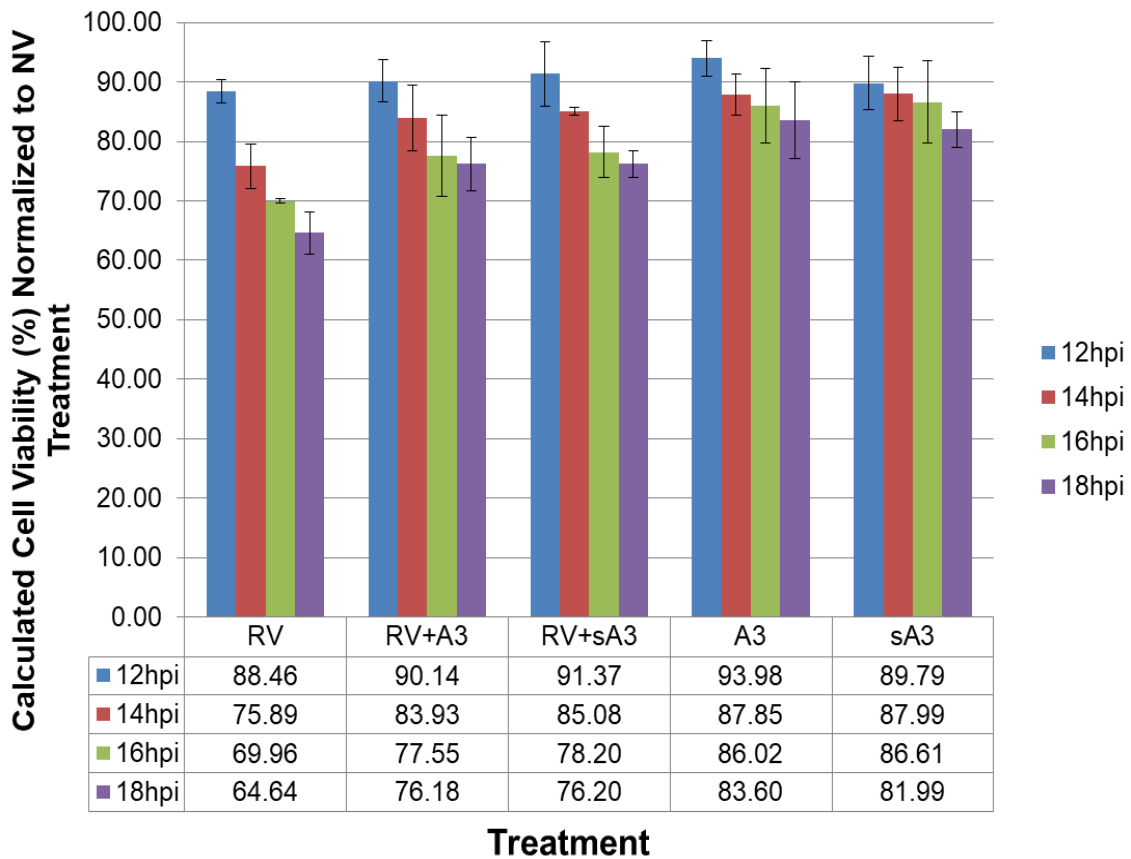**AQueous ONE Viability Assay Results per Treatment 12-18hpi**

Treatment	RV	RV+A3	RV+sA3	A3	sA3
12hpi	88.46	90.14	91.37	93.98	89.79
14hpi	75.89	83.93	85.08	87.85	87.99
16hpi	69.96	77.55	78.20	86.02	86.61
18hpi	64.64	76.18	76.20	83.60	81.99

Figure 24. CellTiter 96 AQ$_{ueous}$ One Solution Cell Proliferation Assay results at 12-18hpi for each treatment. Experiments were conducted three times in triplicate. Data is expressed as mean ±SD.

Caspase-3/7 activity

Caspase 3 and 7 are involved in the apoptosis process and are known to be executioner caspases. The Apo-ONE Homogeneous Caspase-3/7 Assay from Promega was used to investigate the caspase-3/7 activity in HT29.f8 cells with the various treatments. Caspase-3/7 activity was elevated in all treatments at 12hpi. RV only treatments had a sharp drop in caspase-3/7 expression at 14hpi after which it increased again. RV+A3 and RV+sA3 treatments dropped in expression at 14hpi, had slight increases at 16hpi, but significant decreases by 18hpi. A3 and sA3 alone dropped in expression at 14, and 16hpi and started increasing again by 18hpi.

12hpi Caspase-3/7 Activity

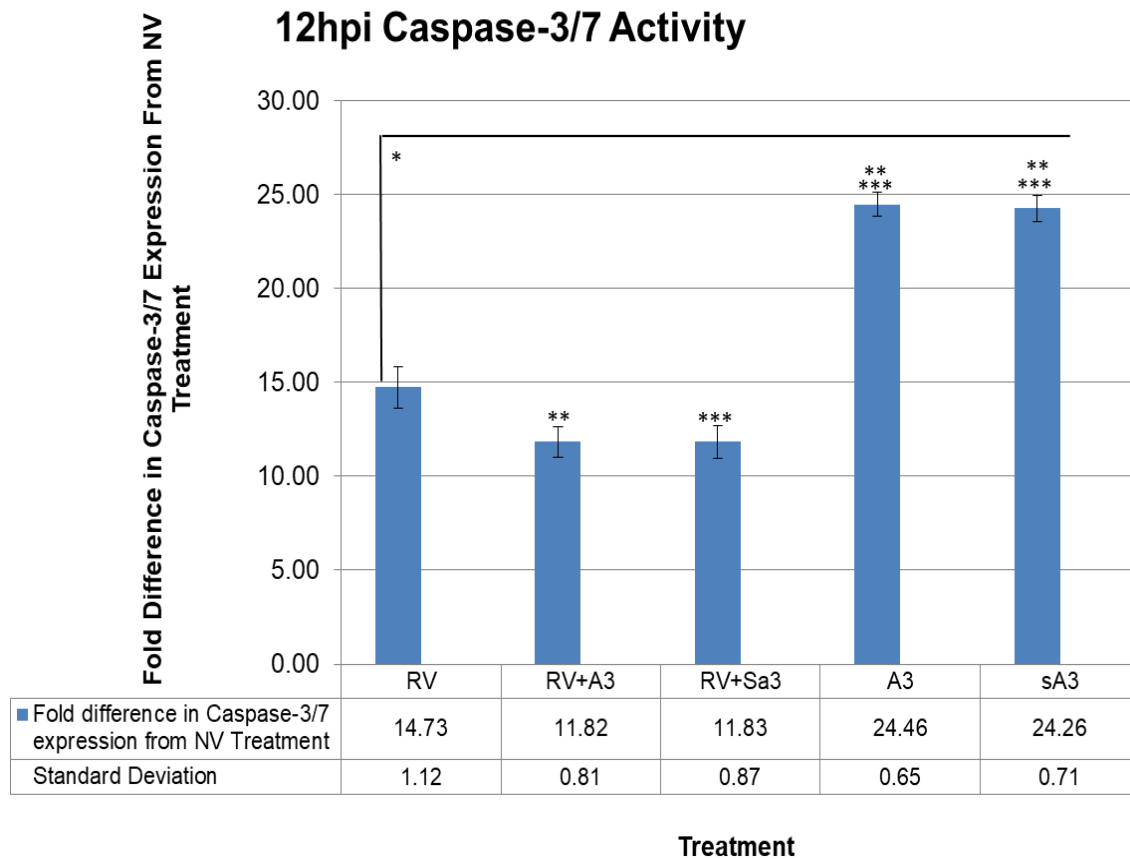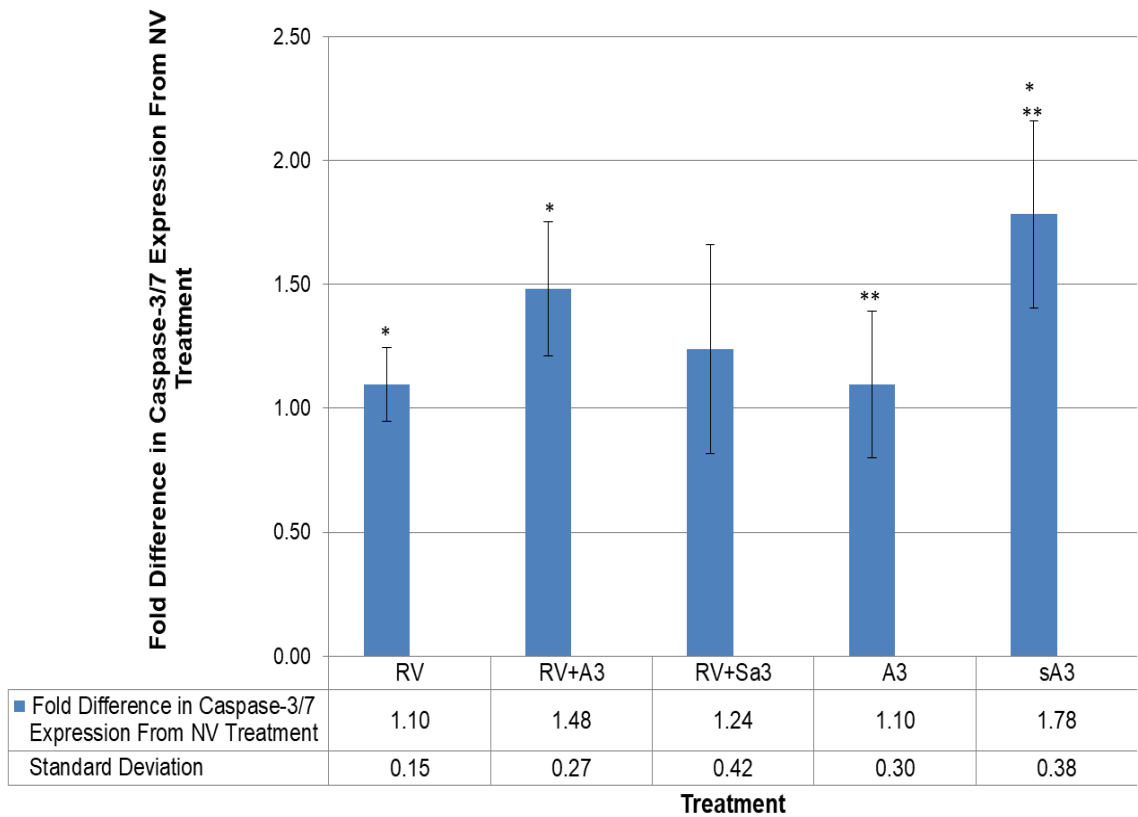|	RV	RV+A3	RV+Sa3	A3	sA3
■ Fold difference in Caspase-3/7 expression from NV Treatment	14.73	11.82	11.83	24.46	24.26
Standard Deviation	1.12	0.81	0.87	0.65	0.71

Treatment

Figure 25. Fold changes in the caspase-3/7 activity observed from NV treated HT29.f8 cells vs. treated cells at 12hpi using the APO3/7 assay. Data shown as mean ±SD. Experiments performed in triplicate three times. Data were statistically analyzed in Microsoft Office Excel 2016 software using a one-way analysis of variance (ANOVA) and a two-tailed Student's t tests (significance level, P <0.05) with Bonferroni's *post hoc* test to correct for multiple comparisons (P <0.005). RV was statistically different from RV+A3 (P= 1.22E-05); RV+sA3 (P=1.39E-05); A3 (P=1.33E-13); and sA3 (P= 2.64E-13). RV+A3 was statistically different from A3 (P= 6.99E-17); and sA3 (P= 1.59E-16). RV+sA3 was statistically different form A3 (P= 1.44E-16); and sA3 (P= 3.12E-16).

14hpi Caspase-3/7 Activity

	RV	RV+A3	RV+Sa3	A3	sA3
Fold Difference in Caspase-3/7 Expression From NV Treatment	1.10	1.48	1.24	1.10	1.78
Standard Deviation	0.15	0.27	0.42	0.30	0.38

Figure 26. Fold changes in the caspase-3/7 activity observed from NV treated HT29.f8 cells vs. treated cells at 14hpi using the APO3/7 assay. Data shown as mean ±SD. Experiments performed in triplicate three times. Data were statistically analyzed in Microsoft Office Excel 2016 software using a one-way analysis of variance (ANOVA) and a two-tailed Student's t tests (significance level, $P < 0.05$) with Bonferroni's *post hoc* test to correct for multiple comparisons ($P < 0.005$). RV was statistically different from RV+A3 ($P= 0.000621$); and sA3 ($P= 5.49E-05$). A3 was statistically different from sA3 ($P= 0.000299$).
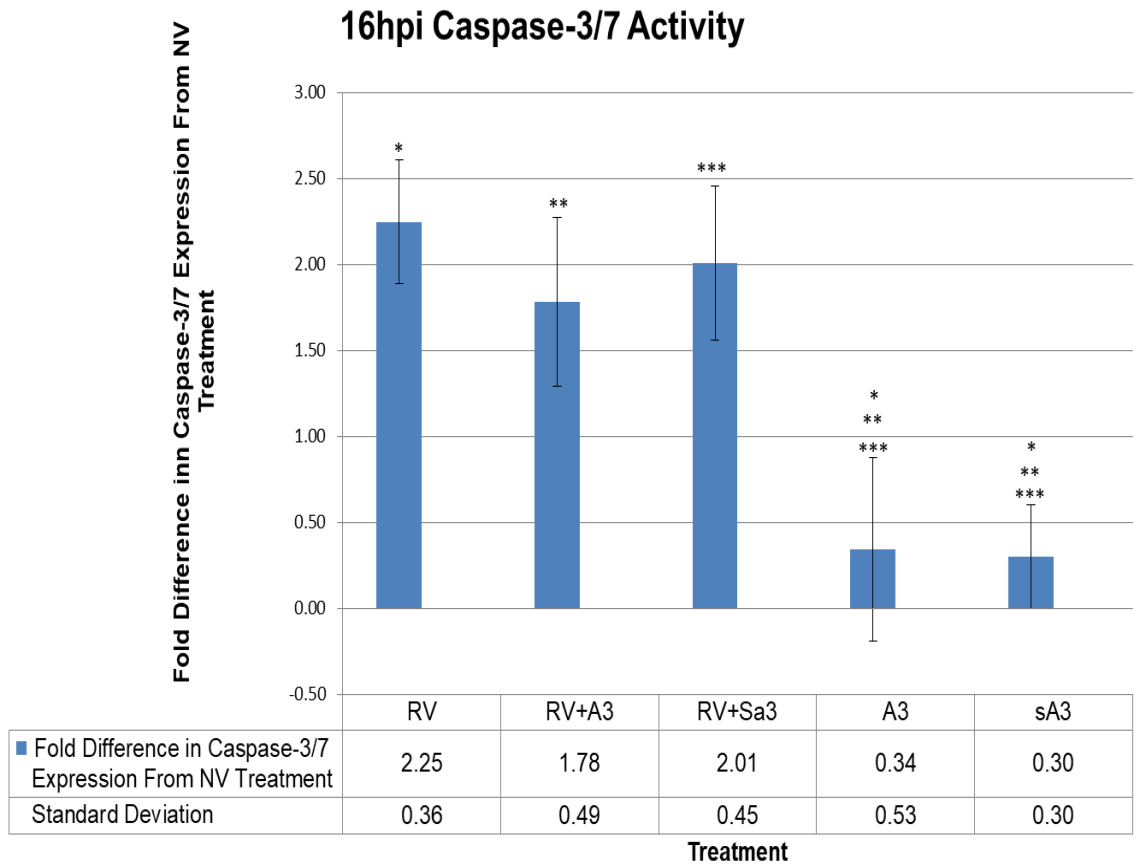
16hpi Caspase-3/7 Activity

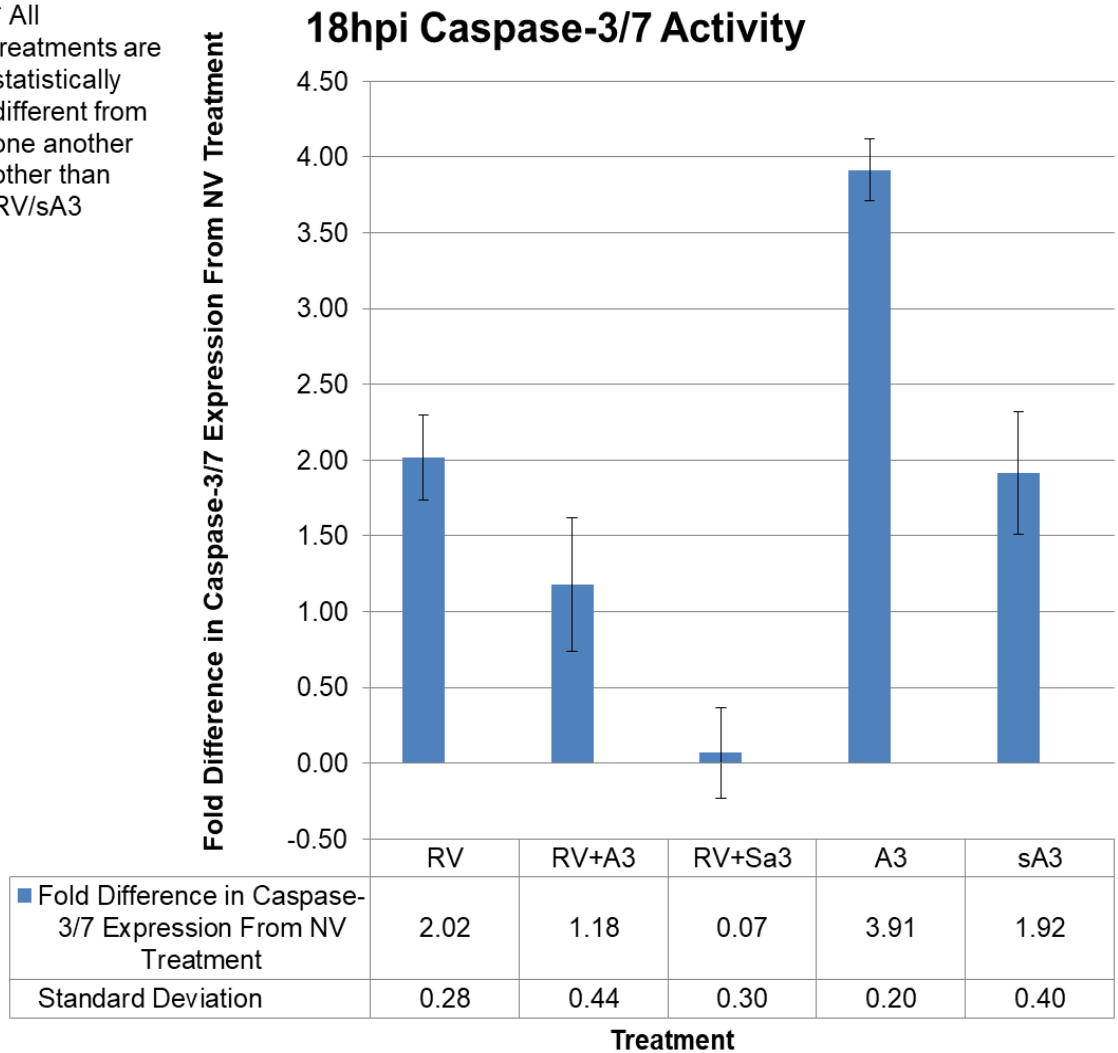|	RV	RV+A3	RV+Sa3	A3	sA3
■ Fold Difference in Caspase-3/7 Expression From NV Treatment	2.25	1.78	2.01	0.34	0.30
Standard Deviation	0.36	0.49	0.45	0.53	0.30

Figure 27. Fold changes in the caspase-3/7 activity observed from NV treated HT29.f8 cells vs. treated cells at 16hpi using the APO3/7 assay. Data shown as mean ±SD. Experiments performed in triplicate three times. . Data were statistically analyzed in Microsoft Office Excel 2016 software using a one-way analysis of variance (ANOVA) and a two-tailed Student's t tests (significance level, P <0.05) with Bonferroni's *post hoc* test to correct for multiple comparisons (P <0.005). RV was statistically different from A3 (P= 2.02E-07); sA3 (P= 1.78E-09). RV+A3 was statistically different from A3 (P= 3.07E-05); and sA3 (P= 1.41E-06). RV+sA3 was statistically different from A3 (P= 3.24E-06); and sA3 (P= 8.47E-08).

* All treatments are statistically different from one another other than RV/sA3

18hpi Caspase-3/7 Activity

	RV	RV+A3	RV+Sa3	A3	sA3
■ Fold Difference in Caspase-3/7 Expression From NV Treatment	2.02	1.18	0.07	3.91	1.92
Standard Deviation	0.28	0.44	0.30	0.20	0.40

Treatment

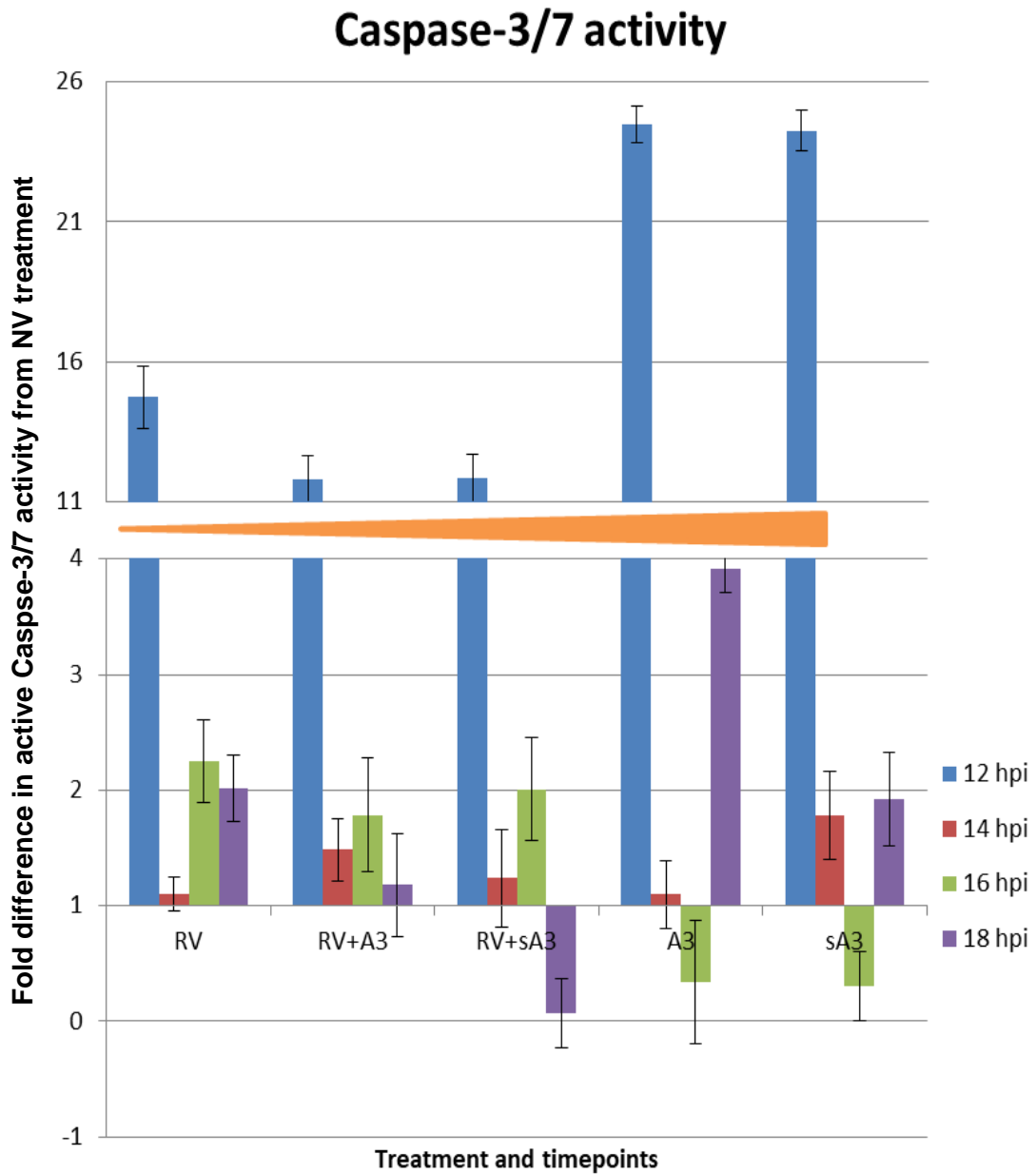Figure 28. Fold changes in the caspase-3/7 activity observed from NV treated HT29.f8 cells vs. treated cells at 18hpi using the APO3/7 assay. Data shown as mean ±SD. Experiments performed in triplicate three times. Data shown as mean ±SD. Experiments performed in triplicate three times. Data were statistically analyzed in Microsoft Office Excel 2016 software using a one-way analysis of variance (ANOVA) and a two-tailed Student's t tests (significance level, P <0.05) with Bonferroni's *post hoc* test to correct for multiple comparisons (P <0.005). RV was statistically different from RV+A3 (P= 0.000364); RV+sA3 (P= 2.38E-10); and A3 (P= 1.31E-11). RV+A3 was statistically different from RV+sA3 (P= 1.94E-05); A3 (P= 9.71E-12); and sA3 (P= 0.001146). RV+sA3 was statistically different from A3 (P= 4.7E-16); and sA3 (P=4.52E-09). A3 was statistically different from sA3 (P= 6.94E-10).

Figure 29. Fold changes in the caspase-3/7 activity observed from NV treated HT29.f8 cells vs. treated cells at 12-18hpi using the APO3/7 assay. Data shown as mean ±SD. Experiments performed in triplicate three times.

DISCUSSION

Previous experiments using the simian RV, SA11.4f, revealed antiviral effects of both A1 and A3 that reduced the amount of released infectious RV and a reduction in NSP4 suggested a decrease in viral replication (Ball *et al.*, 2015). This study investigated the effects of A3 and sA3 on the clonally derived human intestinal cell line, HT29.f8, infected with the human RV strain, Wa. Time course experiments (16 and 18 hpi) were performed to observe the intracellular patterns of the host cell and production of RV particles in RV-infected cells with/without the arachidins. At the same time points, extracellular nanoparticles were counted and measured to determine the diameter size of the populations.

Trypan Blue Cell Viability assay data showed no statistical difference between all groups tested compared to NV. This implies that the arachidins were not toxic to the host cells at 20μM concentrations (Fig. 2). Therefore, any effects observed in this study can be attributed to the mechanism of action of the arachidins.

PFU assays are commonly used to determine titers (PFU/mL) for infectious virus particles (Arnold *et al.*, 2012). Previously, we reported a statistically significant change in the amount of infectious RV produced using the

simian RV, SA11.4f (Ball *et al.*, 2015). This is the first report to demonstrate that the human RV (Wa)-infected cells treated with A3 and sA3 produced significantly fewer infectious RV particles than untreated RV-infected cells (Fig.3). Suggesting that the sA3 has similar antiviral activity as A3 against a human RV strain, Wa, in a human intestinal cell line (HT29.f8).

Initial TEM studies in the Parr laboratory (Lockwood, 2016; Caleb Witcher, 2017) demonstrated intracellular RV particles of two size populations. The two populations observed consisted of a more mature nonenveloped (neRV) population that are of similar sizes of mature infectious RV particles, and the less mature enveloped (eRV) as previously described in the literature (Estes and Greenberg, 2013). At the same time point, TRPS analysis of the supernatants showed extracellular nanoparticles (50-150nm) using the Izon qNano system that had relatively equal number of extracellular particles among the treatments with and without arachidins. However, the size distribution of the particles varied significantly between treatments. This suggests that some of the nanoparticles that are released from RV-infected cells maybe infectious RV particles as these supernatants produced more infectious RV particles (~74nm) than the arachidin treated cells (~116-117nm) as shown with the plaque forming assays. Previous studies infecting Caco-2 cells with RRV (rhesus monkey rotavirus) have shown the presence of extracellular vesicles (EVs) composed of exosomes and apoptotic bodies obtained by filtration/ultracentrifugation or differential

centrifugation (Barreto *et al.*, 2010; Bautista *et al.*, 2015). A recent manuscript has reviewed data that show Picornaviridae and Hepeviridae produce virus particles in fully host-derived lipid bilayers that resemble extracellular vesicles (EV), which are 50 nm–1 µm vesicles released by infected cells (van der Grein *et al.*, 2018). These studies indicate that some of the nanoparticles that our study has measured maybe EVs, therefore they will be further characterized in future studies.

The nucleus/cytoplasm ratio data obtained using TEM and immunofluorescent whole cell studies supported our hypothesis that there was a modulation of the apoptosis pathway with the addition of the arachidins to RV infected HT29.f8 cells. These characteristics of apoptosis have been previously reported in another RV study. This implies modulations cell signaling pathways by A3 and sA3 to achieve cellular homeostasis.

Multiple associations exist between autophagy and apoptosis signaling pathways (Dang *et al.*, 2015; Kroemer & Levine, 2009; Nikoletopoulou *et al.*, 2013; Wang *et al.*, 2015). Previous reports have shown that RV infections lead to cell death using the apoptosis cellular death pathway (Frias *et al.* , 2012). However, recent studies have suggested that the RV nonstructural protein 4 (NSP4) alone triggers the cells to produce autophagosomes, suggesting a change to an autophagy pathway that may be arrested at the autophagosomal stage of development (Crawford *et al.*, 2012). Autophagy can act as both an anti-

viral and pro-viral pathway, and the role of autophagy depends on the virus, the cell type, and the cellular environment (Jackson, 2015). The presence of both pathways as observed with TEM, led to exploration of the molecular and functional connections between the apoptosis and autophagy pathways in RV-infected HT29.f8 cells with and without the arachidins. The qRT-PCR studies conducted at 6, 7, 8, and 9hpi did not show significant fold changes in the expression of select autophagy and apoptosis. However, the upregulation of active caspase 3 and 7 proteins at 12hpi detected using the Apo One 3/7 assay suggests the involvement of the apoptosis pathway that is altered by A3 and sA3. Future studies will explore these pathways on a more global scale using the RT^2 apoptosis and autophagy assays. For example, the RT² Profiler™ PCR Array Human Apoptosis from Qiagen (Qiagen Inc., Germantown, MD) in which 84 or 370 genes of interest can be screened at the same time giving a much more global picture of what is happening in the pathways could be used.

The Apo ONE Caspase-3/7 assay time course study revealed that by 12hpi there was a significant increase in the initiator caspase 3 and 7 activity. Later time points revealed a drastic reduction in caspase 3 and 7 activity. It was noteworthy that there was a statistical decrease in caspae-3/7 activity with the addition of either arachidin to RV infections; however, the arachidins alone had a significantly higher caspase-3/7 activity than any of the test samples. This indicates that both of the arachidins have effects on RV and the cells. A recent

drug screening study has identified the PI3K/mTOR inhibitor, BEZ235, as a regulator of both influenza virus production and cellular metabolic homeostasis (Smallwood, *et al*, 2017). This study shows a potential antiviral agent that affects both an RNA virus' replication and cellular homeostasis that suggests a mechanism of action that modulates cellular homeostasis and inhibits viral infections. This type of therapeutic agent could be very efficient against viral infections without the side effects of causing viruses to mutate and evade the antiviral drugs or vaccines.

Altogether, the data suggests the addition of A3 or sA3 to RV infections has a protective effect on host cells, and that a crosstalk between apoptosis and autophagy inhibits RV morphogenesis. These findings indicate the possibility that RV modulates the switch between autophagy and apoptosis to facilitate their own replication in untreated cells, and suggests that A3 and sA3 restore cellular homeostasis, producing a protective response that has potential therapeutic antiviral activity.

Conflict of interest

The author has no conflict of interest to declare.

References

Akpinar, F., & Yin, J. (2015). Characterization of Vesicular stomatitis virus populations by tunable resistive pulse sensing. *Journal of Virological Methods,* **218**, 71-76*.* DOI: 10.1016/j.jviromet.2015.02.006

Anderson, E. J., & Weber, S. G. (2004). Rotavirus infection in adults. *Lancet Infectious Disease,* **4(2)**, 91-99. DOI: 10.1016/S1473-3099(04)00928-4

Angel, J., Franco, M., & Greenberg, H. (2007). Rotavirus vaccines: recent developments and future considerations. *Nature Reviews Microbiology,* **5(7)**, 529-539. DOI:10.1038/nrmicro1692

Arnold, M., Patton, J. T., & McDonald, S. M. (2009). Culturing, storage, and quantification of rotaviruses. *Current Protocols in Microbiology,* **SUPPL. 15C.** DOI: 10.1002/9780471729259.mc15c03s15

Bakare, N., Menschik, D., Tiernan, R., Hua, W., & Martin, D. (2010). Severe combined immunodeficiency (SCID) and rotavirus vaccination: Reports to the Vaccine Adverse Events Report System (VAERS). *Vaccine,* **28(40)**, 6609-6612. DOI:10.1016/j.vaccine.2010.07.039

Ball, J., Medina-Bolivar, F., Defrates, K., Hambleton, E., Hurlburt, M., Fang, L., Yang, T., Nopo-Olazabal, L., Atwill, R., Ghar, P., & Parr, R. (2015). Investigation of Stilbenoids as Potential Therapeutic Agents for Rotavirus Gastroenteritis. *Advances in Virology,* **2015**, 1-10. DOI: 10.1155/2015/293524

Ball, J., Mitchell, D., Gibbons, T., & Parr, R. (2005). Rotavirus NSP4: A Multifunctional Viral Enterotoxin. *Viral Immunology,* **18(1)**, 27-40. DOI: 10.1089/vim.2005.18.27

Barreto, A., Rodríguez, L.-S., Rojas, O.L., Wolf, M., Greenberg, H.B., Franco, M.A, Angel, J., (2010). Membrane vesicles released by intestinal epithelial cells infected with rotavirus inhibit T-cell function*. Viral Immunol.* **23**, 595–608. DOI: 10.1089/vim.2009.0113

Bautista, D., Rodríguez, L.-S., Franco, M.A., Angel, J., Barreto, A., (2015). Caco-2 cells infected with rotavirus release extracellular vesicles that express markers of apoptotic bodies and exosomes. *Cell Stress Chaperones.* **20**, 697–708. DOI: 10.1007/s12192-015-0597-9

Berardi, V., Ricci, F., Castelli, M., Galati, G., & Risuleo, G. (2009). Resveratrol exhibits a strong cytotoxic activity in cultured cells and has an antiviral action against polyomavirus: potential clinical use. *Journal of Experimental and Clinical Cancer Research,* **28(1),** 96. DOI:10.1186/1756-9966-28-96

Bernstein, D. I. (2009). Rotavirus overview. The *Pediatric Infectious Disease Journal,* **28(Supplement)**, S50-S53. DOI: 10.1097/INF.0b013e3181967bda

Bhowmick, R., Banok, G., Chanda, S., Chattopadhyay, S., & Chawla-Sarkar, M. (2014). Rotavirus infection induces G_1 to S phase transition in MA104 cells via Ca^{+2}/Calmodulin pathway. *Virology,* **454-455**, 270-279. DOI: 10.1016/j.virol.2014.03.001

Bishop, R. (2009). Discovery of Rotavirus: Implications for Child Health. *Journal of Gastroenterology and Hepatology,* **24**, S81-S85. DOI:10.1111/j.1440-1746.2009.06076.x

Bishop, R., Davidson, G. P., Holmes, I. H., & Ruck, B. J. (1973). Virus particles in epithelial cells of duodenal mucosa from children with acute non-bacterial gastroenteritis. *Lancet,* **302(7841)**, 1281-1283. DOI: 10.1016/S0140-6736(73)92867-5

Bobek, V., Kolostova, K., Pinterova, D., Kacprzak, G, Adamiak, J., Kolodziej, J., Boubelik, M., Kubecova, M., and Hoffman, R. M. (2010). A clinically relevant, syngeneic model of spontaneous, highly metastatic B16 mouse melanoma. *Anticancer Research,* **30**, 4799-4804. PMID 21187455 [Indexed for MEDLINE]

Bustin, S., V. Benes, J. Garson, J. Hellemans, J. Huggett, M. Kubista, and R. Mueller et al. (2009). The MIQE Guidelines: Minimum Information for Publication of Quantitative Real-Time PCR Experiments. *Clinical Chemistry,* **55**: 611-622. DOI: 10.1373/clinchem.2008.112797

Chang, J., Lai, Y., Djoko, B., Wu, P., Liu, C., Liu, Y., & Chiou, R. Y. (2006). Biosynthesis Enhancement and Antioxidant and Anti-inflammatory Activities of Peanut *(Arachis hypogaea L.)* Arachidin-1, Arachidin-3, and Isopentadienylresveratrol. *Journal of Agricultural and Food Chemistry,*

54(26), 10281-10287. DOI: 10.1021/jf0620766

Chen, X., Qiao, H., Liu, T., Yang, Z., Xu, L., Xu, Y., Ge, H. M., Tan, R., and Li, E. (2012). Inhibition of herpes simplex virus infection by oligomeric stilbenoids through ROS generation. *Antiviral Research*, **95(1),** 30-36. DOI: 10.1016/j.antiviral.2012.05.001

Chiu, H., Richart, S., Lin, F., Hsu, W., & Liu, H. (2014). The Interplay of Reovirus with Autophagy. *BioMed Research International,* **2014,** 1-8. DOI: 10.1155/2014/483657

Chong, J., Poutaraud, A., & Hugueney, P. (2009). Metabolism and roles of stilbenes in plants. *Plant Science,* **177(3)**, 143-155. DOI: 10.1016/j.plantsci.2009.05.012

Clayton J, Bandy J. (2018). Compositions and methods of synthesizing arachidin-3 from resveratrol. U.S. Patent 9,981,895.

Cook, S. M., Glass, R. I., LeBaron, C. W., & Ho, M. S. (1990). Global seasonality of rotavirus infections. *Bulletin of World Health Organization,* **68**, 171-177. PMID:1694734 PMCID:PMC2393128 [Indexed for MEDLINE]

Cui, H., Bai, S., Huo, Z., Li, J., Sun, J., & An, X. (2015). A cluster of rotavirus enteritis in pediatric liver recipients. *Transplant Infectious Disease,* **17(3)**, 477-480. DOI: 10.1111/tid.12378

DeBloise, R. W., & Bean, C. P. (1970). Counting and sizing of Submicron Particles by the Resistive Pulse Technique. *Review of Science Instruments,* **41(7)**, 909-916. DOI: 10.1063/1.1684724

Djoko, B., Chiou, R., Shee, J., & Liu, Y. (2007). Characterization of Immunological Activities of Peanut Stilbenoids, Arachidin-1, Piceatannol, and Resveratrol on Lipopolysaccharide-Induced Inflammation of RAW 264.7 Macrophages. *Journal of Agricultural and Food Chemistry,* **55(6)**:2376-2383. DOI: 10.1021/jf062741a

Desselberger, U. (2014). Rotaviruses. *Virus Research,* **190**, 75-96. DOI: 10.1016/j.virusres.2014.06.016

Eren, E., Zamuda, K., & Patton, J. T. (2016). Modeling of the Rotavirus Group C Capsid predicts a Surface Topology Distinct From Other Rotavirus Species. *Virology,* **487**, 150-162. DOI: 10.1016/j.virol.2015.10.017

Esona, M. D., & Gautam, R. (2015). Rotavirus. *Clinics in Laboratory Medicine,* **35(2),** 363-391. DOI: 10.1016/j.cll.2015.02.012

Estes, M. K. (2001). Rotavirus and their replication. *Fields Virology,* 1747-1785. ISBN: 9780781760607 0781760607

Estes, M.K., Greenberg, H.., (2013). Rotaviruses, in: Fields Virology. Wolters Kluwer Health/Lippincott Williams & Wilkins, Philadelphia, PA, pp. 1347–1401. ISBN/ISSN: 9781451105636

Farkas, K., Pang, L., Lin, S., Williamson, W., Easingwood, R., Fredricks, R., Jaffer, M. A., & Varsani, A. (2013). A gel Filtration-based Method for the Purification of Infectious Rotavirus Particles for Environmental Research Applications. *Food Environmental Virology,* **5(4)**, 231-235. DOI: 10.1007/s12560-013-9122-4

Flemington, E. K. (2001). Herpesvirus lytic replication and the cell cycle: arresting new developments. *Journal of Virology,* **75(10)**, 4475–4481. DOI: 10.1128/JVI.75.10.4475-4481.2001

Flewett, T. H., & Woode, G. N. (1978). The rotaviruses. *Archives of Virology* **57(1)**, 1-23. DOI: 10.1007/BF01315633

Gambini, J., Ingles, M., Olaso, G., Abdelaziz, K. M., Vina, J., & Borras, C. (2015). Properties of Resveratrol: In Vitro and In Vivo Studies about Metabolism, Bioavailability, and Biological Effects in Animal Models and Humans. *Oxidative Medicine And Cellular Longevity,* **2015**, 1-13. DOI: 10.1155/2015/837042

Gandhi, G. R., Barreto, P. G., Lima, B. D. S., Quintans, J. D. S. S., Araujo, A. A. D. S., Narain, N., Quintans-Junior, L. J., & Gurgrel, R. Q. (2016). Medicinal plants and natural molecules with in vitro and in vivo activity against rotavirus: A systematic review. *Phytomedicine*, **23(14)**, 1830-1842. DOI: 10.1016/j.phymed.2016.11.005

Gardet, A., Brenton, M., Fontanges, P., Trugnan, G., & Chwetzoff, S. (2006). Rotavirus spike protein VP4 binds to and remodels actin bundles of the epithelial brush border into actin bodies. *Journal of Virology,* **80(8)**, 3947-3056. DOI: 10.1128/JVI.80.8.3947-3956

Glass, R. I., Parashar, U. D., Bresee, J. S., Turcios, R., Fischer, T. K., Widdowson, M., Jiang, B., & Gentsch, J. R. (2006) Rotavirus vaccines:

current prospects and future challenges. *The Lancet,* **368(9532)**, 323-332. DOI: 10.1016/S0140-6736(06)68815-6

Greenberg, H. B., & Estes, M. K. (2009). Rotavirus: From Pathogenesis to Vaccination. *Gastroenterology,* **136(6)**, 1939-1951. DOI: 10.1053/j.gastro.2009.02.076

Hu, L., Crawford, S. E., Hyser, J. M., Estes, M. K., & Prasad, B. V. (2012). Rotavirus non-structural proteins: structure and function. *Current Opinion in Virology,* **2(4)**, 380-388. DOI: 10.1016/j.coviro.2012.06.003

Huang, C., Au, L., Chiou, R. Y., Chung, P., Chen, S., Tang, W., Chang, C., Fang, W., & Lin, S. (2010). Arachidin-1, a Peanut Stilbenoid, Induces Programmed Cell Death in Human Leukemia HL-60 Cells. *Journal of Agricultural and Food Chemistry,* **58(23)**:12123-12129. DOI: 10.1021/jf102993j

Heymann, D. L. (2015). Control of communicable diseases manual: an official report of the American Public Health Association. *Washington, DC: APHA Press, an imprint of the American Public Health Association.* ISBN: 978-0-87553-018-5

Jackson, W. (2015). Viruses and the autophagy pathway. *Virology* 479-480: 450-456. DOI: 10.1016/j.virol.2015.03.042

Jayaram, H., Estes, M. K., & Prasad, B. V. V. (2004). Emerging themes in rotavirus cell entry, genome organization, transcription and replication. *Virus Research,* **101(1)**, 67-81. DOI: 10.1016/j.virusres.2003.12.007

Jeandet, P., Delaunois, B., Conreux, A., Donnez, D., Nuzzo, V., Cordelier, S., Clement, C., & Courot, E. (2010). Biosynthesis, metabolism, molecular engineering, and biological functions of stilbene phytoalexins in plants. *BioFactors,* **36(5)**, 331-341. DOI: 10.1002/biof.108

Jiang, V., Jiang., B., Tate, J., Parashar, U. D., & Patel, M. M. (2010). Performance of rotavirus vaccines in developed and developing countries. *Human Vaccine,* **6(7)**, 532-542. DOI: 10.4161/hv.6.7.11278

John, J., Sarkar, R., Muliyil, J., Bhandari, N., Bhan, M. K., & Kang, G. (2014). Rotavirus gastroenteritis in India, 2011–2013: Revised estimates of disease burden and potential impact of vaccines. *Vaccine,* **32**, A5-A9. DOI: 10.1016/j.vaccine.2014.03.004

Kenakin, T., Christopoulos, A., (2013). Signaling bias in new drug discovery : detection , quantification and therapeutic impact**. 12,** 205–216**.** DOI: 10.1038/nrd3954

Lee, L. Y., & Ison, M. G. (2014). Diarrhea caused by viruses in transplant recipients. *Transplant Infectious Disease,* **16(3)**, 347-358. DOI: 0.1111/tid.12212

Leshem, E., Lopman, B., Glass, R., Gentsch, J., Banyai, K., Parasher, U., & Patel, M. (2014). Distribution of rotavirus strains and strain-specific effectiveness of the rotavirus vaccine after its introduction: a systematic review and meta-analysis. *Lancet Infectious Disease,* **14(9)**, 847-856. DOI: 10.1016/S1473-3099(14)70832-1

Liakopoulou, E., Mutton, K., Carrington, D., Robinson, S., Steward, C., Goulden, N., Cornish, J., & Marks, D. (2005). Rotavirus as a significant cause of prolonged diarrheal illness and morbidity following allogeneic bone marrow transplantation. *Bone Marrow Transplantation,* **36**, 691-694. DOI: 10.1038/sj.bmt.1705127

Liu, J. D., Wang, Y. J., Chen, C. H., Yu, C. F., Chen, L. C., Lin, J. K., Liang, Y. C., Lin, S. Y., & Ho, Y. S. (2003). Molecular mechanisms of G0/G1 cell-cycle arrest and apoptosis induced by terfenadine in human cancer cells. *Molecular Carcinogenesis,* **37(1)**, 39–50. DOI: 10.1002/mc.10118

Lockwood, H. (2016). Regulation of the Transcriptome of Rotavirus Infected HT29.f8 cells by Arachidin-3. *Thesis, SFASU.*

Lopman, B. A., Pitzer, V. E., Sarkar, R., Gladstone, B., Patel, M., Glasser, J., Gambhir, M., Atchison, C., Grenfell, B. T., Edmundd, J., Kang, G., & Parashar, U. (2012). Understanding reduced rotavirus vaccine efficacy in low socio-economic settings. *PLoS ONE,* **7(8).** DOI: 10.1371/journal.pone.0041720

Madhi, S. A., Cunliffe, N. A., Steele, D., Witte, D., Kristen, M., Louw, C., Ngwira, B., Victor, J. C., Gillard, P. H., Cheuvart, B. B., Han, H. H., & Neuzil, K. M. (2016). Effect of human rotavirus vaccine on severe diarrhea in African infants. *Malawi Medical Journal,* **28(3),** 108-114. PMCID: PMC5117000 PMID: 27895844

Martin-Latil, S., Mousson, L., Autret, A., Colbere-Garapin, F., & Blondel, B. (2007). Bax Is Activated during Rotavirus-Induced Apoptosis through the

Mitochondrial Pathway. *Journal of Virology* **81(9)**, 4457-4464. DOI: 10.1128/JVI.02344-06

Matthews, R. E. F. (1979). Classification and nomenclature of viruses. Third report of the international committee on taxonomy of viruses. *Intervirology* **12**, 199-206. DOI: 10.1159/000149278

Matthijnssens, J., Ciarlet, M., Heiman, E., Arijs, I., Delbeke, T., Mconald, S. M., Palombo, E. A., Iturriza-Gomara, M., Maes, P., Patton, J.T., Rahman, M., & Van Ranst, M. (2008). Full Genome-based Classification of Rotaviruses Reveals a Common Origin between Human Wa-Like and Porcine Rotavirus Strains and Human DS-1-Like and Bovine Rotavirus Strains. *Journal of Virology*, **82(7),** 3204-3219. DOI: 10.1128/JVI.02257-07

McNulty, M., Curren, W., & McFerren, J. (1976). The morphogenesis of a cytopathic bovine rotavirus in Madin-Darby bovine kidney cells. *Journal of General Virology,* **33(3)**, 503-508. DOI: 10.1099/0022-1317-33-3-503

Mitchell, D. M., & Ball, J. M. (2004). Characterization of a spontaneously polarizing HT-29 cell line, HT-29/cl.f8. *In Vitro Cellular And Developmental Biology—Animal,* **40**, 297-302. DOI: 10.1290/04100061.1

Moss, R., Mao, Q., Taylor, D., & Saucier, C. (2013). Investigation of monomeric and oligomeric wine stilbenoids in red wines by ultra-high-performance liquid chromatography/electrospray ionization quadrupole time-of-flight mass spectrometry. *Rapid Communications in Mass Spectrometry,* **27(16)**, 1815-1827. DOI: 10.1002/rcm.6636

Mohan, K., Muller, J., & Atreya, C. (2008). Defective rotavirus particle assembly in lovastatin-treated MA104 cells. *Archives of Virology,* **153(12),** 2283-2290. DOI: 10.1007/s00705-008-0261-0

Nakamura, M., Saito, H., Ikeda, M., Hokari, R., Kato, N., Hibi, T., & Miura, S. (2010). An antioxidant resveratrol significantly enhances replication of hepatitis C virus. *World Journal of Gastroenterology,* **16(2)**, 184-192. DOI: 10.3748/wjg.v16.i2.184

Nikoletopoulou, V., Markaki, M., Palikaras, K., Tavernarakis, N., (2013). Crosstalk between apoptosis, necrosis and autophagy. *Biochim. Biophys. Acta - Mol. Cell Res.* **1833**, 3448–3459. DOI: 10.1016/j.bbamcr.2013.06.001

Palmara, A. T., Nencioni, L., Aquilano, K., De Chiara, G., Hernandez, L.,

Cozzolino, F., Ciriolo, M. R., & Garaci, E. (2005). Inhibition of influenza A virus replication by resveratrol. *Journal of Infectious Diseases,* **191(10)**, 1719-1729. DOI: 10.1086/429694

Patel, N. C., Hertel, P. M., Estes, M. K., De La Morena, M., Petru, A. M., Noroski, L. M., Revell, P. A., Hanson, I. C., Paul., M. E., Rosenblatt, H. M., & Abramson, S. L. (2010). Vaccine-Acquired Rotavirus in Infants with Severe Combined Immunodeficiency. *New England Journal of Medicine,* **362(4)**, 314-319. DOI: 10.1056/NEJMoa0904485

Patton, J. T., & Spencer, E. (2000). Genome replication and packaging of segmented double-stranded RNA viruses. *Virology,* **277(2)**, 217-225. DOI: 10.1006/viro.2000.0645

Patton, J. T. (2012). Rotavirus diversity and evolution in the post-vaccine world. *Discovery Medicine,* **13**, 85-97. PMCID: PMC3738915 NIHMSID: NIHMS493520 PMID: 22284787

Pattingre, S., A. Tassa, X. Qu, R. Garuti, X. Liang, N. Mizushima, and M. Packer et al. (2005). Bcl-2 Antiapoptotic Proteins Inhibit Beclin 1-Dependent Autophagy. *Cell,* **122**, 927-939. DOI: 10.1016/j.cell.2005.07.002

Payne, D. C., Staat, M. A., Edwards, K. M., Sziagyi, P. G., Gentsch, J. R., Stockman, L. J., Curns, A. T., Griffin, M., Weinberg, G. A., Hall, C. B., Fairbrother, G., Alexander, J., & Parashar, U. D. (2008). Active, population-Based Surveillance for Severe Rotavirus Gastroenteritis in Children in the United States. *Pediatrics,* **122**, 1235-1243. DOI: 10.1542/peds.2007-3378

Parashar, U. D., Gibson, C. J., Bresee, J. S., & Glass, R. I. (2006). Rotavirus and severe childhood diarrhea. *Emerging Infectious Diseases,* **12(2)**, 304-306. DOI: 10.3201/eid1202.050006

Raehal, K.M., Walker, J.K.L., Bohn, L.M. (2005). Morphine Side Effects in β-Arrestin 2 Knockout Mice. *J. Pharmacol. Exp. Ther.* **314**, 1195 LP-1201. DOI: 10.1124/jpet.105.087254

Rao, X., Huang, X., Zhou, Z., & Lin, X. (2013). An improvement of the 2^(–delta delta CT) method for quantitative real-time polymerase chain reaction data analysis. *Biostatistics, Bioinformatics and Biomathematics*, **3(3)**, 71–85. PMID: 25558171 PMCID: PMC4280562

Rasmussen, S.G.F., Choi, H.-J., Fung, J.J., Pardon, E., Casarosa, P., Chae, P.S., DeVree, B.T., Rosenbaum, D.M., Thian, F.S., Kobilka, T.S., Schnapp, A., Konetzki, I., Sunahara, R.K., Gellman, S.H., Pautsch, A., Steyaert, J., Weis, W.I., Kobilka, B.K., (2011a). Structure of a nanobody-stabilized active state of the β(2) adrenoceptor. *Nature.* **469,** 175–180. DOI: 10.1038/nature09648

Rasmussen, S.G.F., DeVree, B.T., Zou, Y., Kruse, A.C., Chung, K.Y., Kobilka, T.S., Thian, F.S., Chae, P.S., Pardon, E., Calinski, D., Mathiesen, J.M., Shah, S.T.A., Lyons, J.A., Caffrey, M., Gellman, S.H., Steyaert, J., Skiniotis, G., Weis, W.I., Sunahara, R.K., Kobilka, B.K., (2011b). Crystal Structure of the β(2)Adrenergic Receptor-Gs protein complex. *Nature.* **477,** 549–555. DOI: 10.1038/nature10361

Roberts, G., S. Yu, Q. Zeng, L. Chan, W. Anderson, A. Colby, and M. Grinstaff (2012). Tunable pores for measuring concentrations of synthetic and biological nanoparticle dispersions. *Biosensors and Bioelectronics* 31: 17-25. DOI: 10.1016/j.bios.2011.09.040

Rzezutka, A., & Cook, N. (2004). Survival of human enteric viruses in the environment and food. *FEMS Microbiology Reviews,* **28(4)**, 441-453. DOI: 10.1016/j.femsre.2004.02.001

Smallwood, H. S., Duan, S., Morfouace, M., Rezinciuc, S., Shulkin, B. L., Shelat, A., … Thomas, P. G. (2017). Targeting metabolic reprogramming by influenza infection for therapeutic intervention. *Cell Reports*, *19*(8), 1640–1653. DOI: 10.1016/j.celrep.2017.04.039

Sobolev, V. S., Potter, T. L., & Horn, B. W. (2006). Prenylated stilbenes from peanut root mucilage. *Phytochemical Analysis,* **17(5)**, 312-322. DOI: 10.1002/pca.920

Stelzueller, I., Wiesmayr, S., Swenson, B., Biebl, M., Goegele, H., Margreiter, R., & Bonatti, H. (2007). Rotavirus enteritis in solid organ transplant recipients: an underestimated problem? *Transplant Infectious Disease,* **9(4)**, 281-285. DOI: 10.1111/j.1399-3062.2007.00251.x

Sugata, K., Taniguchi, K., Yui, A., Nakai, H., Asano, Y., Hashimoto, S., Ihira, M., Yagasaki, H., Takahashi, Y., Kojima, S., Matsumoto, K., Kato, K., & Yoshikawa, T. (2011). Analysis of rotavirus antigenemia in hematopoietic stem cell transplant recipients. *Transplant Infectious Disease,* **14(1)**, 49-56. DOI: 10.1111/j.1399-3062.2011.00668.x

Tate, J. E., Burton, A. H., Boschi-Pinto, C., & Parashar, U. D. (2016). Global, Regional, and National Estimates of Rotavirus Mortality in Children <5 Years of Age, 2000-2013. *Clinical Infectious Disease,* **62(Supplemental 2)**, s96-s105. DOI: 10.1371/journal.pone.0183392

van der Grein, S.G., Defourny, K.A.Y., Slot, E.F.J., Nolte-'t Hoen, E.N.M., 2018. Seminars in Immunopathology Intricate relationships between naked viruses and extracellular vesicles in the crosstalk between pathogen and host. *Semin. Immunopathol.* DOI: 10.1007/s00281-018-0678-9

Velayudhan, L., Van Diepen, E., Marudkar, M., Hands, O., Suribhatala, S., Prettyman, R., Murray, J., Baillon, S., & Bhattacharyya, S. (2014). Therapeutic potential of cannabinoids in neurodegenerative disorders: a selective review. *Current Pharmaceutical Design,* **20(13),** 2218-2230. DOI: 10.15761/CCRR.1000126

Vitaglione, P., Sforza, S., Galavera, G., Ghidini, C., Caporaso, N., Vescovi, P., Fogliano, V., & Marchelli, R. (2005). Bioavailability of trans-resveratrol from red wine in humans. *Molecular Nutrition & Food Research,* **49(5)**, 495-504. DOI: 10.1002/mnfr.200500002

Vogel, R., G. Willmott, D. Kozak, G. Roberts, W. Anderson, L. Groenewegen, and B. Glossop (2011). Quantitative Sizing of Nano/Microparticles with a Tunable Elastomeric Pore Sensor. *Analytical Chemistry* 83: 3499-3506. DOI: 10.1021/ac200195n

Ward, R. L. (1996). Mechanisms of protection against rotavirus in humans and mice. *Journal of Infectious Disease,* **174 (Supplement 1)**, S51-S58. DOI: 10.1097/INF.0b013e3181967c16

Witcher, C. M. (2017). The regulation of rotavirus-infected HT29.f8 and MA104 cells treated with arachidin 1 or arachidin 3. *Electronic Theses and Dissertations.* 98. https://scholarworks.sfasu.edu/etds/98

Wollweber, L. (1990), E. Harlow and D. Lane (Editors), Antibodies: A Laboratory Manual. XIII + 726 S., 50 Abb., 62 Tab. Chapter 10, page 386. Cold Spring Harbor 1988. Cold Spring Harbor Laboratory. DOI: 10.1002/jobm.3620300304

Yakshe, K. A., Franklin, Z. D., & Ball, J. M. (2015). Rotaviruses: Extraction and Isolation of RNA, Reassortant Strains, and NSP4 Protein. *Current Protocols in Microbiology*, John Wiley & Sons, Inc., **2015.** DOI:

10.1002/9780471729259.mc15c06s37

Yang, T., Fang, L., Nopo-Olazabal, C., Condori, J., Nopo-Olazabal, L., Balmaceda, C., & Medina-Bolivar, F. (2015). Enhanced Production of Resveratrol, Piceatannol, Arachidin-1, and Arachidin-3 in Hairy Root Cultures of Peanut Co-treated with Methyl Jasmonate and Cyclodextrin. *Journal of Agriculture and Food Chemistry,* **63(15)**, 3942-3950. DOI: 10.1021/jf5050266

Yin, Y., Metselaar, H. J., Sprengers, D., Peppelenbosh, M. P., & Pan, Q. (2015). Rotavirus in organ transplantation: Drug-virus-host interactions. *American Journal of Transplantation,* 15**(3)**, 585-593. DOI: 10.1111/ajt.13135

VITA

Rebekah Napier-Jameson graduated from Delta State University with Bachelors in Biology and Bachelors in Environmental Science in December 2015. She entered graduate school at Stephen F. Austin State University, Nacogdoches, Texas in August 2016 and will receive a Master of Science degree in Biotechnology. After completion of her Master of Science degree in Biotechnology at Stephen F. Austin State University she will start pursuing her PhD in Biology at Southern Methodist University, Dallas, Texas in the Fall of 2018.

Permanent Address: 71 Vantil Road, Farmall, Chartwell West,

Randburg, Gauteng,

South Africa, 2194

Email Address: napierjameson@gmailcom@gmail.com

Style manual designation: Journal of Virological Methods

This thesis was typed by Rebekah Napier-Jameson.